IOP Publishing | Bureau International des Poids et Mesures Metrologia

Metrologia **60** (2023) 015002 (40pp) https://doi.org/10.1088/1681-7575/ac8c99

Gas flow standards and their uncertainty

John D Wright[1,*], Shin-Ichi Nakao[2], Aaron N Johnson[1] and Michael R Moldover[1]

[1] National Institute of Standards and Technology, Gaithersburg, MD, United States of America
[2] Flowcol, Yokohama, 235-0045, Japan

E-mail: john.wright@nist.gov

Received 24 May 2022, revised 11 August 2022
Accepted for publication 25 August 2022
Published 12 December 2022

Abstract

We review primary and working gas flow standards that are used to calibrate gas flow meters. For each type of primary standard, we describe the principles and practical considerations of its operation and describe one example implementation. We identify the practical limits of the example's performance, and, in many instances, we provide an uncertainty budget for a typical flow. The reviewed standards span the flow range 2.2×10^{-7} g s^{-1} to 520 kg s^{-1}. The references point to standards that operate at higher and at lower flows. The reviewed standards include volumetric flow standards (piston and bell provers, pressure–volume–temperature–time standards, rate of rise standards), static and dynamic gravimetric flow standards, and velocity $\times$ area standards such as critical flow venturis, laser doppler anemometer surveys, and multipath-ultrasonic meters. Finally, we describe working standard flow meters used in parallel to attain higher flows than economically practical via primary methods.

Keywords: gas flow, primary standard, working standard, uncertainty

(Some figures may appear in colour only in the online journal)

Introduction

This review describes gas flow standards that are used as references to calibrate flow meters. These standards measure the flux of mass per unit time passing through a flow meter that is undergoing calibration to produce a *meter calibration factor* that will be used in future applications of the meter. Flow standards can be classified as (1) primary standards or (2) working standards [1].

Primary gas flow standards are traceable to the international system of units (SI) through length, mass, time, pressure, or temperature and have the lowest available uncertainty. They are not calibrated versus other flow standards. Because of their complexity and expense, primary standards are generally found only in national metrology institutes and a few commercial labs. In sections 1 and 2, we discuss primary standards for gas flows that operate on the 'bucket and stop-watch' principle. In section 3 we discuss three types of flow meter that can be used as primary flow standards by measuring the average velocity over a well-known cross-sectional area: critical nozzles, laser Doppler anemometers (LDA), and ultrasonic time-of-flight meters.

A *working standard* is a flow meter with demonstrated long-term calibration stability (reproducibility) that is used to calibrate other flow meters. Working standards have significant advantages in size, cost, complexity, speed, and ease of operation compared to primary standards. There are many gas flow meter types used as working standards including laminar, critical flow venturi (critical nozzle), Coriolis, ultrasonic, turbine, and positive displacement meters. Working standards are often used in parallel to measure large flows that would be impractical to measure using a primary standard (section 4).

Figure 1 illustrates the 'bucket and stopwatch' method for measuring the flow of a fluid to calibrate a flow meter. The operator measures the time required to fill a bucket of known volume. Dividing the collected volume by the fill time gives the volumetric flow. An analogous approach for measuring gas flow is shown on the right side of figure 1. The gas flows through the meter under test (MUT) into an inverted, graduated cylinder that is initially filled and sealed with water. The

* Author to whom any correspondence should be addressed.

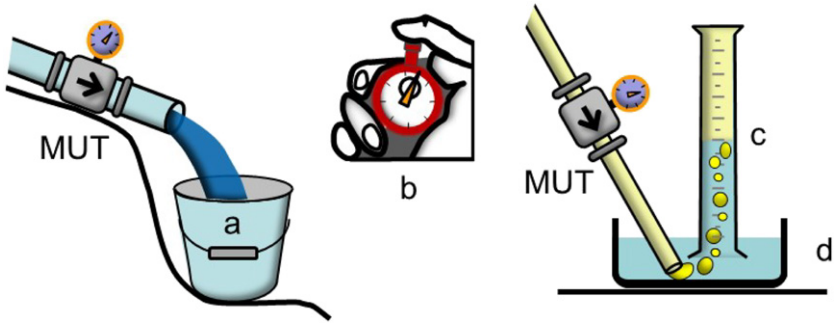

Figure 1. Bucket (a) and stopwatch (b) methods for measuring the volumetric flow of left: liquid and right: gas to calibrate a flow meter under test (MUT). An inverted graduated cylinder (c) and a trough filled with liquid (d) form a measuring volume for the gas flow.

operator measures the time required for the gas–liquid interface to move between two marks on the graduated cylinder. This basic system can measure flows with uncertainties[3] less than 10%.

Low-uncertainty gas flow standards are usually sophisticated versions of the bucket-and-stop-watch approach; they measure the change of mass in a measuring volume (V_M) over a designated time interval. These standards deliver gas flow uncertainties of <0.1% by attending to many details including accurate mass determinations (by measuring either the gas density and volume in the measuring volume or by weighing the vessel) and accurately accounting for buoyancy and density changes in connecting volumes. Low-uncertainty instruments must be used to measure mass, pressure, and temperature. The required low uncertainty is often challenged by pressures and temperatures that are nonuniform and rapidly changing.

Figure 2 shows a generic constant-volume primary standard calibrating a MUT. Flow (and a timer) can be started or stopped by opening or closing the valve located on the measuring tank. Flow from the MUT exhausts into the inventory volume (V_I) depicted by the diagonal shading in the figure, and subsequently accumulates in the measuring tank with volume (V_M). By applying conservation of mass to the control volume, indicated by the dashed lines surrounding $V_I + V_M$, the instantaneous mass flux entering the control volume equals the rate of mass accumulation in the inventory volume and measuring volume. The time-averaged mass flow over a collection period beginning at time t_i and ending at t_f is

$$\dot{m} = \frac{\mathrm{d}m}{\mathrm{d}t} = \frac{\left(m_{M,f} - m_{M,i}\right) + V_I\left(\rho_{I,f} - \rho_{I,i}\right)}{t_f - t_i}, \qquad (1)$$

where the term $\left(m_{M,f} - m_{M,i}\right)$ is the difference between the final (f) and initial (i) masses of the measuring tank (m_M) and the term $V_I\left(\rho_{I,f} - \rho_{I,i}\right)$ is the mass change in the inventory volume V_I calculated from the product of the density change

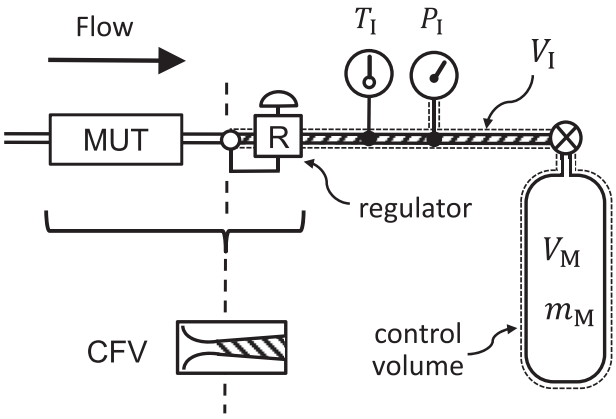

Figure 2. A generic primary gas flow standard. The upstream boundary of the inventory control volume V_I (shaded region) is either a meter under test (MUT) and an upstream pressure regulator or a critical flow venturi (CFV). The downstream boundary is the measuring tank with volume V_M.

$\left(\rho_{I,f} - \rho_{I,i}\right)$ of the gas in V_I and the denominator is the time interval between the initial and final measurements.

The *inventory volume* (shaded by diagonal lines in figure 2) is called the 'connecting volume' by some authors. It includes the volumes of the gauges measuring the inventory pressure (P_I) and the inventory temperature (T_I) and their connections. In equation (1), the second term in the numerator accounts for the possibility that the mass of gas in the inventory volume may not be the same at the start and the stop of the flow measurement. As the measuring volume fills, the pressure increases in the inventory volume cause *storage effects* (sometimes called line-pack effects). Therefore, not all of the gas that passes through the MUT reaches the measuring volume. The density ρ_I of the gas in V_I can be calculated from pressure and temperature measurements and an equation of state for the gas. However, such measurements are difficult when conditions change rapidly in V_I. To reduce the uncertainty contribution from the inventory volume, primary standards are designed so that the mass change in V_I is several orders of magnitude less than the mass accumulated in the measuring volume. This is accomplished by designing the inventory volume approximately 1000 times smaller than

[3] Unless otherwise stated, all uncertainties in this manuscript are two standard uncertainties corresponding to an approximate confidence interval of 95% or, equivalently, with the coverage factor $k = 2$. A standard uncertainty corresponds to a 68% confidence level.

the volume of the measuring tank ($V_I < V_M/1000$), and, when possible, matching the initial and final temperature and pressure in V_I to keep the density change small: $\rho_{I,f} - \rho_{I,i} \ll \rho_{I,f}$.

The test section of a flow standard is the location where the MUT is installed (upstream from the inventory volume in figure 2). The meter factors of flow meters are sensitive to the velocity profile in the test section, i.e., whether the velocity profile is symmetric and fully developed or not. Long straight runs of pipe with constant cross-sectional dimensions are the best flow conditioners but this is difficult to provide for large diameter flow meters. Alternatively, flow conditioners (e.g., perforated plates) can be installed upstream from the test section to approximate the velocity profiles produced by long straight runs. Proper installation and flow conditioning of various MUTs is not the scope of this review, but information can be found in reference [2]. The test section should also have stable pressure and temperature.

Primary standards can be classified as gravimetric or volumetric, depending on the method of determining the change in mass in the measuring volume. The design and operation of the measuring volume is optimized for the selected method. Although figure 2 depicts a fixed measuring volume that collects gas during the flow measurement, some primary standards use a fixed measuring volume that discharges gas, thereby acting as the source of flow (i.e., a blow-down system). Furthermore, other primary standards are based on measuring volumes that change during gas accumulation or discharge (e.g., piston prover, bell prover). A gravimetric primary standard uses a nearly constant volume measuring tank and measures the tank's mass with a balance (a weigh scale). Section 3 gives details regarding further classification by whether methods are dynamic or static, i.e., whether the mass of gas is measured while it is changing or in a steady state.

For volumetric methods, the change in mass is determined by measuring the density changes of the gas in a measuring tank of known internal volume

$$\dot{m} = \frac{\mathrm{d}m}{\mathrm{d}t} = \frac{\left(\rho_{M,f}V_{M,f} - \rho_{M,i}V_{M,i}\right) + V_I\left(\rho_{I,f} - \rho_{I,i}\right)}{t_f - t_i}, \qquad (2)$$

where we replaced the mass of gas in the measuring tank in equation (1) with the product of density and volume $m_M = \rho_M V_M$. Volumetric primary standards have measuring tanks of either constant volume or changing volume (e.g., gas from the MUT pushes a piston or liquid interface through a measured volume). For constant volume measuring tanks, equation (2) applies with the initial and final volumes equal $V_{M,i} = V_{M,f}$. Alternatively, for an expanding (or contracting) measuring tank the initial volume is often zero $V_{M,i} = 0$. (See figure 3.) Ideally, the process is both isobaric and isothermal so that initial and final densities in the measuring tank are equal $\rho_{M,f} \approx \rho_{M,i}$. Section 1 discusses how both types of measuring tanks are applied.

We note that most of the standards described here can be used either upstream or downstream from the MUT. The preferred arrangement is often determined by the pressure requirements for the MUT. Equations (1) and (2) are the basis for calculating mass flow for gravimetric and volumetric primary standards, respectively. Minor adjustments may be necessary for specific applications (e.g., multiple inventory volumes, the blow-down mode of operation, dynamic weighing). For example, equations (1) and (2) remain valid in blow-down mode provided the mass flow is taken to be negative to reflect mass leaving the control volume.

In addition to categorizing primary gas flow standards by either 'gravimetric' or 'volumetric', we categorize them by the means used to establish a calibration's start and stop times. A *flying start/stop* system has a *diverter*. When a diverter is used, the gas flows through the MUT into a path that bypasses the collection tank. When the flow has become steady at the value specified for the calibration, the diverter valves rapidly switch the flow from the bypass into the collection tank. The valves generate precise start and stop signals for a timer while minimizing disruption of the temperature and pressure in the test section upstream of the MUT. In contrast, a *standing start/stop system* (such as shown in figure 2), has neither a diverter nor a bypass. Instead, a blocking valve is opened and the flow rapidly ramps up from zero to the set point. At the end of the collection, the blocking valve is closed and the flow ramps down to zero. Long collection periods are required to compensate for uncertainties resulting from the unsteady ramping processes. For low flows, the measuring tanks can be made sufficiently large to facilitate long collection times; however, this is not practical for large flows. As a result, primary standards that calibrate large flow meters use diverter systems to establish steady-state flow conditions.

The flow output from the MUT is averaged during the same time interval $t_f - t_i$ that flow is collected in the tank and compared to the average flow resulting from equations (1) and (2) to arrive at a meter factor or discharge coefficient for the MUT. Alternatively, the mass change in the numerator of equations (1) and (2) can be divided by the integrated flow output by the MUT during $t_f - t_i$.

The response of MUTs to flow transients is governed by the non-zero response times of their mechanisms and their associated instruments. The transient responses cannot be characterized by calibration with primary standards that provide the time-averaged flow. Therefore, calibrations are performed with steady-state flow conditions at the MUT. Two versions of MUT are shown in figure 2: (1) a critical flow venturi (or CFV or critical nozzle) and (2) a generic MUT with a fast-acting upstream pressure regulator[4]. CFVs are converging–diverging nozzles of specified shapes used with a sufficiently large gas pressure drop that the gas attains sonic velocity near the smallest cross section (the throat) [3, 4]. Under these 'critical' flow conditions, the mass flow can be calculated from the throat area, the

[4] An upstream pressure regulator is sometimes called a back-pressure regulator. In this application it is used to maintain an approximately constant pressure at the outlet of the meter under test. The set point of the regulator during calibration matches the pressure the MUT is exposed to during application to minimize flow measurement errors due to pressure sensitivity of the MUT.

gas properties, the upstream pressure, and the upstream temperature. CFVs are often calibrated versus a primary gas flow standard and then used as working standards to calibrate other flow meters (see section 4). They are best suited to flows larger than 0.022 g s^{-1} (or 1 L min^{-1}). Below that, boundary layer and non-equilibrium effects lead to increasing uncertainty [5] and laminar flow meters are generally preferred as working standards [6]. The critical flow condition at the throat of a CFV prevents the rising pressure in the tank and inventory volume from perturbing the steady-state conditions upstream at the MUT. This makes it a valuable working standard when the primary standard imposes changing pressure conditions in the test section. For other flow meter types, steady-state pressure conditions in the test section should be established by an upstream pressure regulator.

Many of the standards described in this article require filling a tank with pressurized gas; therefore, there are serious safety concerns that are not addressed here. For example, (1) a pressurized gas system must have relief valves or burst disks to avoid explosions in case of accidental over pressurization, (2) filling a tank too rapidly can weaken it and cause failure due to overheating, and (3) a gas tank must only be used for a certain number of fill/empty cycles before it is re-inspected or retired [7].

In this review, we will use the mass flow units g s^{-1} or kg s^{-1} and volume flow units cm^3 min^{-1}, L min^{-1}, or m^3 min^{-1}. For readers interested in volume flow, we will assume that the gas is dry air at 101.325 kPa and 0 °C and leave it to the reader to calculate flows for other gases or conditions that may be of interest. We note that for the small gas flow standards described herein, nitrogen (not dry air) is often used because its properties are so well known. But this will have little influence on the nominal volume flows quoted in this review because the molar masses of nitrogen and dry air differ by only 3.4%.

No calibration is complete without a statement of its uncertainty and the confidence level of the uncertainty. Example uncertainty analyses for particular implementations of each method for a particular flow comprise a large portion of this article. We hope that the analyses and the accompanying explanations of how we estimated components will be a useful reference for others. Excellent references are available on the general topic of uncertainty [8–11], therefore, we will assume that the reader has either a good understanding of the subject or will refer to these references. Brief general information about uncertainty analysis is given in the explanation of table 1.

Most of the uncertainty analyses used as examples herein have been validated by international comparisons organized by the Working Group for Fluid Flow and the Comité International des Poids et Mesures. The results of comparisons are collected in reports that can be found in the Key Comparison Database (https://bipm.org/kcdb/). The most relevant comparison reports are [12–17] in which many of the piston provers, bell provers, *PVTt*, rate of rise, gravimetric, and working flow standards used as examples herein have successfully validated their uncertainty claims.

The uncertainty (and cost) of a gas flow standard depends on the quality of the sensors used and how the system is operated. For these reasons, the reader should not conclude that one method is better than another based on the uncertainty values given here: a different implementation of the method can have a better or worse uncertainty. Also, uncertainty is just one of the deciding factors in selecting a method along with ease of use, cost, size, safety, etc.

1. Volumetric flow standards

Volumetric gas flow standards determine mass flow by calculating the density of gas collected in a known volume over a measured time interval. The density is calculated via a properties database such as REFPROP [18] (or an equation of state) using measurements of the gas's composition, pressure, and temperature. In the following sections we describe the piston prover, bubble meter, bell prover, *PVTt*, and rate of rise standards.

1.1. Piston provers

The piston prover is one of the most commonly used primary flow standards, for both gases and liquids. The measuring volume of a piston prover is a right circular cylinder, with a well-known and uniform inside diameter, containing a sealed piston that is slightly smaller in diameter [19]. The cylinder's dimensions and the speed of the piston determine the fluid flow at the entrance/exit of the cylinder. By the continuity equation, the mass flow, after inventory corrections, is $\dot{m} = \overline{\rho}\overline{u}A$ where $\overline{\rho}$ and $\overline{u}$ are the average density and speed of the fluid or piston over the cross-sectional area A of the cylinder. Piston provers have been used to measure flows spanning 12 orders of magnitude: from 8.6×10^{-11} g s^{-1} [20] to 170 g s^{-1} [21] (4×10^{-6} cm^3 min^{-1} to 8 m^3 min^{-1}).

In one design for gas flow (figures 3 and 4), a circumferential groove around the piston retains a ring of mercury to form a low-friction seal between the piston and the glass cylinder. Mercury is hazardous, so other seal types are more popular now. Initially, gas flows through the MUT and exhausts through a bypass valve. The piston prover of the type shown in figure 3 exhausts to the room and must operate near atmospheric pressure. When the bypass valve is closed, a small excess pressure (≈0.5 kPa) pushes the piston up the glass cylinder. As the piston rises, its leading edge is detected by pairs of collimated light beams and photodetectors near each end of the measuring volume. The photodetectors generate signals that trigger a timer that measures the collection time, $t_f - t_i$. The piston prover mass flow is calculated via:

$$\dot{m}_{PP} = \frac{V_M \rho_{M,f} + V_I\left(\rho_{I,f} - \rho_{I,i}\right)}{(t_f - t_i)}. \tag{3}$$

The first term in the numerator is the mass of gas collected in the measuring volume V_M between the start and stop sensors and the second term accounts for any density change in the inventory volume V_I during the collection interval. Temperatures and pressures determined using sensors located near

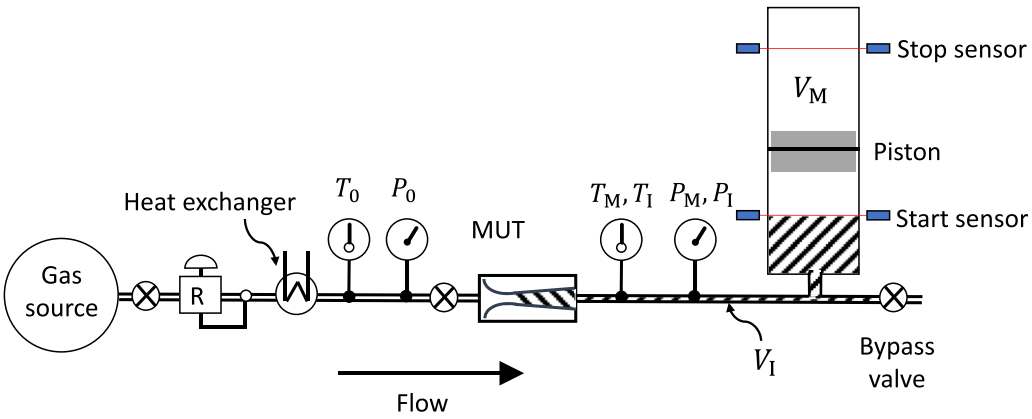

Figure 3. Schematic of a CFV calibration via a piston prover. The sensors labelled P_0 and T_0 are necessary for calculating flow from a CFV. The piston prover pressure and temperature sensors should be located as close to the measuring volume as practical.

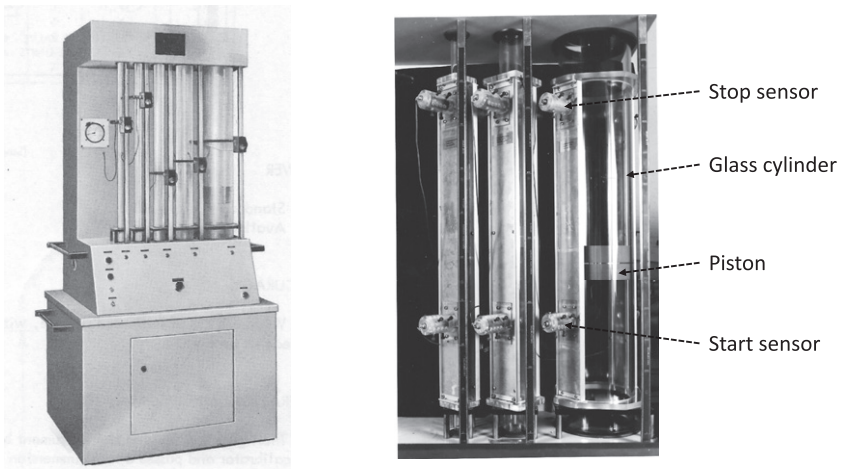

Figure 4. Left: model 1050 mercury sealed piston provers manufactured by George K. Porter Inc./Brooks Instrument Division[5] that were used at National Institute of Standards and Technology (NIST), the national metrology institute of the United States from 1962 to 2003. Reproduced with permission. Photo courtesy of Brooks Instrument, LLC. Right: the inside diameters of the glass cylinders were 1.90 cm, 4.44 cm, and 14.4 cm. The largest cylinder has the piston elevated and the mercury seal is visible. In this implementation, optical sensors produce trigger signals to start and stop a timer. Adapted with permission from [19].

the entrance of the cylinder are combined with an equation of state to calculate the density. Usually, only one pressure and one temperature sensor are used. Note that $\rho_{M,f}$ is the spatial-average density of the gas in the measuring volume at the stop time t_f. However, the spatial average at a particular time is difficult to measure because it is difficult to distribute sensors throughout the volume in which there is a moving piston. Instead, most systems average a number of readings immediately preceding t_f from sensors near the entrance to the cylinder.

Undetected leaks past the seal of a piston prover are a source of error. To leak-check a piston prover, use flow to raise the piston in the cylinder and shut an isolation valve immediately upstream from the MUT. Measure the change in piston position (perhaps by hand, with a ruler) over a period of many minutes. Note that the piston can rise if the trapped gas expands due to barometric pressure drop or temperature rise. Therefore, it is also necessary to measure the initial and final density of the gas in the cylinder and inventory volumes. Then, equation (3) gives the leak flow if V_M is replaced by the volume displaced by the piston's motion during the leak-test interval.

The measuring volume V_M is determined by measuring the inside diameter of the cylinder at many locations along the cylinder's length and by measuring the height between the start and stop switches. The start sensor position should be located sufficiently far away from the bottom rest position that the piston reaches a steady state velocity.

The significance of the inventory volume term scales with V_I/V_M, but is usually small (and often assumed negligible) because pressure and temperature conditions are stable and $\rho_{I,f} \cong \rho_{I,i}$. The pressure in the inventory volume and at the outlet of the MUT changes depending upon whether the piston is at the bottom rest position or 'floating'. This does not have significant impact on the calibration of a CFV, but it can disrupt steady-state flow conditions for most other meter types (e.g., a laminar flow meter). In some piston provers, the bypass valve can be adjusted to float the piston above the bottom rest to

avoid the pressure changes. But some automated systems use actuated valves that do not float the piston causing transient conditions in the test section (figure 5).

The bubble meter is a lower cost but higher uncertainty analog to the mercury sealed piston prover, with the piston replaced by a soap film [23, 24]. To operate a bubble meter, a squeeze bulb is used to raise the level of a soap solution and generate a soap bubble at the bottom of the collection cylinder (figure 6). Then, the metered gas flow pushes the soap film up the cylinder. The time to travel from a start to a stop position is generally measured by eye using a stopwatch, but some automatically timed versions have been developed. The measuring volume is affected by the thicknesses of the soap film on the cylinder wall. Also, if a dry gas flow is being measured, the gas stream will entrain vapor as it passes over the soap solution at the bottom of the collection cylinder and over the solution coating the cylinder's walls. This water vapor is gas that has not passed through the MUT, but it does enter the measuring volume. For an aqueous soap solution and a dry air flow at 24 °C, entrained water vapor can comprise as much as 3% of the collected gas. A correction assuming that the gas attains 50% relative humidity can be made, thereby reducing the uncertainty due to the sealant's vapor pressure to half of the 3% value.

Many variations on the piston prover technique exist. Some piston provers utilize a continuous piston position measuring sensor (such as a laser interferometer, an ultrasonic sensor, or a linear encoder) so that the velocity of the piston is measured [25, 26]. There are versions of the piston prover which do not use a mercury seal, but instead have a 'clearance seal': a gap of about 10 μm between a piston made of graphite composite and the borosilicate glass collection cylinder. These piston provers either apply a correction for the Hagen–Poiseuille flow of gas leaking past the piston or treat the leak as a source of uncertainty [27–31].

Cignolo *et al* [32, 33] use a motor to push an O-ring sealed piston into a cylinder, taking advantage of the fact that an external diameter can be measured more accurately than an internal one. Figure 7 shows the largest of these designs at the Instituto di Metrologia G. Colonnetti (IMGC) in Italy. This design has been scaled down to measure flows of 2.2×10^{-5} g s^{-1} (1 cm^3 min^{-1}) [34]. Piston provers with O-ring seals are also used to measure high-pressure gas flows [21, 35, 36].

To support standards for vacuum pressure calibrations, piston provers with O-rings, sliding seals, or bellows seals have been used to measure flows as small as 8.6×10^{-11} g s^{-1} (4×10^{-6} cm^3 min^{-1}) [20, 37–39]. Piston provers with seals of these types can accommodate a wider range of pressure differences across the seal. The *dynamic expansion* method uses flow to generate a vacuum reference pressure. Flow from the piston prover passes through an orifice of known diameter to a downstream volume evacuated by a vacuum pump. For molecular flow conditions (pressures <1 Pa), the measured flow is combined with gas kinetic theory and the orifice's diameter to calculate the pressure in the volume upstream from the orifice.

An example of this type of piston prover is shown in figure 8 [40]. It uses an O-ring-sealed piston to generate flows between 2.2×10^{-7} g s^{-1} (0.01 cm^3 min^{-1}) and 2.2×10^{-3} g s^{-1} (100 cm^3 min^{-1}). It can be used as a flow source or sink. A feedback loop controls the motor's speed to maintain stable

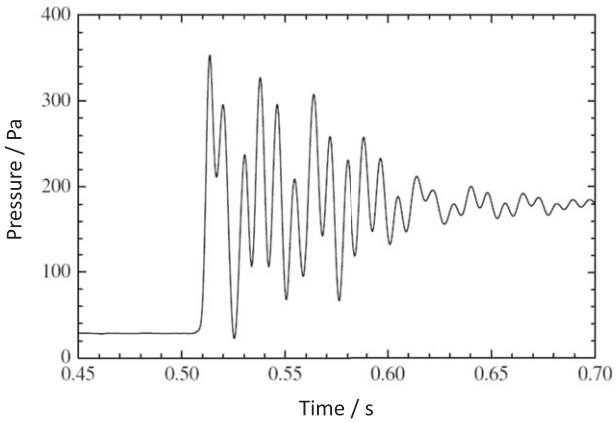

Figure 5. Damped pressure fluctuations caused by closing the bypass valve on a clearance-sealed piston prover. The start sensor should be located high enough on the cylinder that these fluctuations decay. Reproduced from [22]. 2011 BIPM & IOP Publishing Ltd. All rights reserved.

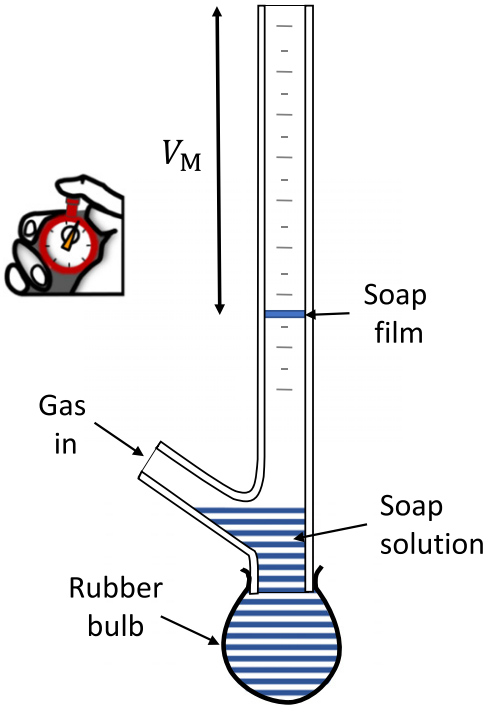

Figure 6. A bubble meter uses a reservoir of soap solution to create a soap film that is pushed up a graduated glass cylinder by the flow [24].

[5] Certain commercial equipment, instruments, or materials are identified in this paper to foster understanding. Such identification does not imply recommendation or endorsement by NIST, nor does it imply that the materials or equipment identified are necessarily the best available for the purpose.

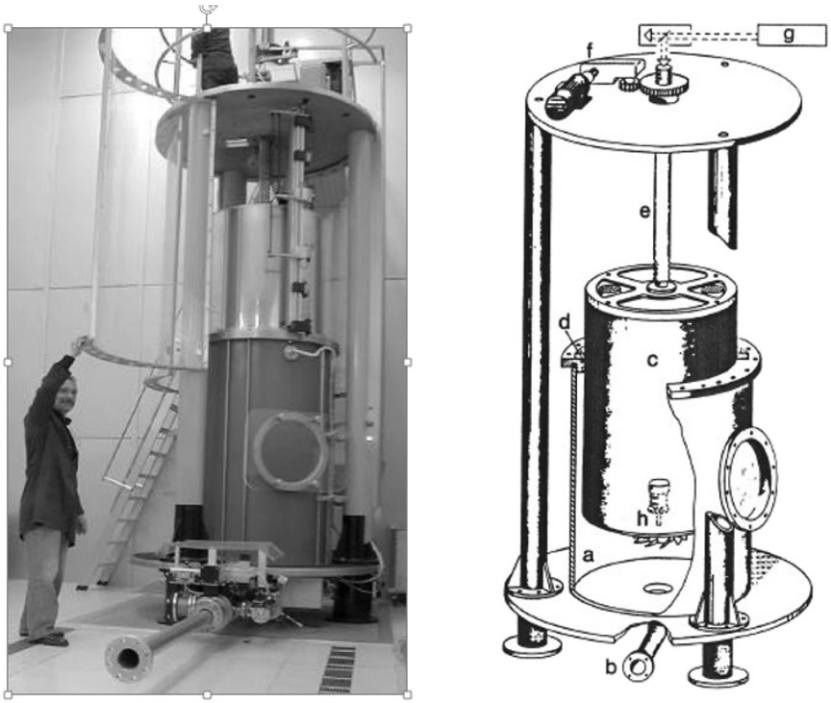

Figure 7. O-ring sealed 1.2 m^3 piston prover at IMGC Italy. Gas from volume (a) is expelled through outlet (b) by descending piston (c) that is sealed at (d). The piston is driven by ball screw (e) and motor (f). The piston's position is measured with laser interferometer (g). Fan (h) mixes air for temperature uniformity but adds heat to the system. Reproduced with permission from [33].

pressure (and flow) conditions and the piston's position is measured using a linear encoder. A 'guard' pressure on the outside of the seal maintains a low differential pressure across the O-ring seal to reduce leakage past the sliding seal. At low flows, outgassing of seal materials is a concern and must be quantified.

Uncertainty analysis: the format in table 1 will be used throughout this paper to report the results of uncertainty analyses. The first column gives the name of the input variable x_i (or uncertainty component). The second column refers to notes below the table that give brief explanations of the origin of each component. The third and fourth columns list the value for the input variable x_i and its standard uncertainty expressed as a percentage of x_i, i.e., $100 \times u(x_i)/x_i$,. However, the last two uncertainty components [leaks and type A $(s/\sqrt{n})$] are expressed as a percentage of the flow. A standard uncertainty corresponds to a 68% confidence level. The normalized sensitivity coefficient $S_i = \left(x_i/\dot{m}\right)\left(\partial\dot{m}/\partial x_i\right)$ of the measurand to the input variable [8] is listed in column five. The last column gives the relative significance of each component to the total uncertainty calculated via a ratio of variances: $\mathrm{Contrib}_i(\%) = 100 \times S_i^2\left(\frac{u(x_i)}{x_i}\right)^2 / \sum_{i=1}^{N} S_i^2\left(\frac{u(x_i)}{x_i}\right)^2$.

The repeatability of flow measurements made with a flow standard must be included in its uncertainty analysis [41, 42]. The repeatability is evaluated by making multiple measurements of the meter factor of a MUT. It is customary for laboratories to use their *best existing device* (BED), i.e., the flow meter with the smallest repeatability that is available to the laboratory [43] to calculate the sample standard deviation of the mean (or standard error) $s/\sqrt{n}$. Here s is the standard deviation of the meter factor (expressed as % of the average meter factor) and n is the number of repeated measurements, generally in the range $5 \leqslant n \leqslant 10$ at each flow set point.

The guide to the expression of uncertainty in measurement or GUM [10] categorizes uncertainty components as types A or B depending upon whether or not they are statistically determined. The only type A component in table 1 is the repeatability of the flow measurement when calibrating the BED.

The uncertainty components are combined and multiplied by a coverage factor $k = 2$ to obtain the expanded uncertainty (corresponding to approximately 95% confidence level) for the mass flow listed at the bottom of the table. In most cases, uncertainty components are uncorrelated and are combined by taking the root-sum-of squares (RSS) of the weighted components. However, there are important exceptions to this in flow measurement, e.g., reference flow meters used in parallel (section 4). There are other cases where correlated uncertainties would reduce the uncertainty of the flow standard, such as when the same pressure sensor is used to measure a pressure change or the same balance is used to measure a mass change. In our examples, the more conservative approach is applied (assuming the uncertainties are uncorrelated and using the RSS of components). We use the RSS because the portions of the uncertainty components that are correlated (e.g., the reference used to calibrate the sensor) are small compared to the uncorrelated components (e.g., calibration drift, repeatability).

There are many published uncertainty analyses for piston provers and a typical value for the expanded uncertainty is 0.2% [19, 44]. However, piston provers for flows as small

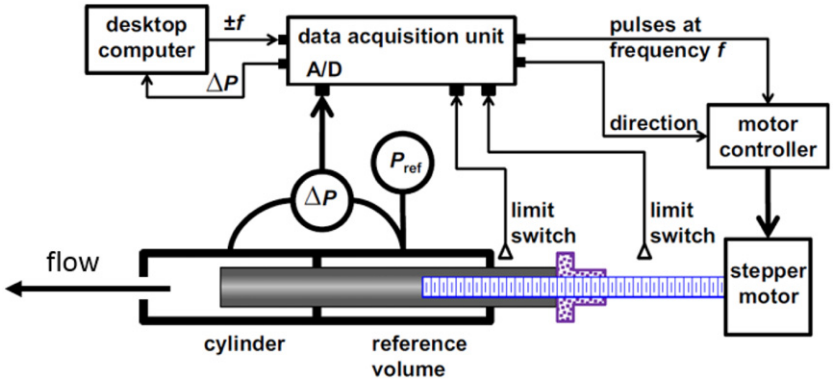

Figure 8. A piston prover with O-ring seals for flows as low as 2.2×10^{-7} g s^{-1} (0.01 cm^3 min^{-1}). Reprinted from [40], Copyright 2014, with permission from Elsevier.

Table 1. Uncertainty of the 4.44 cm diameter piston prover shown in figure 4 for 2.2×10^{-2} g s^{-1} (1 L min^{-1}).

Input variable (x_i)	Notes	x_i value	$u(x_i)/x_i$/%	S_i	Contrib./%
Cylinder volume, V_M	a	0.71 L	0.016	1	6
Gas density, $\rho_{M,f}$	b	1.14 g L^{-1}	0.053	1	68
Collection time, $(t_f - t_i)$	c	38 s	0.009	−1	2
Inventory mass change, $V_I(\rho_{I,f} - \rho_{I,i})$	d	2.8×10^{-5} g	0.007	0.5	0
Leaks	e	2.2×10^{-6} g s^{-1}	0.010	1	2
Type A ($s/\sqrt{n}$)	f	6.5×10^{-6} g s^{-1}	0.030	1	22
Expanded uncertainty (95%)	$\boldsymbol{U(\dot{m})/\dot{m}} = 0.13\%$				

[a]Based on 25 evenly spaced internal diameter measurements, start to stop sensor length, piston rocking, thermal expansion caused by environmental temperature changes.
[b]Includes pressure, temperature calibration, temperature errors due to spatial non-uniformity, equation of state, gas composition.
[c]Timer calibration, timer actuation.
[d]Inventory volume and density uncertainty.
[e]Measured via a floating piston as described in text.
[f]Based on calibration data from a laminar flow meter.

as 8.6×10^{-11} g s^{-1} (4×10^{-6} cm^3 min^{-1}) must contend with leaks and outgassing components that are insignificant for large gas flows and have uncertainty of 1% or more [20]. Here, we examine the uncertainty of the 4.44 cm, mercury-sealed piston prover shown in figure 4 that was used at NIST from 1962 to 2003 [19].

Mass flow measurements made with a piston prover are subject to uncertainties in the determination of the measuring volume, gas density, collection time, inventory mass change, leaks or outgassing, and the type A uncertainty of the BED.

The average temperature of the gas in the full measuring volume is often the largest source of uncertainty in a piston prover standard. The measured temperature is that of the gas flowing across a temperature sensor in the pipe leading to the cylinder, but the desired temperature is the spatial average of the gas in the full cylinder. For many prover calibrations, gas cools as it expands through regulators and through the MUT. These expansions lead to temperature gradients and differences between the temperature of the gas and the prover's walls. Hence the gas temperature is spatially non-uniform and changes over time. Kutin *et al* [45] found that the uncertainty caused by these effects is approximately linearly related to the temperature difference between the gas and the wall and the sensitivity coefficient depends on the flow. Some standards utilize heat exchangers to keep the gas temperature close to room temperature and reduce these uncertainty components. It is also important to maintain well controlled environmental conditions in the laboratory housing the flow standard to avoid temperature gradients in the volume of collected gas.

The piston can tip or rock slightly within the cylinder because it has a smaller diameter. This effect generates a volume uncertainty. In small piston provers, the piston can move in a 'stick-slip' manner, i.e., stop moving momentarily then move rapidly due to pressure build up. The stick-slip motion is due to electrostatic forces or irregularities of the cylinder's inside diameter; it increases the timing uncertainty and type A uncertainty.

1.2. Bell provers

Bell provers have been used as gas flow standards for more than 150 years. Their principle of operation is similar to that of a piston prover. Both use a sealed, moving boundary to collect a known volume of gas. The measuring volume of a bell prover (figure 9) consists of (1) a cylindrical tank containing sealing

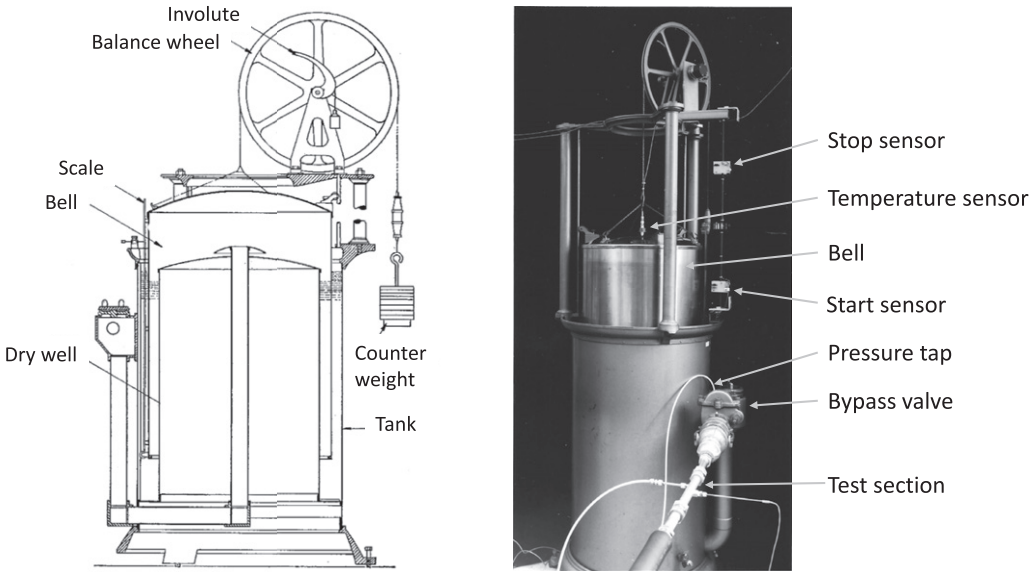

Figure 9. Left: schematic of a bell prover. Reproduced with permission from [46] and right: one of three bell provers used as national standards at NIST until 2003. Reproduced with permission from [19]. The measuring volume between the start and stop sensors was 114 L.

liquid and (2) a bell-shaped gas measuring tank that is open at the bottom. The most common sizes range between 50 L and 500 L and some as large as 50 m^3 have been built. Typical bell prover expanded uncertainty is 0.17% [44] but particular implementations have reported uncertainty as low as 0.06% [25].

The bell's weight is nearly balanced by counterweights so that it can be raised by a small differential pressure (≈1 kPa). When a bypass valve is closed, gas flows to the underside of the bell and the bell rises past start and stop time sensors to collect a known volume of gas during a measured time interval. A smaller counterweight is mounted on an involute-shaped cam to provide compensation for buoyancy effects as the bell's immersion in the sealing liquid changes. Rollers and guide rods stabilize the bell's lateral position as it moves upwards. Temperature is usually measured with a single sensor installed at the top of the bell. Pressure is measured at a tap in the bell's inlet piping.

The measuring volume has an internal 'dry well' to produce an annular space that reduces the necessary volume of sealing liquid. The sealing liquid should have a low vapor pressure so that its vapor is not a significant portion of the gas collected in the bell and so that it does not have to be replenished frequently due to evaporation. The sealing liquid should also have a low kinematic viscosity so that the films of liquid on the bell's wall drain rapidly and do not contribute a large uncertainty to the measuring volume of the bell.

The equation of flow is the same as for the piston prover (equation (3)) and like the piston prover, the flow can also be based on the velocity of the bell rather than the time to traverse start and stop positions. The bell prover's measuring volume V_M is calculated from measurements of the internal diameter and the length between start and stop switches, with corrections. The external diameter of the bell is measured by 'strapping', i.e., measuring its circumference at many vertical positions. In the strapping approach, the internal diameter is calculated by subtracting twice the bell's wall thickness from the external diameter. Alternatively, gas can be transferred in batches between a reference volume (e.g., a Stillman standard) and the bell in a process called 'bottling', but this approach introduces uncertainties due to gas temperature measurements [47].

The measurement of the volume of a bell prover is complicated by the liquid sealant. The slightly elevated internal pressure of the bell causes the oil level to be lower inside the bell than outside. Also, as the bell rises out of the oil during a collection, the metal walls of the bell displace less of the oil, and consequently the oil level falls. Finally, oil adheres to the inner and outer surfaces of the bell as the bell rises, changing the measuring volume [48]. The oil drains from the walls and the volume remaining on the walls is proportional to the square root of the ratio of kinematic viscosity of the sealant to the drain time [49], so the volume occupied by the oil layer depends on the collection time. Using low kinematic viscosity oil reduces this oil adherence effect. The bell prover in figure 9 used oil with kinematic viscosity of 0.047 $cm^2\ s^{-1}$ and it had uncertainty due to oil adherence of 0.01%.

Closing the bypass valve causes pressure changes within the bell and leads to an oscillatory motion between the inner and outer bell oil surfaces. (See figure 10.) The start time sensor should be positioned high enough that these oscillations fully decay before the timed collection begins [50–52]. In addition, the bell should be well counterbalanced and travel smoothly so that pressure fluctuations within the bell during a collection are negligible. Significant pressure fluctuations lead to changes in the level of the sealing liquid leading to uncertainties in the bell measuring volume and unsteady conditions in the test section.

So far, we have described the bell prover as ascending while it collects gas from the MUT, but a bell prover can also be operated as a flow source while it descends [53]. In

Table 2. Uncertainty of the 114 L bell prover shown in figure 9 for 2.2 g s^{-1} (100 L min^{-1}).

Input variable (x_i)	Notes	x_i value	$u(x_i)/x_i$/%	S_i	Contrib./%
Tank volume, V_M	a	114 L	0.059	1	48
Gas density, $\rho_{M,f}$	b	1.14 g L^{-1}	0.045	1	28
Collection time, $(t_f - t_i)$	c	68.3 s	0.009	−1	1
Inventory mass change, $V_I(\rho_{I,f} - \rho_{I,i})$	d	1.3×10^{-3} g	0.011	0.09	0
Leaks	e	2.2×10^{-4} g s^{-1}	0.010	1	1
Type A ($s/\sqrt{n}$)	f	8.6×10^{-4} g s^{-1}	0.040	1	22
Expanded uncertainty (95%)	$\boldsymbol{U(\dot{m})/\dot{m}} = 0.17\%$				

[a]Based on outside diameter (strapping) and wall thickness measurements, start to stop sensor displacement, tilting (rocking) of the bell, sealing liquid film drainage and thickness, thermal expansion caused by environmental temperature changes.
[b]Includes spatial non-uniformity of temperature, pressure and temperature calibration, equation of state, gas composition.
[c]Timer calibration and actuation.
[d]Inventory volume and density uncertainty.
[e]Based on leak tests performed by raising the bell under zero flow conditions.
[f]Based on calibration data from a critical flow venturi.

the descending mode, the bell is held in a raised position and gas initially flows from the room, through the open bypass valve, through the MUT, and to a vacuum pump or to the inlet of a blower. When conditions in the flow meter are stable, the bypass valve is closed, the bell is released, and gas is pulled through the MUT from the bell, causing the bell to fall. Once the bell passes the lower, stop position, the bypass valve is reopened. The descending mode has the advantage of lower uncertainty for the average temperature of the gas in the bell. A descending mode bell prover at the Physikalisch-Technische Bundesanstalt (PTB) in Germany has uncertainty as low as 0.06% [25]. A disadvantage is that the descending mode allows the MUT to be calibrated only near atmospheric pressure. In the ascending mode, gas is provided from a pressure source and the MUT can be calibrated over as wide a range of pressures as is available from a compressor or a gas cylinder.

Uncertainty analysis: (table 2) the bell prover and piston prover uncertainty categories are similar, with additional components related to the measuring volume, such as sealing liquid level changes and liquid film adherence to the bell's walls. Temperature sampling uncertainty due to spatial non-uniformity is another significant component. The temperature is usually measured with a single sensor at the top of the bell. Like the piston prover, the temperature sampling uncertainty depends on the magnitudes of the flow and temperature differences between the incoming gas, the bell prover's materials, and the environment.

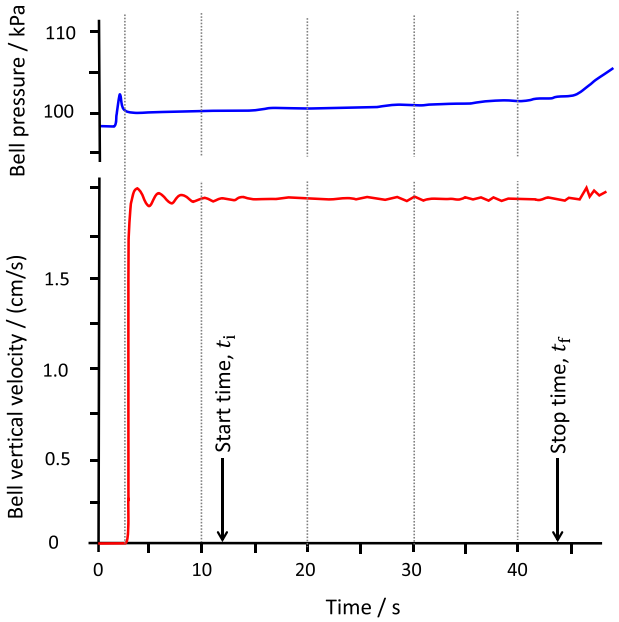

Figure 10. Time dependence of pressure and velocity for a 48 L bell prover during a collection at a flow of 1.94 g s^{-1} (90 L min^{-1}). Note the initial damped oscillation of the bell's velocity due to the change in pressure when the bypass valve is closed and the resulting oil level fluctuations. The increase in the pressure inside the bell during the collection is caused by imperfect counterbalancing of the bell's weight because of buoyancy changes as the bell rises out of the sealing liquid.

1.3. The floppy bottle

Bignell and Choi [54] developed a 'floppy' volumetric standard that uses a flexible diaphragm that moves back and forth within a pair of concentric metal spheres (figure 11). The inner sphere is perforated. The travel time of the diaphragm is measured as it alternates between opposite sides of the constraining spherical volume. A differential pressure sensor indicates when the diaphragm is full and starting to push against the perforated walls and switches actuated valves to direct the flow to one side of the diaphragm or the other. The spherical volume is ≈25 L and the 95% confidence level flow uncertainty is 0.15%. Because this method is rarely used, we have not included an uncertainty table and readers should refer to [54] for more details.

1.4. Pressure, volume, temperature, and time standard (PVTt)

The *PVTt* method uses a flying start/stop and measures the mass change in the measuring volume from the gas density and the known V_M [55]. Temperature and pressure measurements of the gas in V_M under steady state conditions are measured

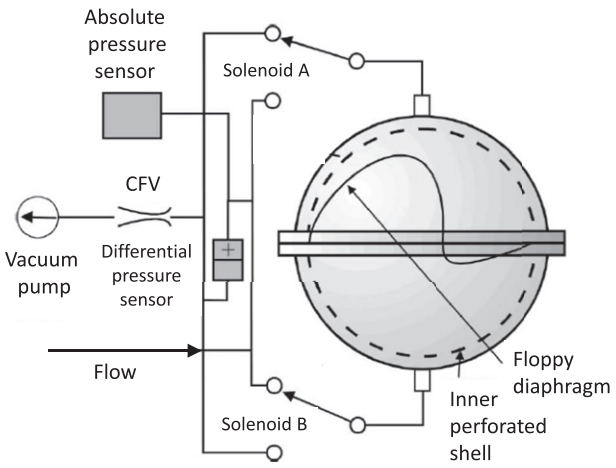

Figure 11. A floppy bottle flow standard. Reprinted from [54], Copyright 2001, with permission from Elsevier.

before and after filling. The mass flow is calculated from the product of the gas density change and V_M, divided by the collection time:

$$\dot{m}_{PVTt} = \frac{V_M(\rho_{M,f} - \rho_{M,i}) + V_I(\rho_{I,f} - \rho_{I,i})}{(t_f - t_i)}, \qquad (4)$$

where $\rho_{M,f}$, $\rho_{M,i}$, $\rho_{I,f}$, $\rho_{I,i}$ are the final and initial gas densities in the tank and inventory volumes calculated from the pressure and temperature measurements and the gas composition using a properties database or the real gas equation of state.

The *PVTt* system shown in figure 12 is composed of:

- A source of gas with a shut-off valve.
- A downstream pressure regulator and heat exchanger to maintain steady conditions at the test section.
- The MUT (in this case a critical nozzle) and the pressure and temperature sensors necessary to measure T_0 and P_0 to calculate the nozzle flow.
- A diverter unit, i.e., valves that allow the gas to be switched from a bypass path to the measuring tank. The diverter also produces trigger signals to start and stop a timer. The bypass may exhaust to a vacuum pump, to atmospheric pressure, or to a back-pressure regulator.
- An inventory volume V_I with instrumentation to measure gas density changes therein (shaded with diagonal lines in figure 12).
- A measuring volume V_M with pressure and temperature sensors to allow calculation of the density of the gas in V_M.
- A valve connecting V_M to a vacuum pump so that V_M can be emptied between collection cycles.

The procedure for making a mass flow measurement is:

- Install the MUT in the test section and ensure there are no significant leaks in the system. In figure 12, the MUT is a critical flow venturi.
- Set the flow through the MUT by choosing a set point pressure with the regulator. Flow is initially directed to the bypass path.
- Evacuate V_M with the vacuum pump, wait for any remaining gas in V_M to reach steady state conditions, and measure its initial pressure and temperature ($P_{M,i}$ and $T_{M,i}$).
- Once there are steady state conditions at the nozzle, measure the initial pressure and temperature in the inventory volume ($P_{I,i}$ and $T_{I,i}$), divert flow from bypass to the tank and start a timer (triggered by the diverter unit).
- Measure the pressure and temperature in the nozzle approach pipe during the time that V_M is filling.
- Fill the tank to a high enough pressure that it can be measured with sufficient uncertainty, but not so high as to lose critical conditions at the nozzle.
- Divert flow to the bypass path and measure the final pressure and temperature in the inventory volume ($P_{I,f}$ and $T_{I,f}$). The timer is stopped by a trigger signal from the diverter unit to measure the collection time ($t_f - t_i$).
- Stop the flow or move to the next flow set point.
- Wait for V_M to reach steady state conditions and measure the final pressure and temperature of its contents ($P_{M,f}$ and $T_{M,f}$).

PVTt standards are used at the National Metrology Institute of Japan/Advanced Industrial Science and Technology (NMIJ/AIST) in Japan (figure 13) [56, 57], the National Institute of Metrology in China [58, 59], National Institute of Metrology Australia [60], the national metrology institute in Taiwan [61], and at NIST in the United States (figure 14) [55, 62, 63]. The NMIJ standard pulls air from the environment through a nozzle under test into the evacuated measuring tank. The NIST standard uses dried air from a compressor or from pressurized gas cylinders, allowing a nozzle to be calibrated over a wider range of inlet pressures.

Tank sizes: the NIST flow standard shown in figure 14 has two measuring volumes: 34 L and 677 L to accommodate a wide range of flows and, in a range of overlap, to allow comparisons between flow measurements using the different volumes. The 34 L measuring volume is a single 15 cm diameter tank and the 677 L volume is a manifold of eight tanks, each 20 cm in diameter. As shown in figure 17, the range and uncertainty of flow covered by this *PVTt* system is dependent on the desired uncertainty, the resolution of the time and pressure measuring devices, and the final tank pressure.

NIST's *PVTt* standards are filled over periods ranging from 20 s to many hours. The maximum flow for the 34 L measuring volume is nominally 2.2 g s^{-1} (100 L min^{-1}); the maximum for the 677 L measuring volume is 43 g s^{-1} (2000 L min^{-1}). The minimum flow capability of a *PVTt* system is determined by how long the operator is willing to wait for the pressure in the tank to rise to a value that can be measured with acceptable uncertainty: if the pressure change between the initial and final conditions is too small, the transducer resolution will be a large uncertainty contributor. By waiting longer, the pressure rises to higher values, solving the resolution issue. As always, leaks can be a problem, especially for small flows. In summary, the size of the measuring tank is determined from the relationship between the desired uncertainty, the flow to be calibrated,

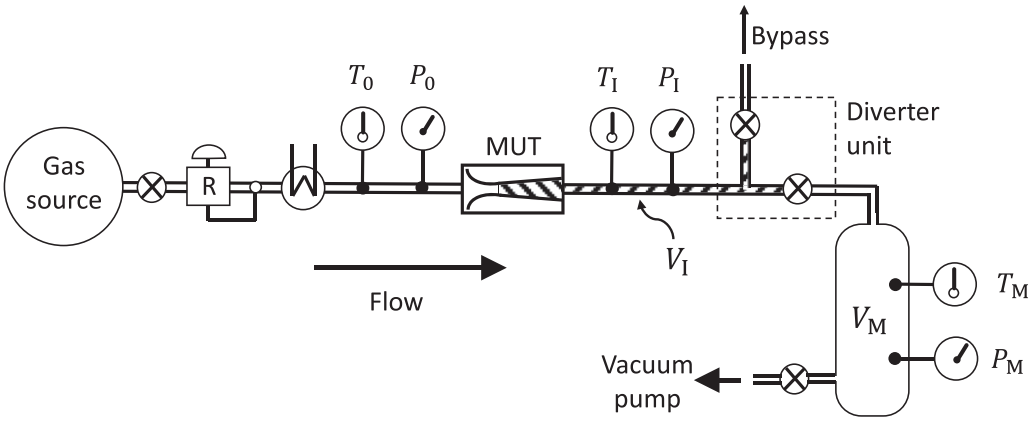

Figure 12. A schematic diagram of a *PVTt* gas flow standard.

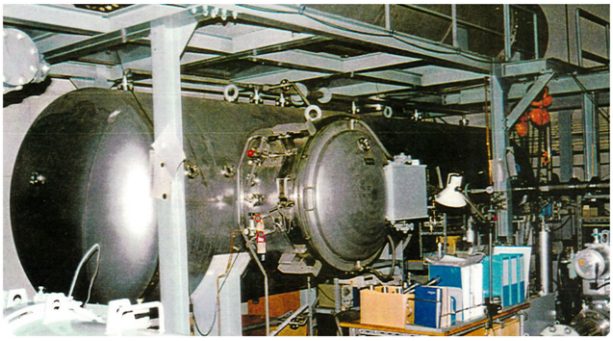

Figure 13. The 13 m^3 *PVTt* system of NMIJ/AIST is surrounded by a recirculating, temperature-controlled water jacket.

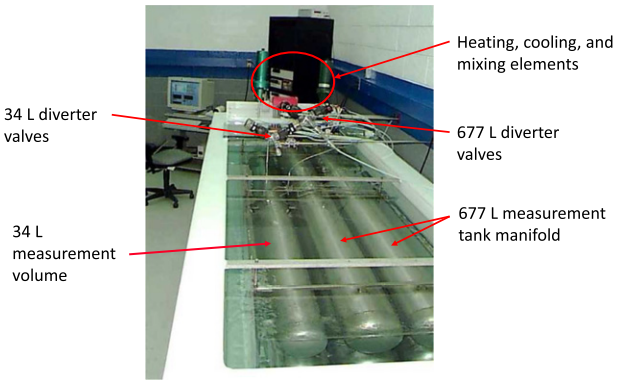

Figure 14. A photograph of the NIST 34 L and 677 L *PVTt* measuring tanks submerged in a temperature-controlled water bath. Adapted with permission from [70].

the minimum size of a detectable leak, and the collection time.

Temperature measurement: measuring a low uncertainty spatial average temperature of the gas in the full *PVTt* tank is challenging. Flow work [64] heats the gas as the tank fills and the gas stratifies: warm, lower-density gas rises to the top of the tank and colder gas moves to the bottom [65]. After the collection is complete, the gas cools due to heat transfer from the environment through the tank's walls, setting up convection currents in the gas, but this process is slow, and it may take many hours for the gas in large tanks to reach thermal equilibrium with the surroundings. For large tanks, stratification of the room's temperature may prevent the temperature of the gas in V_M from ever becoming spatially uniform [65]. Both the NMIJ system shown in figure 13 and the NIST system shown in figure 14 have recirculating, temperature-controlled water surrounding V_M that eliminates the effects of the environmental temperature stratification [56].

To improve the average temperature measurement, some *PVTt* system designers average the measurements from many temperature sensors and locate sensors strategically, placing more sensors where larger temperature gradients are expected (near the tank's walls) [65]. A fan can be installed inside a tank to mix the collected gas and hasten steady state, but the fan adds heat to the system.

The NIST *PVTt* standard shown in figure 14 reduces temperature uncertainty caused by flow work and stratification by dividing the measuring volume into 2.5 m long tanks of small diameter ($\leqslant$20 cm) and submerging them in a recirculating water bath with its temperature controlled to match the nominal room temperature (296.5 K) [55]. An acrylic duct surrounds the tanks and a propeller recirculates the water to ensure that there are no stagnant zones in the water. The water bath is temporally and spatially uniform to 0.002 K. The use of multiple, small-diameter tanks ensures a large surface-to-volume ratio that facilitates heat transfer between the gas and the surrounding water. Within 20 min, the gas's temperature equilibrates with the water's temperature. The equilibration is confirmed by the asymptotic decline of the pressure of the gas in the tank (figure 15). The final gas temperature is obtained by measuring the water temperature.

For small flows, a water bath is not necessary: the measuring tank is an adequate heat sink for the gas it collects and a measurement of the temperature of the tank's wall determines the gas's temperature with a low uncertainty. Figure 16 shows Nakao's design at the NMIJ/AIST [66] in which two tanks (400 cm^3 and 100 cm^3) spanning different flow ranges are machined into a large piece of metal. Each tank is filled with copper wool to promote rapid thermal equilibration between

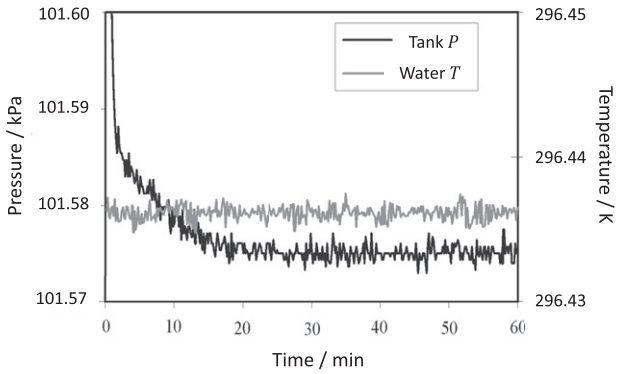

Figure 15. The equilibration of the pressure and temperature in the measuring tank immediately following a filling of the NIST 34 L *PVTt* standard at 0.54 g s^{-1} (25 L min^{-1}). Adapted with permission from [70].

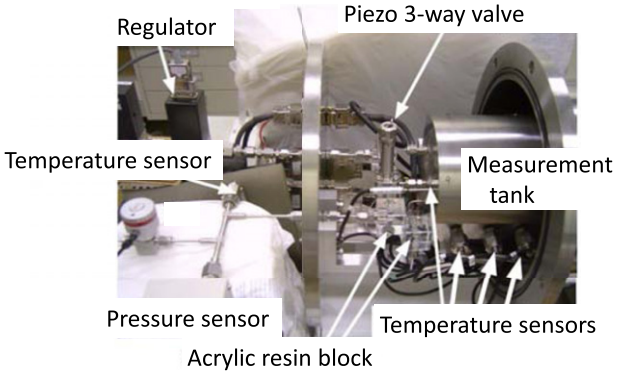

Figure 16. A *PVTt* system for low gas flow at NMIJ/AIST with the vacuum chamber open to show the metal tank that contains two measuring volumes.

the tank and the gas within it. The tanks are housed in a vacuum chamber to isolate them from room temperature variations. The test section and pressure gauge are connected to the measuring tanks via an acrylic block to reduce heat conduction from the surroundings. The diverter valve in this system is a combination of two piezo-electric valves that do not generate heat. Temperature sensors embedded in the metal block are used to obtain the gas's temperature.

Thermostating large (i.e., several cubic meter) tanks for large *PVTt* systems is impractical, so researchers are pursuing acoustic resonance techniques to measure low uncertainty spatially-averaged temperatures despite stratification of the gas [67]. Acoustic thermometry applies the relationship between the resonant frequency of a gas-filled volume and the speed of sound to calculate the temperature of the gas. Preliminary results show that a cylindrical tank with a horizontal axis has longitudinal acoustic modes that produce accurate average temperatures despite stratification.

Inventory volume: the inventory volume V_I of a *PVTt* standard contains some gas that passed through the critical nozzle but did not flow into the measuring tank. For example, if the pressure in V_I was 100 kPa at the start of a collection and if the measuring tank were filled to 200 kPa, there would be twice the mass of gas in V_I at the end of the collection as there was at the beginning. Quantifying the change of mass of gas in the V_I and estimating its uncertainty is a challenge. The second term in the numerator of equation (4), $V_I(\rho_{I,f} - \rho_{I,i})$ accounts for this storage effect, but it is difficult to measure ρ_I accurately. Keeping V_I as small as practical reduces the inventory correction and its uncertainty contributions. But if V_I is too small, the short interval when both the bypass and measuring tank are closed by the diverter unit (the 'dead-end time') can lead to high pressure in V_I and the loss of stable pressure and flow conditions at the MUT.

There are various ways to handle the inventory volume correction [68, 69], including making the dead-end time as short as a few milliseconds and making measurements of $P_{I,i}$, $T_{I,i}$, $P_{I,f}$, and $T_{I,f}$ as accurately as possible. Unfortunately, the accuracy of measurements of $P_{I,i}$, $T_{I,i}$, $P_{I,f}$, and $T_{I,f}$ at the instants that the gas collection begins and ends are limited because the sensors' response times limit their ability to track rapidly changing conditions in the inventory volume. The *PVTt* system at NIST uses a mass cancellation technique: the start and stop times of the collection are selected from data recorded at 3000 Hz during the dead-end intervals so that $P_{I,f} = P_{I,i}$ which leads to $T_{I,f} = T_{I,i}$, $\rho_{I,f} \approx \rho_{I,i}$, and $V_I(\rho_{I,f} - \rho_{I,i}) \approx 0$ [55]. This approach does not rely on the pressure sensor to provide instantaneous time response, rather it assumes: (1) the diverter unit produces similar start and stop transients in the inventory volume, and (2) the pressure sensor has good short-term reproducibility. A disadvantage of this approach is the requirement that the initial and final inventory pressures (and hence tank pressure) match. The match condition limits the mass of gas that can be collected in V_M because the tank cannot be filled to a higher pressure than the initial pressure in the inventory volume.

Determining the measuring tank's volume: the internal volume of the *PVTt* measuring tank V_M must be known with low uncertainty at the final pressure and temperature (or as a function of pressure and temperature). It can be measured by: (1) a gas gravimetric method, (2) a liquid gravimetric method, or (3) a gas expansion method.

In the *gas gravimetric method*, a leak-free gas weighing tank is filled with a pure gas with a low-uncertainty equation of state (e.g., nitrogen), weighed, connected to, and discharged into the evacuated *PVTt* tank through a shut off valve. The weighing tank is weighed again to determine the mass of gas discharged. The pressure and temperature in the *PVTt* tank before and after the addition of gas are used to calculate the density change in the *PVTt* tank. The volume of the *PVTt* tank is calculated via equation (5), which is based on the conservation of mass:

$$V_{M,grav} = \frac{m_f - m_i}{(\rho_{M,f} - \rho_{M,i})} - V_{extra}. \quad (5)$$

The numerator is the mass change of the weighing tank (corrected for buoyancy, see section 2.1) and V_{extra} represents the extra volume temporarily connected to the tank for the purpose of introducing the gas from the weighing tank to the *PVTt* tank (usually a small volume of tubing and a valve body). The extra volume is calculated from dimensional measurements

or measured by liquid volume transfer methods (a graduated syringe). The NIST 34 L and 677 L *PVTt* volumes were determined by the gas gravimetric method by filling the volumes to 100 kPa while they were immersed in the thermostatted water bath at 296.5 K. These volume determinations were made at the values of pressure and temperature that are normally used when the *PVTt* standard calibrates customer's meters, thereby eliminating the need to measure the tanks' volumes as a function of pressure and temperature.

For the *liquid gravimetric method*, the unknown volume is weighed empty, then filled with a liquid of known density (e.g., water or mercury), and an equation similar to equation (5) is applied. This method is not well-suited to a *PVTt* measurement volume because it is impractical to completely remove air bubbles from tubes and pressure gauges that are part of V_{M}.

For the *gas expansion method* [70], another tank of known volume V_1 that is instrumented with temperature and pressure sensors is used as a reference. By pressurizing one tank, connecting it to the other, and opening a valve between them, the change in gas density in the two volumes gives the unknown volume. From conservation of mass, the unknown volume by the expansion method is:

$$V_{\mathrm{M,exp}} = \frac{\left(\rho_{1,i} - \rho_{1,\mathrm{f}}\right)V_1}{\left(\rho_{\mathrm{M,f}} - \rho_{\mathrm{M,i}}\right)} - V_{\mathrm{extra}}. \tag{6}$$

As for the gravimetric approach, there may be small extra volumes necessary to connect the known and unknown volumes that must be quantified by other means, but by keeping V_{extra} small, the uncertainty from this source is manageable.

Uncertainty analysis: (table 3) the uncertainty of all flow standards is flow dependent, as shown in figure 17 for the NIST 34 L and 677 L *PVTt* standards. For both standards, leaks dominate uncertainty for small flows and inventory uncertainties grow for high flows. The tank volumes 34 L and 677 L were chosen to facilitate an overlapping flow range enabling comparisons. Together, both volumes span more than 5 decades of flow, 2.2×10^{-4} g s^{-1} to 43 g s^{-1} (10 cm^3 min^{-1} to 2000 L min^{-1}) with expanded uncertainty of 0.025% or less. Both standards have wide flow ranges with uncertainty <0.016% ($k = 2$) where the largest uncertainty component (up to 84%) results from the uncertainty of the pressure of the full tank. The full tank pressure contributes uncertainty during both (1) determination of the tank volume and (2) a flow measurement. If the volume and flow measurements are made with the same pressure sensor, their uncertainty might be considered correlated, leading to a reduced uncertainty in the flow measurement. Because the largest uncertainty source for the pressure measurements is calibration drift and the volume and flow measurements are separated in time, the pressure uncertainty is considered uncorrelated.

The dashed lines in figure 17 show flow ranges where the systems could be used but generally are not. For instance, a flow of 1.1 g s^{-1} (50 L min^{-1}) takes more than 10 min to fill the 677 L tank while the 34 L system fills in 41 s, so the 34 L system is used to save the operators' time even though the uncertainty is slightly larger.

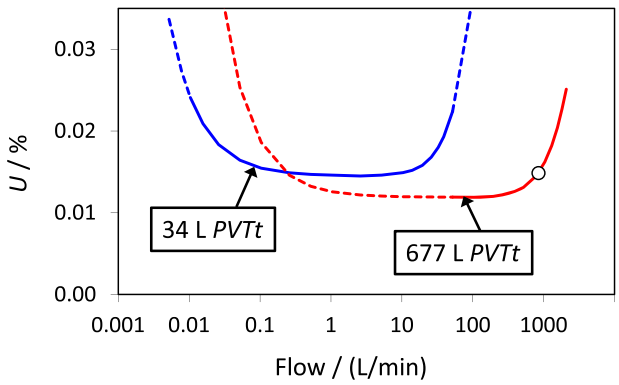

Figure 17. Expanded uncertainty of mass flow measurements from the NIST 34 L and 677 L *PVTt* standards plotted versus flow. A circle marks the case detailed in the example *PVTt* uncertainty analysis. Dashed lines show ranges that are possible but generally not used for time efficiency or uncertainty reasons.

In the following subsections we discuss the major components of uncertainty for the NIST *PVTt* standards and calculate the uncertainty for the 677 L system at a flow of 22 g s^{-1} (1000 L min^{-1}) which corresponds to the circle plotted in figure 17.

Tank volume: the *PVTt* tank volume was determined by the gas gravimetric method and equation (5). The volume measurement was performed eight times using nitrogen on some occasions and argon on others to challenge the procedure and the calculations. High-purity dry gases were used to reduce uncertainties from possible impurities. A substitution procedure was used to weigh the pressurized tank so that the major uncertainty components for the mass of gas discharged to the *PVTt* tank were: balance resolution, buoyancy corrections, reference mass uncertainty, and repeatability (10% of the volume uncertainty). Most of the uncertainty (84%) of the volume determination is the final density in the *PVTt* tank which can be traced to the uncertainty of the pressure measurement for the full tank.

Gas density: the normalized sensitivity coefficient for the initial gas density is $\frac{\rho_{\mathrm{M},i}}{\dot{m}}\frac{\partial \dot{m}}{\partial \rho_{\mathrm{M},i}} \approx \frac{-\rho_{\mathrm{M},i}}{\rho_{\mathrm{M,f}} - \rho_{\mathrm{M},i}}$. We used the symbol '≈' because we assumed that the change in mass in the inventory volume was negligibly small to make an algebraic simplification. Initially, the *PVTt* tank is evacuated to a pressure of 0.02 kPa and then it is filled to 100 kPa (and because $\rho_{\mathrm{M}} \propto P_{\mathrm{M}}$), the normalized sensitivity coefficient for $\rho_{\mathrm{M,i}}$ is −0.0002. Therefore, a poor measurement of the initial density introduces little uncertainty to the mass flow measurement. The normalized sensitivity coefficient for the final tank density $= \frac{\rho_{\mathrm{M,f}}}{\rho_{\mathrm{M,f}} - \rho_{\mathrm{M},i}}$, is approximately unity; therefore, it is 5000 times more important to have low uncertainty values for the pressure, temperature, composition, and equation of state for the full tank than for the empty tank.

Inventory mass change: the mass change in the inventory volume is considered zero in the flow calculation due to the mass cancellation procedure, but the inventory volume still

Table 3. Uncertainty of the NIST 677 L *PVTt* flow standard at 22 g s^{-1} (1000 L min^{-1}).

Input variable (x_i)	Notes	x_i value	$u(x_i)/x_i$/%	S_i	Contrib./%
Tank volume, V_M	a	677.9 L	0.0041	1	26
Initial gas density, $\rho_{M,i}$	b	2.27×10^{-4} g L^{-1}	5.0	−0.0002	2
Final gas density, $\rho_{M,f}$	b	1.14 g L^{-1}	0.0037	1	22
Inventory mass change	c	1.3 g	3.2	0.0017	44
Collection time, $(t_f - t_i)$	d	35.1 s	0.0005	−1	0
Leaks	e	1.7×10^{-7} g s^{-1}	~ 0	1	0
Type A $(s/\sqrt{n})$	f	4.4×10^{-4} g s^{-1}	0.0020	1	6
Expanded uncertainty (95%)	$\boldsymbol{U}(\dot{\boldsymbol{m}})/\dot{\boldsymbol{m}} = 0.016\%$				

[a]Measured by gas gravimetric method. Largest component is full tank density due to pressure uncertainty.
[b]Pressure, temperature, equation of state, and gas composition.
[c]Used estimated uncorrelated uncertainties, verified by comparison and multiple diversions.
[d]3000 Hz data acquisition rate, rectangular distribution, applied for both start and stop times.
[e]Periodically measured by pressure decay test.
[f]Based on calibrations of a critical flow venturi.

introduces uncertainty. The most significant uncertainty components (due to sensor time constants) are correlated between the start and stop diversions. For instance, the inventory's temperature is measured incorrectly low by the same amount at both the start and stop conditions due to slow sensor response time; therefore, most errors from temperature (and pressure) sensors cancel out. But inconsistencies in the pressure and temperature fields in V_I between the start and stop diversions exist and probably increase at higher flows. Uncorrelated uncertainties in inventory temperature and pressure were estimated with a function that increases for increasing flow. This assumption was validated by comparisons between the 34 L and 677 L standards and by performing multiple diversions during one collection to intentionally multiply the uncertainties generated by the diversion and the inventory volume [70]. Comparisons of the two systems with their 20:1 volume ratio were used to verify the difficult to characterize inventory uncertainty. The normalized sensitivity coefficient is equal to the mass change in the inventory divided by the mass change in the whole *PVTt* system. At the largest flow 43 g s^{-1} (2000 L min^{-1}) for the system, this inventory component contributes 75% of the uncertainty budget; but the contribution decreases to 44% at 22 g s^{-1} (1000 L min^{-1})

Collection time: the collection time is determined by a pair of redundant counters that are triggered by signals from the diverter valve. The interval determined by the counters is corrected for inventory-mass-cancellation after the run using records from the pressure and temperature sensors acquired at 3000 Hz during the start and stop dead-end times. The time uncertainty is dominated by the time resolution of 1/3000 Hz = 0.33 ms. The standard uncertainty related to periodic counter calibrations (0.01 ms) is only a minor contributor. Following the GUM section 4.3.7 [9] and assuming a rectangular probability distribution for the time uncertainty leads to a standard uncertainty of $0.33\ \text{ms}/\sqrt{6} = 0.134$ ms. Taking the RSS of two uncertainties of this magnitude (for the start and stop times) gives a standard uncertainty for the collection time of 0.19 ms.

1.5. Rate of rise (RoR) standard

The rate of rise method uses equipment similar to a *PVTt* standard (shown in figure 12). Valves are used to evacuate the measuring tank with a vacuum pump and then the tank is filled with gas from the MUT. A RoR standard does not require a carefully designed diverter unit because flow is calculated from a time series of mass values, not precisely measured *static* values at the start and stop times [71]. Hence, the RoR method is a *dynamic* volumetric method because the pressure and temperature measurements used to calculate the mass of gas are made while their values are changing, not in a steady state. One advantage of the dynamic method is that the operator can monitor the flow during the calibration. RoR can be applied to a measuring volume V_M that is used as either a gas sink or as a gas source. Here, we describe the use of V_M as a gas sink.

For many years the semiconductor manufacturing industry has used the RoR method to calibrate mass flow controllers. Some have used chemical vapor deposition chambers as the measuring volume [71]. The RoR method is well suited to small flows where the temperature uncertainties caused by flow work are small. (See below.) Some RoR measuring tanks are filled with metal spheres to improve the heat transfer between the gas and its surroundings. NIST applies the RoR method at flows below 2.2×10^{-3} g s^{-1} (100 cm^3 min^{-1}) using the 34 L *PVTt* measuring tank in a temperature-controlled water bath. When used for *PVTt* measurements, the 34 L measuring tank is normally filled from 0.02 kPa to 100 kPa; for a flow of 2.2×10^{-5} g s^{-1} (1 cm^3 min^{-1}), this would take 24 days! The RoR method utilizes the same equipment to measure small gas flows with good uncertainty in a much shorter time. During a typical flow meter calibration, the NIST RoR standard will collect 3600 measurements of pressure and temperature at 10 s intervals for each flow set point. Alternatively, the *PVTt* method could be used with a smaller measuring tank [66]; however, the RoR method allows NIST's existing collection system (with 677 L and 34 L tanks) to calibrate small flows efficiently.

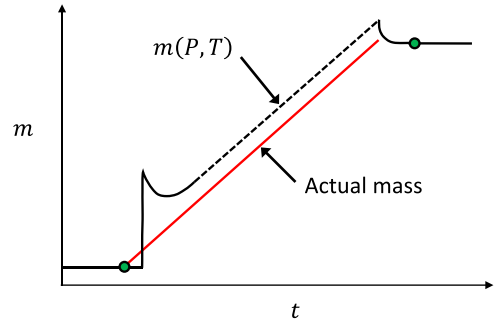

Figure 18. For RoR, mass flow is calculated from the slope of the measured mass (dashed line) versus time data collected during filling or discharge of V_M. The measured mass is based on temperature (and pressure) measurements that have errors caused by flow work and sensor response times. The actual mass (solid line in figure 18) differs from the measured mass, especially for large flows into a small V_M. In contrast with an RoR standard, a *PVTt* standard uses initial and final masses that are calculated at static or steady-state conditions (circles) to reduce errors due to flow work.

The rate of rise method calculates the rate of change of mass during the tank filling process:

$$\dot{m}_{\mathrm{RoR}} = \frac{\mathrm{d}}{\mathrm{d}t}[(V_M + V_I)\rho(P,T)], \tag{7}$$

where V_M and V_I are the measuring volume and inventory volumes respectively and t is time. The gas density $\rho(P,T)$ is calculated from a properties database like REFPROP [18] or an equation of state. The simplest mass flow calculation takes the mass difference between sequential readings and divides by the time interval between the readings:

$$\dot{m}_i = \frac{m_i - m_{i-1}}{t_i - t_{i-1}}. \tag{8}$$

Here $m_i = (V_M + V_I)\rho(P_i, T_i)$. Equation (8) will yield mass flow values with a large variance (and possibly even negative values) due to noise in the pressure and temperature readings. Therefore, to reduce the variance of the real time mass flow values, it is common to use running averages of $\dot{m}_i$, i.e.,

$$\dot{m}_{\mathrm{RoR},i} \cong (V_M + V_I)\left[\sum_{i=1}^{\mathrm{MA}} \frac{\rho\left(P_{i+1}, T_{i+1}\right) - \rho(P_i, T_i)}{t_{i+1} - t_i}/\mathrm{MA}\right], \tag{9}$$

where the variable MA is an integer that defines a moving-average filter over a range of MA density measurements. As illustrated in figure 19, a moving average of 10 or 100 points reduces noise arising from pressure resolution.

The slope of mass versus time can also be calculated via a first-order least squares regression [8] with N time and mass data pairs,

$$\dot{m} = \frac{N\sum_{i=1}^{N} t_i m_i - \sum_{i=1}^{N} t_i \sum_{i=1}^{N} m_i}{N\sum_{i=1}^{N} t_i^2 - \left(\sum_{i=1}^{N} t_i\right)^2}. \tag{10}$$

The NIST RoR system uses either a mass flow controller or a pressure controller to ensure that the flow from the MUT is stable within ±0.2% or better. Any data including transients due to out-of-control environmental temperatures are not processed. The uncertainty due to flow instability is negligible because the MUT's response time is short compared to the averaging interval (⩾1 h) and because both the RoR data and the MUT data are averaged over identical intervals. To visually qualify data that will be used to calculate the mass flow via equation (10), we first plot the RoR flow based on equation (9) with MA = 100.

One can also calculate the meter factor by dividing the difference between two masses in the data record ($m_{M,f} - m_{M,i}$) by the integrated mass flow measured by the MUT. The initial and final masses $m_{M,i}$ and $m_{M,f}$ can be chosen from the data record at times where the data are unaffected by the start and stop transients and for differences in mass measurements that are large enough to produce acceptable uncertainty due to instrumentation, particularly balance uncertainty. This approach is described in more detail in section 2.2 which covers the static gravimetric method.

Flow work: flow work adds enthalpy and increases the temperature of the gas in the measuring volume during filling [64]. (Here, we assume that density changes from leaks and the thermal and pressure expansion of the tank are negligibly small.) The challenges of accounting for flow work increase if the measuring volume is filled rapidly. After the filling stops, the gas's pressure declines as it cools into thermal equilibrium with the surroundings. Mass conservation dictates that the average gas density remains constant during thermal equilibration. Figure 20 illustrates equilibration following filling of NIST's 34 L tank by a comparatively large flow: 0.11 g s^{-1} (5 L min^{-1}). In this case, the temperature of the gas was approximately 2.5 K warmer than the water bath immediately after filling. The decreasing pressure is due to the decreasing gas temperature, and the time required for pressure stabilization is the thermal time constant of the system, in this case approximately 170 s.

Flow work does not generate temperature errors in the *PVTt* standard because the temperature is measured only during thermal equilibrium, both before and well after filling is complete. (The *PVTt* measurement times are represented by circles in figure 18.) Temperature errors, if uncorrected, are an important uncertainty component for RoR flow measurements.

Wright *et al* used a lumped-parameter heat transfer model to estimate the temperature difference between the gas and water ($T_{err} = T_{gas} - T_{water}$) while the tank was filling [72]. They found that the dimensionless variable Γ which enters into the ratio {heat transfer from the gas to its surroundings}/{energy input to gas from flow work) is a key parameter. We define:

$$\Gamma = \left[\frac{hA}{c_V \dot{m}}\right], \tag{11}$$

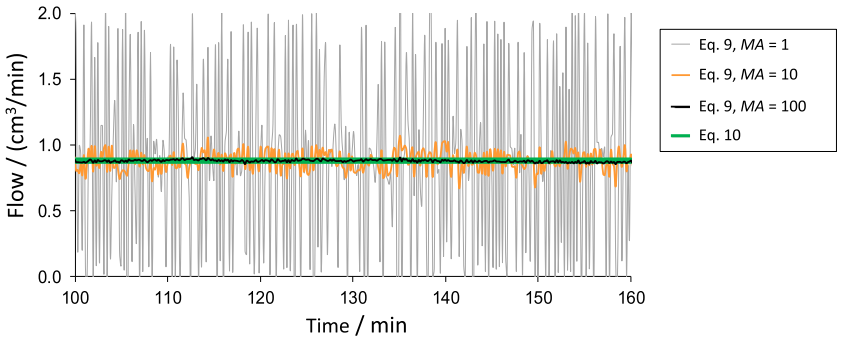

Figure 19. Raw and processed RoR data. The green line is the result of a least squares regression (equation (10)); the noisy lines result from three moving averages (equation (9) with MA = 1, 10, 100). The moving averages allow one to monitor the flow's stability while data is collected before applying equation (10).

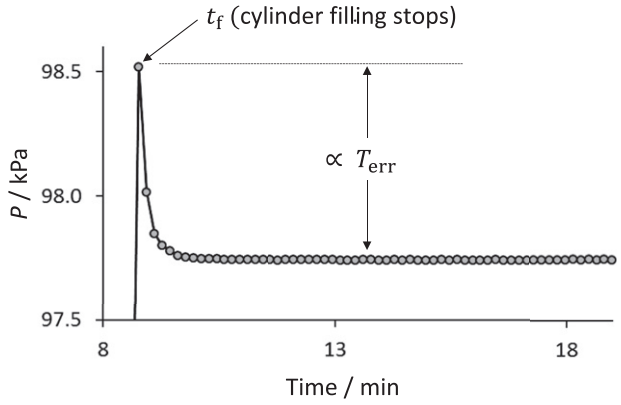

Figure 20. Pressure in the 34 L tank versus time at the end of a 0.11 g s^{-1} (5 L min^{-1}) collection. Because of the flow work during filling, the gas was warmer (and therefore at higher pressure) than the water bath at time t_f.

where A is the surface area of the measuring tank, h is the convective heat transfer coefficient between the gas and the tank's walls, and c_V is the constant-volume heat capacity of the gas.

The model applies conservation of mass and energy to the filling tank to predict the temperature error:

$$T_{err} = T_{gas} - T_{water} = T_{water}\left[\frac{(T_{in}/T_{water})\gamma - 1}{1+\Gamma}\right] \times \left[1 - \left(\frac{\dot{m}t}{m_i} + 1\right)^{-(1+\Gamma)}\right], \quad (12)$$

where T_{in} is the temperature of the gas entering the tank from the MUT, T_{water} is the temperature of the environment surrounding the tank (in this case, a water bath), $\gamma = c_P/c_V$ is the constant-pressure to constant-volume ratio of the gas's specific heats, m_i is the initial mass of gas in the tank before filling begins, and t is the time measured from the beginning of the fill.

The lumped-parameter analysis assumes that the gas is well stirred and that the tank wall's temperature matches the water bath's temperature, so that the heat transfer from the gas to the tank walls is the limiting heat transfer process. The analysis shows the importance of maximizing the tank's surface area and that the temperature error depends on the specific heats of the gas being measured. Errors in the pressure measurement were avoided by placing the pressure connection on the gas measuring tank [72].

Uncertainty analysis : (table 4) the uncertainty of RoR gas flow measurements depends upon the flow, as illustrated in figure 21 for NIST's 34 L measuring tank. For a particular RoR system and gas species, the temperature and pressure errors due to flow work can be quantified by plots such as figure 20 and corrected as a function of the flow. In this uncertainty analysis, we do not correct the temperature and pressure errors due to flow work. Instead, we treat them as uncertainties.

For flows between 2.2 × 10^{-5} g s^{-1} (1 cm^3 min^{-1}) and 4.3 × 10^{-3} g s^{-1} (200 cm^3 min^{-1}), the 34 L RoR flow standard has uncertainties between 0.05% and 0.12%. For this range of flows, the dominant uncertainties result from leaks, repeatability of the BED (a laminar flow meter was used), and the measurements of volume and density. At flows <2.2 × 10^{-5} g s^{-1} (1 cm^3 min^{-1}), the uncertainty is primarily due to the leak corrections and at flows >4.3 × 10^{-3} g s^{-1} (200 cm^3 min^{-1}), the RoR flow uncertainty is dominated by the uncorrected temperature errors from flow work T_{err}.

The uncertainty components included in the analysis are:

Volume of the measuring tank and inventory volume: note that the rate of rise method requires one to know the sum of the tank and inventory volumes, i.e., $V_M + V_I$. For the NIST 34 L system, the standard uncertainty of $V_M + V_I$ is 9.7 cm^3 or 0.028% [72].

Change in gas density: we measured the pressure in V_M with a pair of pressure sensors that are linear within 1 Pa in the range 20 kPa ⩽ P ⩽ 130 kPa and have a resolution of 1 Pa. The RoR system is used only at pressures greater than 20 kPa. Below 20 kPa, additional uncertainties are generated by the transient responses of the pressure and temperature sensors and the MUT [72]. The uncertainty of the water bath temperature is 0.012 K. When using nitrogen gas and thermodynamic data from REFPROP [18], the uncertainty of the compressibility factor $P\mathcal{M}/(\rho\mathcal{R}T)$ is 20 parts in 10^6 and the uncertainty of the molar mass $\mathcal{M}$ from impurities is negligible [70]. The universal gas constant $\mathcal{R}$ is a defined quantity and has zero uncertainty. These uncorrelated uncertainty components of the gas density calculation are combined by RSS.

Table 4. Uncertainty of the NIST 34 L rate of rise flow standard at 2.2×10^{-3} g s^{-1} (100 cm^3 min^{-1}).

Input variable (x_i)	Notes	x_i value	$u(x_i)/x_i$/%	S_i	Contrib./%
Tank volume, $V_M + V_I$	a	34.13 L	0.028	1	39
Gas density change, $\Delta\rho_M$	b	0.352 g L^{-1}	0.013	1	48
Slope calculation and flow stability	c	~0	~0	1	0
Collection time ($t_f - t_i$)	d	5588 s	~0	−1	0
Leaks	e	1.1×10^{-8} g s^{-1}	~0	1	0
Type A ($s/\sqrt{n}$)	f	1.8×10^{-7} g s^{-1}	0.008	1	13
Expanded uncertainty (95%)		$\boldsymbol{U(\dot{m})/\dot{m}} = 0.065\%$			

[a]Measured by gas gravimetric method. Largest component is full tank density due to pressure uncertainty.
[b]Includes pressure, temperature calibration, temperature errors due to flow work, resolution, equation of state, gas composition.
[c]Data is prequalified for stability, N is large.
[d]Collection time must be long enough to ensure low uncertainty pressure change.
[e]Periodically measured by pressure decay test as a function of tank pressure. Leaks are significant at lower flows. See figure 21.
[f]Based on calibration data from laminar flow meters.

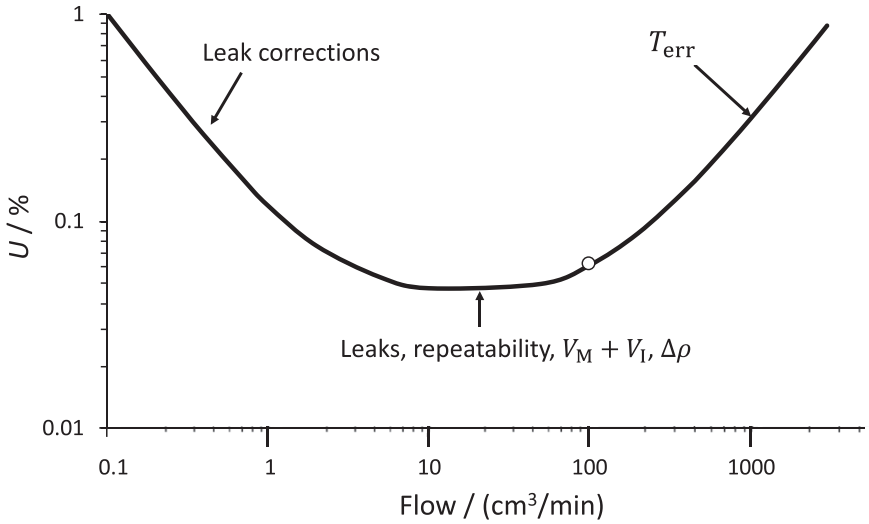

Figure 21. Expanded uncertainty versus flow for the NIST 34 L rate of rise flow standard. The circle identifies the result of the RoR uncertainty analysis detailed in table 4.

As discussed above, flow work leads to uncertainty in the gas temperature that grows with increasing flow. The resulting temperature and pressure uncertainties are correlated, of known sign, and are not combined by RSS, but rather by addition. For the 34 L RoR standard, these temperature uncertainties become the dominant contributors at flows greater than about 2.2×10^{-3} g s^{-1} (100 cm^3 min^{-1}).

For the NIST 34 L standard, a minimum of 1 h of 0.1 Hz data ($N = 360$ points) are processed to produce one RoR flow measurement. At flows below 2.2×10^{-5} g s^{-1} (1 cm^3 min^{-1}), data are collected for 18 h or more ($N \geqslant 6480$) so that the pressure change is $\geqslant$1 kPa in order to reduce the uncorrelated uncertainty of the pressure and temperature sensors. This is necessary because the normalized sensitivity coefficients $S_i = \left(x_i/\dot{m}\right)\left(\partial\dot{m}/\partial x_i\right)$ for the pressures and temperatures used in the RoR calculation are inversely proportional to $P_N - P_1$. To illustrate the issue, consider the simplified case of a RoR measurement based on only two points, $m_1 = (V_M + V_I)\rho(P_1, T)$ and $m_2 = (V_M + V_I)\rho(P_2, T)$ separated by $\Delta t = t_2 - t_1$ so that $\dot{m}_{RoR} = (m_2 - m_1)/\Delta t$. If the 95% confidence level uncertainty due to non-linearity of the pressure sensor is 0.001 kPa, $P_1 = 20$ kPa, and $P_2 = 20.1$ kPa, this uncorrelated pressure uncertainty would lead to a mass flow uncertainty of 0.001 kPa/(20.1–20 kPa) = 1%. By filling the tank longer to increase the pressure change (and increase N), this uncertainty is reduced.

Time measurements: the computer's clock and software determine the accuracy of the time measurements. The clock is periodically compared to NIST reference time (time.gov) over intervals of several days. Based on these measurements, the time uncertainty of the data acquisition system is 1 ms. For data records >20 s, this uncertainty component is <0.005%.

Slope calculation and flow stability: the uncertainty in calculation of slope via equation (10) is insignificant if data are collected for a sufficiently long interval and if the flow is sufficiently stable during that interval. The uncertainty in the mass values m_i in equation (10) is at least 2.5 times larger than the uncertainty in the time values t_i, allowing us to apply the simplest expression for the expanded uncertainty of the slope calculation [8]:

$$U(a_1) = 2\left[\frac{\frac{\sum_{i=1}^{N}(m_i - a_1 t_i - a_0)^2}{N-2}}{\sum_{i=1}^{N} t_i^2 - \frac{\left(\sum_{i=1}^{N} t_i\right)^2}{N}}\right]^{\frac{1}{2}} = \frac{4\sqrt{3}s(m)}{\sqrt{N^3 - N}\Delta t}, \quad (13)$$

where a_0 and a_1 are the zeroth and first order coefficients of the fit to the mass versus time data. (Here we have used a_1 instead of $\dot{m}$ to avoid confusion. Equation (13) gives the uncertainty related to the fitting process, not the total uncertainty of the mass flow.) The quantity $s(m)$ is the sample standard deviation of the mass fit residuals and Δt is the time interval between successive mass measurements. We used example data sets to quantify $s(m)$ for a range of flows and it led to $<0.01\%$ uncertainty contribution to the mass flow. Pressure or flow regulators are necessary to generate stable flows at the MUT. The collected data are visually assessed prior to final processing to assure low values of $s(m)$ and negligible uncertainty from flow instability.

Leaks: the flow due to leaks or outgassing for the 34 L system has been measured over the range of tank pressures used during RoR measurements. The RoR flow measurements are corrected using a fit to the leak versus pressure data. The uncertainty of the leak correction is 1.1×10^{-8} g s^{-1} (5×10^{-4} cm^3 min^{-1}). This is based on the residuals of the fits of sets of leak versus tank pressure data collected over several years. Much lower leak rates can be attained by using materials and fittings that are designed for vacuum systems. Even if the leaks were zero, adsorption and desorption of gas from the system's walls and outgassing from gaskets will generate 'virtual leaks' that must be quantified.

2. Gravimetric flow standards

Gravimetric standards use a weigh scale (balance) to measure the mass of the gas delivered from (or collected in) a measurement volume V_M. (See figure 22.) During a calibration, the gas flows through a test section and the MUT during a measured time interval. A static gravimetric system weighs V_M while it is separated from the test section and the MUT, before and again after delivering (or collecting) the gas. Hence the mass of V_M is not changing (i.e., static) while it is measured. Figure 22 is a schematic of a static gravimetric system while gas is flowing into V_M. When the weighed tank is the source of the flow, this system is often called a blow-down system.

In a dynamic gravimetric standard (figure 29), V_M is weighed while it is connected to the test section and the gas is flowing into (or out of) it. The method is called *dynamic* because the mass is measured while it is changing.

2.1. Static gravimetric standard with flying start/stop

Figure 21 is a schematic diagram of a static gravimetric standard utilizing the flying start/stop approach [73–75]. The test apparatus comprises:

- A source of gas with a shut-off valve.
- A downstream pressure regulator and heat exchanger to maintain steady conditions at the test section.
- The MUT (in this case a critical nozzle) and the pressure and temperature sensors necessary to measure T_0 and P_0 to calculate the nozzle flow.
- An upstream pressure regulator located after the MUT if the MUT is not a critical nozzle.
- A diverter unit, i.e., valves that allow the gas to be switched from a bypass path to the measuring tank. The diverter also produces trigger signals to start and stop a timer. The bypass may exhaust to a vacuum pump or to atmospheric pressure. The inventory volume (hatched) is the internal volume of the pipes that connect the MUT and diverter unit to the tank. The inventory volume has pressure and temperature instrumentation ($P_{I1}, T_{I1}, P_{I2}, T_{I2}$) needed to measure gas density changes.
- A measuring tank (V_M) that can be disconnected from the inventory volume for weighing.
- A balance inside a wind screen for weighing V_M before and after it is filled.

Figure 23 is an example of a large static gravimetric flow standard [74]. A gravimetric standard for natural gas (NG) at 6 MPa at flows up to 5.4 kg s^{-1} and expanded uncertainty of 0.044% is described by Ren *et al* [76].

The procedure for making a mass flow measurement is:

- Install the MUT in the test section and ensure there are no significant leaks.
- Empty V_M and weigh it with the balance.
- Connect V_M to the diverter unit.
- Set the flow through the MUT by choosing a set point pressure with the regulator. Flow is initially to the bypass path.
- Once conditions at the MUT stabilize, measure the initial pressure and temperature in the inventory volume, divert flow from bypass to V_M and start a timer (triggered by the diverter unit).
- Measure P_0 and T_0 (the pressure and temperature in the MUT approach pipe) while V_M is filling.
- Fill V_M to a high enough pressure that the mass of gas can be measured with small uncertainty, but not so high that the flow at the MUT becomes unsteady.
- Divert flow to the bypass path and measure the final pressure and temperature in the inventory volume. The timer is stopped by a diverter valve signal.
- Stop the flow.
- Disconnect the full V_M and weigh it with a balance.

Figures 24 and 25 show photographs of a static gravimetric system at NMIJ/AIST [77]. The facility has two calibration lines, one for flows between 1.7×10^{-3} g s^{-1} (79 cm^3 min^{-1}) and 0.17 g s^{-1} (7.9 L min^{-1}) and the other for flows between 0.17 g s^{-1} and 0.83 g s^{-1} (39 L min^{-1}). Each line is provided with a nozzle holder for mounting a critical nozzle and has diverter valves downstream. Pressure and temperature sensors are used to measure the mass change in the inventory volume. Figure 25 shows chambers enclosing two balances used to measure the mass of the measuring tank. The large one on the right is a mechanical balance with a resolution of 0.1 mg

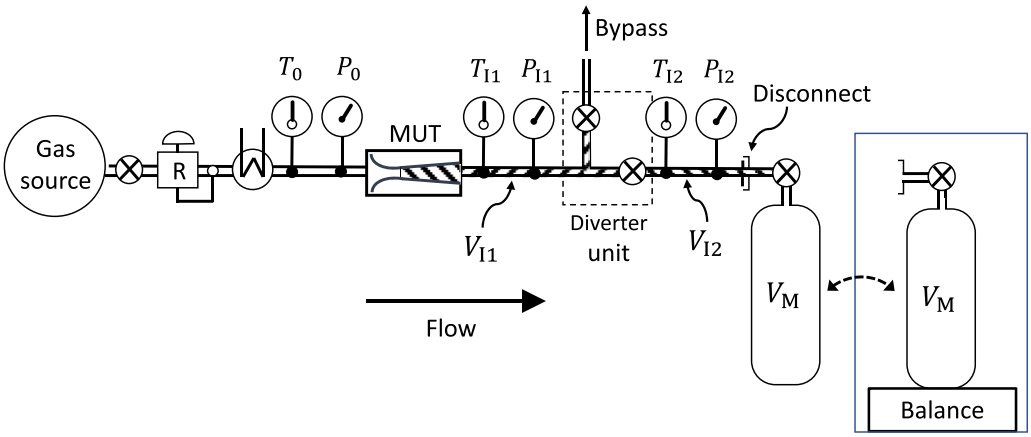

Figure 22. A schematic diagram of a flying start/stop static gravimetric flow standard.

Figure 23. A gravimetric standard for flows up to 43 kg s^{-1} (2000 m^3 min^{-1}) at the Southwest Research Institute. Reproduced with permission from [74]. Photo courtesy of Southwest Research Institute.

and the electronic balance placed in the left chamber has a resolution of 0.01 mg.

Stability of the supply gas pressure: pressure fluctuations of the test gas flowing into the test section cause flow instability. A pressure controller downstream from the gas source reduces flow fluctuations and improves the performance of the calibration facility and the MUT. The automatic pressure controller used in the NMIJ/AIST calibration facility can control the pressure within ±5 Pa of the pressure set point in the pressure range of 50 kPa to 700 kPa.

Temperature effects: temperature control is more difficult than pressure control. Since the calibration of high-resolution balances is sensitive to temperature fluctuations in the room, it is desirable to install the entire calibration facility (including the balance) in a temperature-controlled room. The room housing the NMIJ/AIST standard has a temperature stability of ±1 °C and changes less than 0.1 °C during a collection. Furthermore, the balance is housed in a chamber as shown in figure 25. Even in a temperature-controlled room, calibrations are affected by gas temperature changes accompanying pressure changes in regulators, the MUT, and the measuring tank. For low uncertainty flow measurements, it is necessary to wait for steady temperature conditions in the system. For small flows, the connecting piping serves as a heat exchanger with the room air. For larger flows, a heat exchanger can reduce the time needed to return the gas to a steady temperature, thereby reducing temperature measurement errors.

Careful attention should be paid to the location of the test section and to room ventilation. The NMIJ/AIST facility shown in figures 24 and 25 is built on an open framework to allow circulation of the room air near the test section.

Diverter unit: a single, three-way ball valve can be used to divert flow between the bypass and the V_M. When a typical, commercially available 3-way valve is used to switch the flow direction, there is a short interval in which the two downstream flow paths are simultaneously open. This allows gas that did not pass through the MUT to move from the bypass into V_M, thereby generating a measurement error. To reduce the error, high speed ball valves can be used; however, the error is not zero. Instead of using a ball valve, the calibration facility of NMIJ/AIST [78] uses two valves (figure 24) with a controller that allows adjustable opening and closing times. One valve is located on the bypass; the other is located on the measurement tank path. The opening and closing times of the two valves are adjusted so that both lines are never open simultaneously. Instead, there is a short 'dead-end time' when both valves are closed. (The two-valve system is also called a 'zero overlap' system [79]). The dead-end time is brief (<10 ms) so the pressure rise in the inventory volume causes only a minor disruption of steady flow at the MUT. Figure 24 is a photograph of the diverter unit used at NMIJ/AIST. The flow from the

Table 5. Uncertainty of the NMIJ/AIST flying start/stop static gravimetric flow standard for a flow of 0.06 g s^{-1} (2.8 L min^{-1}).

Input variable (x_i)	Notes	x_i value	$u(x_i)/x_i$/%	S_i	Contrib./%
Tank mass change $(m_{M,f} - m_{M,i})$	a	1.8 g	0.028	1	24
Inventory mass change	b	~0 g	0.020	1	13
Collection time $(t_f - t_i)$	c	30 s	0.020	−1	13
Leaks	d	1.6×10^{-11} g s^{-1}	~0	1	0
Type A $(s/\sqrt{n})$	e	2.4×10^{-5} g s^{-1}	0.040	1	50
Expanded uncertainty (95%)		$\boldsymbol{U(\dot{m})/\dot{m}} = 0.11\%$			

[a]Includes balance resolution, buoyancy corrections via reference tank.
[b]Includes density and inventory volume components.
[c]6 ms out of 30 s minimum collection.
[d]Measured by pressure decay test.
[e]Measured during calibration of best existing device, in this case, a critical flow venturi.

MUT is switched to the bypass or the measuring tank by valves 1 and 2. The opening and closing times of each valve are detected by sensors attached to the valves [78].

Measuring the tank mass and buoyancy corrections: an object weighed in air has an 'apparent' mass m_A that is less than its true (or *in vacuo*) mass because of a buoyant force equal to the external volume of the object V_{obj} multiplied by the density of the surrounding air ρ_{air}. The true mass can be calculated from:

$$m = m_A + \rho_{air} V_{obj} = \frac{m_A}{\left(1 - \frac{\rho_{air}}{\rho_{obj}}\right)} \approx m_A \left(1 + \frac{\rho_{air}}{\rho_{obj}}\right). \quad (14)$$

Typical density values for the air and the weighed tank are 0.001 g cm^{-3} and 1 g cm^{-3} respectively, so buoyancy corrections are approximately 0.1% in this application.

Commercial balances usually apply corrections based on assumed values for the densities of the air and V_{obj}. To obtain the lowest-uncertainty mass measurements, it is necessary to turn off the balance's assumed corrections and apply buoyancy corrections using the actual air density and object volume (or object density). The air density can be calculated from pressure, temperature, and humidity measured in the environment surrounding the tank when it is weighed [80, 81].

The external volume of the tank (V_{obj}) is a function of its temperature and internal pressure:

$$V_{obj} = V_{ref}[1 + \lambda(P - P_{ref})][1 + 3\alpha(T - T_{ref})], \quad (15)$$

where V_{ref} is the external volume of the tank assembly at some convenient reference pressure and temperature conditions (P_{ref} and T_{ref}), λ is the pressure expansion coefficient of the tank assembly, α is the linear thermal expansion coefficient of the tank material, and T and P are the temperature and internal pressure of the tank at the time of the mass measurement. A practical alternative to equation (15) is to measure the external volume of the tank assembly at normal room temperature and various pressures and fit the external volume to the apparent mass for each gas species for which the tank will be used.

The coefficients in equation (15) are small: typical values are $\lambda = 1.59 \times 10^{-10}$ Pa^{-1} and $\alpha = 2.4 \times 10^{-5}$ K^{-1}. Because equation (15) is applied to a buoyancy effect of only 0.1%, this correction is negligible for most flow measurements. For example, ignoring pressure effects for the tank assembly shown in figure 27 would lead to errors in the tank mass change of only 0.003% [82].

The sensitivity of the tank mass measurements to errors in the environmental conditions is relatively low, i.e., errors of several percent of the room temperature, pressure, and humidity can be tolerated without significant impact on the mass flow measurements. Also, the uncertainties in the buoyancy corrections are highly correlated when measuring mass differences. Therefore, tank mass uncertainty is driven by the drift of the balance's zero and gain caused by changes in the environmental conditions and vibration: 0.5 mg. A robust substitution weighing program [80] helps to keep the mass uncertainties nearly as small as the balance resolution.

The static gravimetric system of NMIJ/AIST corrects for buoyancy effects using an alternative to substitution weighing. Two nearly identical tanks are weighed: one is a reference tank; the other is the measuring tank that collects the test gas. Because the buoyancies of the two tanks are approximately equal, the influence of the buoyancy on the mass difference makes a negligible contribution to the mass flow uncertainty. This two-tank approach also reduces the uncertainty impact of the drifts in the balance's scale factor and zero.

Inventory volume corrections: in section 1.4 describing the *PVTt* method, we described a 'mass cancellation method' that matches the initial and final densities in the inventory volume resulting in a negligible inventory volume correction. However, 'mass cancellation' cannot be applied to the static gravimetric method because the collection tank must be filled to a high pressure so that the collected mass is significant relative to the tank's mass. Therefore, at the stop diversion, the inventory volume contains some gas that passed through the MUT but did not flow into the measuring tank. The change of the mass of gas in the inventory volume needs to be added to the mass in the measuring tank as in equation (1). Since inventory corrections can be minimized by reducing the inventory volume, a small V_I is preferable. But, for small inventory volume and large flow, the dead-end time of the diverter unit must be short to avoid a high enough pressure to cause unsteady flow at the MUT (i.e., loss or upstream pressure control by the upstream pressure regulator or loss of critical flow through the nozzle) during the diversion process.

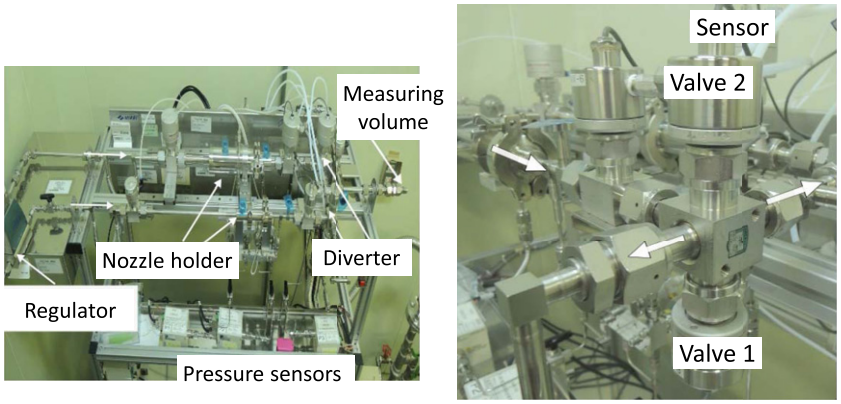

Figure 24. Pictures of the test section and diverter unit of the static gravimetric system of NMIJ/AIST.

Flow equation: the mass flow of the NMIJ/AIST static gravimetric standard $\dot{m}_{\mathrm{SG}}$ is calculated using an equation analogous to equation (1), but with a second inventory volume term. The mass flow through the MUT obtained from the calibration facility of figure 22 is:

$$\dot{m}_{\mathrm{SG}} = \frac{\left(m_{\mathrm{M,f}} - m_{\mathrm{M},i}\right) + V_{\mathrm{I1}}\left(\rho_{\mathrm{I1,f}} - \rho_{\mathrm{I1,i}}\right) + V_{\mathrm{I2}}\left(\rho_{\mathrm{I2,f}} - \rho_{\mathrm{I2,i}}\right)}{t_{\mathrm{f}} - t_{\mathrm{i}}}, \tag{16}$$

where the subscripts I1 and I2 refer to the two inventory volumes in figure 22.

As explained above, buoyancy corrected values of $m_{\mathrm{M,f}}$ and $m_{\mathrm{M,i}}$ can be measured by weighing the difference between the measuring tank and a reference tank of approximately the same external volume. The inventory corrections can be simplified by noting that the initial densities differ for I1 and I2, but the final densities in I1 and I2 are equal, so:

$$\dot{m}_{\mathrm{SG}} = \frac{\left(W_{\mathrm{M,f}} - W_{\mathrm{M},i}\right) + (V_{\mathrm{I1}} + V_{\mathrm{I2}})\rho_{\mathrm{f}} - V_{\mathrm{I1}}\rho_{\mathrm{I1},i} - V_{\mathrm{I2}}\rho_{\mathrm{I2},i}}{t_{\mathrm{f}} - t_{\mathrm{i}}}, \tag{17}$$

where W represents the difference in the balance readings between the measuring and reference tanks and $\rho_{\mathrm{f}} = \rho_{\mathrm{I1,f}} = \rho_{\mathrm{I2,f}}$.

Uncertainty analysis: table 5 summarizes the uncertainty of the NMIJ/AIST gravimetric flow standard described above.

2.2. Static gravimetric standard with standing start/stop

The static gravimetric standard with standing start/stop compares the mass change in a source tank of compressed gas to the integrated mass flow from the MUT [83]. A schematic of a static gravimetric standard in shown in figure 26 and its components are:

- A pressurized measuring volume V_{M} with a shut-off valve and a fitting that allows the tank to be disconnected from the rest of the system for weighing.
- A pressure regulator and heat exchanger to provide stable flow conditions at the MUT as V_{M} discharges.
- The MUT with associated instrumentation.

Figure 25. The balances of the static gravimetric system of NMIJ/AIST.

- A balance inside a wind screen with pressure, temperature, and humidity sensors for buoyancy corrections.

The procedure for making a mass flow measurement is:

- Install the MUT and ensure there are no significant leaks in the system between V_{M} and the MUT.
- Set the pressure regulator for the desired pressure at the MUT.
- If the tank had contained a different gas, purge the tank by repeated filling and discharge to ensure the necessary purity of the test gas. Fill V_{M} with pressurized gas. The filling process generates flow work that will heat the gas and V_{M}. Observe safety precautions to avoid tank failure. Wait until the tank returns to room temperature before weighing.
- Weigh the full V_{M}. Make buoyancy corrections to obtain the mass of the full V_{M}.
- Connect V_{M} to the test section.
- Begin recording (or totalizing) the flow measured by the MUT and start flow by opening V_{M}'s shut-off valve.
- Allow V_{M} to discharge long enough that (1) the mass change of gas in V_{M} and (2) the ramp up (and down)

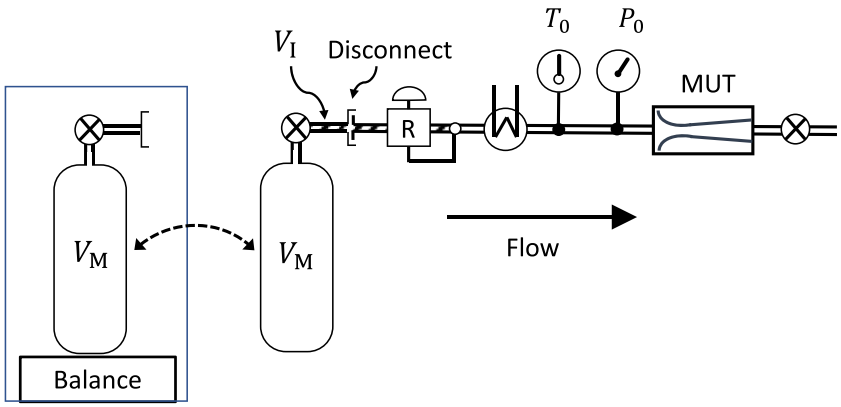

Figure 26. A schematic of a standing start/stop static gravimetric gas flow standard.

of flow through the MUT lead to acceptable uncertainty contributions.

- Close the shut-off valve and stop recording (or totalizing) the flow from the MUT.
- Wait for the tank to return to room temperature and weigh the empty V_M.

A reliably leak-free fitting must be used for the disconnect because it is impractical to test for leaks (except with soap solution) once the test procedure commences.

Figure 27 is a photograph of a gravimetric standing start/stop system used at NIST. In this picture the MUT is a laminar flow meter and the flow output by the MUT is displayed and recorded by a laptop computer for later numerical integration in a spreadsheet.

The measuring volume: the measuring volume V_M in NIST's standard is made of aluminum: using a material of lower {density/(yield strength)} allows the balance to have a smaller full scale and better resolution. This reduces the uncertainty of the tank mass change (the mass of gas discharged). The measuring volume is separated from the test section at the vertical black line in figure 27, so the weighed portion includes two shut-off valves and a regulator. Polymer parts of the weighed equipment have been replaced with metal parts because many polymers gain or lose moisture from the room air and cause mass errors. Note that measuring tanks made from composite materials should be avoided for this application because they also change mass depending on the environmental humidity conditions. The tank is refilled through a port on the upstream side of the brass regulator. Care is taken to purge ambient air from the pipes used to fill the tank to maintain pure gas in V_M.

Weighing V_M: the tank is manually weighed by substitution weighing using a 10 kg full scale balance with resolution of 1 mg. Substitution weighing alternately places an object of unknown mass and a set of reference masses on a balance and uses the ratio of the balance readings (with zero corrections) to obtain the weight of the object [80]. The weighing is conducted inside a wind screen to prevent interference from air currents in the room. The pressure, temperature, and humidity are measured inside the wind screen and used to apply buoyancy

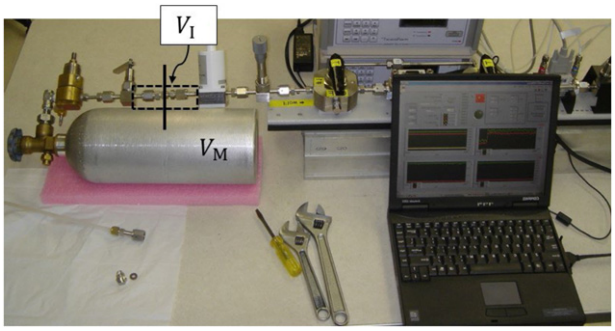

Figure 27. A picture of a standing start/stop static gravimetric standard at NIST being used to calibrate a laminar flow meter. The vertical black line shows where V_M is disconnected from the test section for weighing.

corrections. The environmental temperature is controlled to ± 1 K to minimize convective forces on the balance and a correction is made to account for the expansion of V_M with internal pressure (equation (15)). With these buoyancy corrections, we estimate the standard uncertainty of the mass change is 4.5 mg.

Inventory volume: in figure 27, the inventory volume V_I is surrounded by a dashed rectangle. The inventory corrections are negligible because V_I is only 3 cm^3 and because the mass change in V_I is due mainly to changes in the molar mass (contamination of the test gas by room air). Ignoring inventory corrections entirely leads to a standard uncertainty of 1 mg when the test gas is nitrogen. (Before the shut-off valve is opened, the pressure and temperature in V_I equals the room conditions and when the flow is turned off, the operator waits for flow through the meter to drop to zero, i.e., the pressure and temperature in V_I return to room conditions again.)

Flow equations and uncertainty (table 6): the ratio of the difference between the final and initial tank masses ($m_{M,f} - m_{M,i}$) to the integrated mass measured by the MUT (m_{MUT}) gives the calibrated meter factor.

The time record of the flow from the MUT is integrated using a numerical method (e.g., the trapezoidal rule) to obtain the totalized mass measured by the meter between the time that

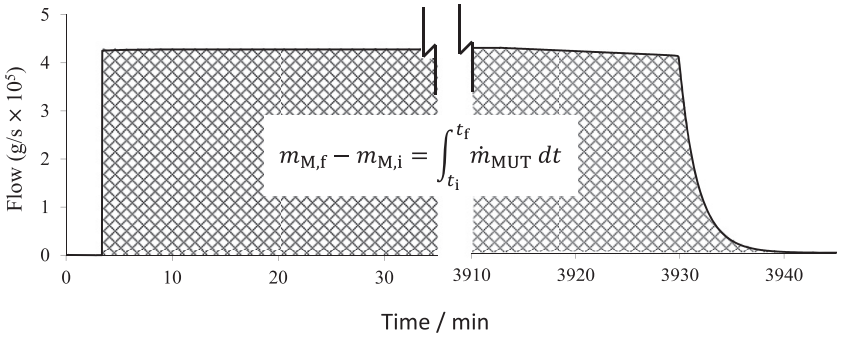

Figure 28. Time dependence of the mass flow indicated by a laminar flow MUT. The nominal flow is 4.3×10^{-5} g s^{-1} (2 cm^3 min^{-1}).

Table 6. Uncertainty of the NIST static, standing start/stop gravimetric flow standard for a flow of 4×10^{-5} g s^{-1} (1.9 cm^3 min^{-1}).

Input variable (x_i)	Notes	x_i value	$u(x_i)/x_i$/%	S_i	Contrib./%
Tank mass change $(m_{M,f} - m_{M,i})$	a	9.4 g	0.048	1	28
Inventory mass change	b	0.001 g	0.010	1	1
Integration errors	c	0.006 g	0.064	1	50
Collection time $(t_f - t_i)$	d	235 620 s	0.004	−1	∼0
Leaks	e	3.9×10^{-10} g s^{-1}	∼0	1	∼0
Type A $(s/\sqrt{n})$	f	106×10^{-8} g s^{-1}	0.04	1	20
Expanded uncertainty (95%)	$\boldsymbol{U}(\dot{\boldsymbol{m}})/\dot{\boldsymbol{m}} = 0.18\%$				

[a]Includes balance resolution, reference mass uncertainty, buoyancy corrections.
[b]Based on making no inventory correction, nitrogen test gas.
[c]Assumed a quarter of a triangular area covering the stop transient.
[d]10 s out of 235 620 s integration.
[e]Measured by pressure decay test.
[f]Measured during calibration of best existing device, in this case a laminar flow meter.

the shut-off valve is opened (t_i) and closed (t_f),

$$m_{MUT} = \int_{t_i}^{t_f} \dot{m}_{MUT} dt \cong \sum_{i=1}^{N} \frac{\dot{m}_{MUT,i-1} - \dot{m}_{MUT,i}}{2} \Delta t, \quad (18)$$

where Δt is the time increment in the data record. The uncertainty of the numerical integration depends on the time resolution, the stability of the flow, the time response of the meter, and other factors. A well-designed flying start/stop system has a diverter that does not perturb the steady-state conditions at the MUT. In contrast, the standing start/stop system has ramp-up and ramp-down conditions by definition; therefore, the MUT's response time can more easily affect the calibration results. For a perfect step function between zero flow and steady state conditions, the numerical integrations introduce negligible uncertainty, but for short integration intervals, the ramp-up and ramp-down events can be the dominant sources of uncertainty.

Figure 28 plots the time dependence of a flow meter output during a calibration. The calibration started when the shut-off valve was opened (at $t = 3$ min) and stopped at $t = 3930$ min. The details of figure 28 depended on the particular regulators, valves, flow meters, etc shown in figure 27. The start and stop events were not perfect step functions and the meter response was not instantaneous, introducing uncertainty to the numerical integration. The uncertainty can be reduced by making the mass change in the tank large compared to the uncertainty introduced by the start and stop transients. For figure 28, a crude estimate of the integration error (a quarter of a triangular area of the stop transient) produces a standard uncertainty 6 mg, which is 0.064% of the 9.4 g integrated flow.

The 95% confidence level uncertainty of this particular flow measurement is 0.18%. Because V_M can hold as much as 420 g of nitrogen, the uncertainty related to the start and stop transients (and the weighing process) can be reduced by extending the measurement time (and increasing the mass change), but this may not be practical; this single flow measurement took nearly three days to complete table 6).

2.3. Dynamic gravimetric standard

Figure 29 is a schematic diagram of a dynamic gravimetric system. The components of this type of flow standard are:

- A compressed gas tank functioning as a measurement volume V_M with a shut-off valve resting on a balance, both inside a wind screen so that air currents do not influence the tank's weight.
- A data acquisition system that records the readings of the balance (and other sensor readings) as the gas tank discharges through the MUT.

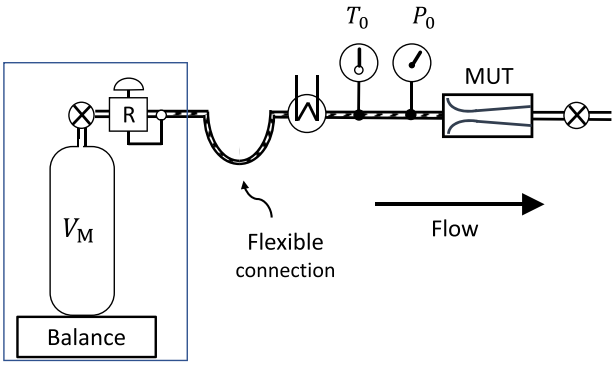

Figure 29. Schematic diagram of a dynamic gravimetric system.

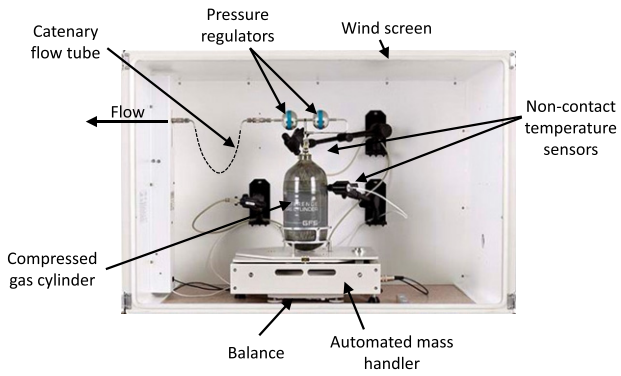

Figure 30. The dynamic gravimetric gas flow standard developed by Fluke Inc. Reproduced with permission by Fluke Corporation.

- Sensors to measure the pressure, temperature, and relative humidity of the air surrounding the tank to make buoyancy corrections.
- A regulator and heat exchanger to stabilize the gas pressure and temperature at the MUT.
- A flexible connection between the sub-system on the balance and the test section to minimize the variation of forces between these two parts of the system during tests.
- The MUT with appropriate instrumentation and downstream isolation valve for leak testing.

To use a dynamic gravimetric gas flow standard:

- Fill V_M with the test gas following necessary safety and purging requirements. Wait for V_M to return to room temperature.
- Place V_M on the balance and connect it to the downstream portion of the system. Test for leaks between V_M and the MUT using the isolation valves and a pressure sensor.
- Open the V_M's valve and the downstream isolation valve to initiate flow. Flow is controlled by the pressure regulator and/or a flow controller in the test section.
- Periodically record time-stamped balance and environmental sensor readings and calculate the time-dependent, buoyancy-corrected mass of the tank and its change with respect to time. Also record the flow readings from the MUT.
- After sufficient gas has flowed through the MUT to satisfy uncertainty considerations, close V_M's shut off valve or change the flow set point.

The dynamic gravimetric method has been used at the Laboratoire National d'Essai (LNE) in France [84], at the PTB in Germany [85], at HORIBA STEC Co. in Japan [86], and is sold commercially by Fluke, Inc. [87]. Two implementations are shown in figures 30 and 31.

The dynamic gravimetric method weighs a tank filled with a test gas and determines the mass flow through the MUT from the rate of change of the buoyancy-corrected tank mass. This method has the advantage of not requiring a carefully designed diverter unit to switch the flow from a bypass path. Instead, a simple on/off valve that does not generate timing triggers can be used. The mass flow calculations use data acquired during steady flow; therefore, the calculations are not affected by the flow transients generated by the valve's operation.

The dynamic gravimetric method is usually applied in the blow-down mode while the MUT discharges into the atmosphere or into a vacuum pump. It is usually applied to low flows ($<$0.22 g s^{-1} or 10 L min^{-1}) so that heat transfer from the surroundings maintains the entire system near room temperature. For larger flows, adiabatic expansion of the gas flowing out of V_M significantly cools the tank. The ambient air surrounding V_M also cools, descends, and loads the balance. At large flows, water vapor in the surrounding air can condense or freeze on the cold tank causing even larger mass measurement errors. As shown in figure 29, a heat exchanger can be placed before the test section to improve temperature stability at the MUT.

One of the challenges of the dynamic gravimetric method is ensuring that the forces imposed on the balance by connecting wires or tubes are either negligible or constant. For example, if the sub-system on the balance and the test section were connected by a rigid tube, the balance would not accurately detect the mass change of the tank as the tank discharges. To minimize the forces, some researchers have connected the tank assembly to the MUT using a thin-walled, flexible, coiled tube (pigtail) while others used a catenary shape, as shown in figure 30 [88].

Note that the pressure regulators in figures 30 and 31 are part of the tank assembly that is weighed by the balance. In general, it is better to minimize the mass of the weighed components. This allows the use of a balance with a smaller full-scale range and a correspondingly finer resolution; the finer resolution reduces the uncertainty of weighing the gas that flows out of the tank. However, it is desirable to include the pressure regulator in the tank assembly to maintain a stable pressure in the flexible connecting tube while the tank pressure decreases during a flow measurement. If the pressure changes, the decreasing Bourdon tube forces caused by a decreasing pressure in a pigtail would cause errors in the balance's reading. Also, if the pressure and temperature in the connecting tube are nearly constant, the initial and final conditions of the inventory volume are nearly constant, and the inventory volume correction is often negligible.

In common with other gravimetric methods, buoyancy corrections are applied. The tank's temperature and internal pressure are used to correct the tank external volume. The internal

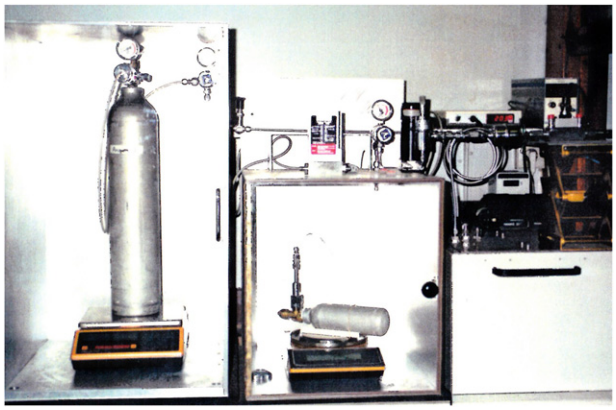

Figure 31. A picture of two dynamic gravimetric systems in the Laboratoire National d'Essai circa 2003 [84].

pressure need not be measured with a sensor: it can be related to the tank's mass and gas species, as previously described. The temperature of the tank is measured with non-contact thermometers to avoid extra weight and parasitic forces from connecting wires. Some implementations of the dynamic gravimetric method make buoyancy corrections negligible by housing the collection tank in a vacuum chamber [86, 89]. Making the mass measurements in vacuum also eliminates forces due to natural convection currents flowing over the surfaces of the collection tank caused by temperature differences between the tank and the environment [90].

The dynamic gravimetric method is often used for smaller flows that require collecting data for many hours. For long collections, the calibration stability of the balance and its sensitivity to changing environmental conditions are a concern. The system in figure 30 has an automated mass handling ('auto-zeroing') system that can alternately weigh: (1) the tank, (2) nothing, or (3) a reference mass. This mass handling system allows one to monitor and correct for the balance's zero and gain drift during long tests.

Flow equations and uncertainty (table 7): the slope of the buoyancy corrected mass versus time data yields the mass flow, using the same equations given for the rate of rise method (equations (8)–(10)).

As for the RoR method, the meter factor can be calculated in the same manner described for the static gravimetric method: by dividing the difference between two masses in the data record ($m_{M,f} - m_{M,i}$) by the integrated mass flow measured by the MUT (m_{MUT} from equation (18)). The initial and final masses $m_{M,i}$ and $m_{M,f}$ can be chosen from the data record at times where the data are unaffected by the start and stop transients.

Similar to other methods covered herein, the uncertainty of the flow measurement is highly dependent on the particular way the method is implemented, e.g., the specifications of the balance, the performance of the tank assembly, etc. The uncertainty is also highly dependent on the operating procedures. For example, the data collection intervals must be long enough for significant mass changes, significant leaks must be avoided, buoyancy corrections must be performed correctly, etc.

We illustrate the connections between the uncertainty of a standard's instrumentation, the operating procedures, and the flow range by considering the equipment for the standard shown in figure 30. Time uncertainties for this standard are on the order of 0.02 s at the 95% confidence level. Therefore, measuring mass change over intervals of 200 s or longer will keep time uncertainty contributions to the flow measurement below 0.01%. Also, the 95% confidence level uncertainty for the mass change measurement is approximately 1 mg. Hence, to limit the uncertainty due to mass measurement to 0.1% or less, the mass change should be 1000 times 1 mg, i.e., 1 g or larger. For nitrogen, these procedures lead to collection times of 1.3 h for a 2.2×10^{-4} g s^{-1} (10 cm^3 min^{-1}) flow, 0.13 h for 2.2×10^{-3} g s^{-1} (100 cm^3 min^{-1}), etc. Based on this procedure, we will now generate an uncertainty analysis using either equation (10) or a long average of the results from equation (8) for a collection time >100 s and a mass change >1 g.

Change in the tank mass: this component covers uncertainty in the mass flow measurement that is related to the calibration and operation of the balance. The standard uncertainty of a single mass measurement (0.31 mg) is the RSS of the standard uncertainties due to: the balance non-linearity (0.19 mg), zero corrections (0.25 mg), and repeatability (0.23 mg). Two or more mass measurements are required to measure the mass change of the gas in V_M. We will treat those two mass measurement uncertainties as uncorrelated and combine them by RSS even though they are measured by the same balance because the linearity, zero correction, and repeatability are not correlated for two mass measurements. Combining two mass uncertainties of 0.31 mg by RSS gives a standard uncertainty a mass change measurement of 0.55 mg ($k = 1$).

The zero correction uncertainty is based on analysis of the periodic, automatically collected zero data such as those plotted in figure 32. Also plotted is the change in the zero between adjacent zero checks ('zero change') and the environmental air density.

Slope calculation and flow stability: similar to the rate of rise method, these components must be controlled by collecting data over a sufficiently long interval and prequalifying the data. It is based on the standard deviation of the residuals of the best fit equation as described in section 1.5 on the rate of rise method and equation (13).

Changes in room conditions and the inventory volume: the storage effect correction is proportional to the product of the connecting volume and the fractional change in absolute temperature. For example, a 0.5 °C temperature change on a 10 cm^3 connecting volume during a 1 h flow measurement generates a flow uncertainty of 3.2×10^{-8} g s^{-1} (0.0015 cm^3 min^{-1}). Insulating the connecting tubing will dampen the effect of room temperature changes on the dynamic gravimetric flow measurements.

2.4. Liquid displacement standard

The liquid displacement standard [91] uses gas from the MUT to push an oil out of a sealed container into a gravimetric liquid flow standard. The oil should have a low vapor pressure and

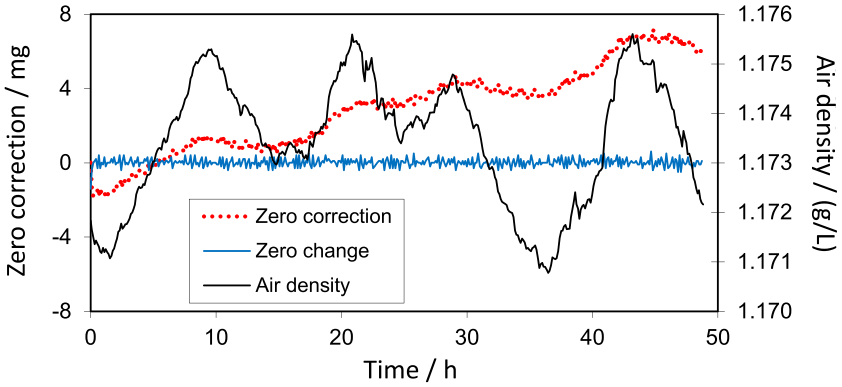

Figure 32. A sample set of balance zero correction data.

Table 7. Uncertainty of a dynamic gravimetric flow standard for a flow of 1.1×10^{-3} g s^{-1} (50 cm^3 min^{-1}).

Input variable (x_i)	Notes	x_i value	$u(x_i)/x_i$/%	S_i	Contrib./%
Tank mass change $(m_{M,f} - m_{M,i})$	a	1.1 g	0.050	1	72
Slope calculation and flow stability	b	0.006 g	0.010	1	3
Inventory mass change	c	1×10^{-5} g	0.001	1	0
Collection time $(t_f - t_i)$	d	1000 s	0.001	−1	0
Leaks	e	3.9×10^{-10} g s^{-1}	~0	1	0
Type A $(s/\sqrt{n})$	f	3.2×10^{-7} g s^{-1}	0.030	1	25
Expanded uncertainty (95%)	$\boldsymbol{U(\dot{m})/\dot{m}} = 0.12\%$				

[a]Includes balance resolution, zero, linearity, buoyancy corrections, forces from natural convection.
[b]Assumes flow is kept stable, $u(m)/u(t) \geqslant 2.5$, and N is $\geqslant 5 \times 10^4$.
[c]Based on making no inventory correction, 0.5 K h^{-1} room temperature change, nitrogen.
[d]Rectangular probability distribution applied to 23 Hz sampling for start and stop times.
[e]Measured by pressure decay test.
[f]Measured during calibration of best existing device, in this case a laminar flow meter.

low kinematic viscosity. During operation of the standard, gas flows through the MUT to the oil-filled tank. The incoming gas displaces oil from the tank and pushes it through a pipe to the gravimetric flow standard. A measurement of the liquid mass flow, as well as temperature and pressure measurements made at appropriate locations in the system, permits calculation of the gas flow in the test section. The 'actual' volumetric flows of the gas and liquid are equal (not their mass flows), so it is necessary to know the density of both media to calculate the mass flow of gas. The liquid displacement method takes advantage of the relative simplicity of a liquid diverter valve as compared to a gas diverter. Also, the greater density of a liquid relative to a gas makes the gravimetric liquid flow measurement relatively low in uncertainty. Because this method is not widely used, the reader is referred to reference [91] for more information about operation and uncertainty.

3. Velocity × area standards

The largest gas flow standards that we described above reach flows of approximately 40 kg s^{-1} (1860 m^3 min^{-1}) [74]. Large standards grow in size and expense in rough proportion with the flow. For flows greater than about 0.3 kg s^{-1} (14 m^3 min^{-1}), *velocity × area* methods that measure the gas velocity in a pipe of known area are more practical. Alternatively, several moderately sized meters can be calibrated versus a primary standard and used in parallel. (See section 4.) In section 1.1, we described a primary standard that could also be called a velocity × area method. It measures the speed of a piston that determines the average velocity of the gas $\overline{u}$ in a cylinder and applies the continuity equation $\dot{m} = \overline{\rho u} A$ to determine the flow. Here A is the cross-sectional area of the cylinder and $\overline{\rho}$ is the average density of the gas.

Velocity × area methods apply empirical and theoretical knowledge of fluid mechanics to estimate the velocity profile, including topics such as boundary layers and the transition from laminar to turbulent flow [92]. For example, in viscous flows, the velocity is zero at the solid boundaries and the maximum velocity occurs at the point furthest from the boundaries. A fully developed laminar velocity profile in a circular pipe will be parabolic, while that for a turbulent flow will depend on the pipe's roughness and the Reynolds number, i.e. the ratio of inertial forces to viscous forces. Near elbows, valves, or any geometry other than a long straight conduit of constant dimensions, the velocity profile is complicated and challenging to measure.

Flow in large conduits (e.g., smokestacks) can be quantified by measuring the profile with a velocity sensor inserted through the wall on a support rod and numerically integrating the axial velocity over the cross-sectional area. This is a

primary gas flow measurement. However, its uncertainty is often >5% for at least four reasons: (1) the flow often has a complex time dependence, (2) the integration of the flow in a cross-section has errors, (3) the velocity sensor changes the velocity profile due to blockage effects, and (4) the cross-sectional area is uncertain [93]. Here we focus on flow standards used in well controlled circumstances that use non-intrusive velocity sensors and can achieve uncertainty <1%.

3.1. Critical flow venturis (nozzles)

Critical flow venturis (CFVs, sometimes called nozzles) are converging-diverging orifices with a large enough pressure difference across the smallest cross section (the throat) that the gas attains the speed of sound [3, 4] (figure 33). Compressible flow theory indicates that this critical flow condition occurs for downstream-to-upstream pressure ratios <0.5. But thanks to pressure recovery in the diverging section, critical flow can often be maintained for pressure ratios <0.9. Under these *critical* conditions, the equation for the mass flow $\dot{m}_{R*}$ is derived from the continuity equation:

$$\dot{m}_{R*} = C_d A C_R^* P_0 \sqrt{\frac{\mathcal{M}}{\mathcal{R} T_0}}, \tag{19}$$

where, A is the cross-sectional area of the nozzle throat, C_d is the dimensionless discharge coefficient calculated from calibration data (or theory), P_0 and T_0 are the pressure and temperature at the stagnation condition upstream from the nozzle, $\mathcal{R}$ is the universal gas constant, $\mathcal{M}$ is the molar mass of the gas, and C_R^* is a dimensionless gas property called the critical flow function. It is related to the speed of sound and density on an adiabat and is available from a property database such as REFPROP [18]. The discharge coefficient corrects for errors in the throat diameter as well as momentum and boundary layer effects. The necessary inputs to calculate flow are the throat area, the gas properties, and the upstream pressure and temperature of the gas. Examples of how to calculate the flow through a CFV and best practices for their application are given in documentary standards [3, 4]. Reference [3] includes example uncertainty analyses as do references [6, 94].

Most users calibrate their critical nozzle versus a reference flow standard over a range of inlet pressures and fit the discharge coefficient C_d as a function of the Reynolds number to correct for departures of the theoretical flow from the mass flow measured by the reference standard. The throat diameter is used as the length scale when calculating the Reynolds number for a CFV: $\mathrm{Re} = (4\dot{m})/(\pi d \mu)$, where d is the throat diameter and μ is the gas dynamic viscosity. Used this way, critical nozzles are excellent working standards for flows $>2.2 \times 10^{-2}$ g s^{-1} (1 L min^{-1}) that can provide 0.1% uncertainty flow measurements.

The simplest physical model for the CFV assumes that the entire throat cross-section has velocity equal to the speed of sound, but more sophisticated models account for momentum effects and boundary layers on the nozzle walls [95–98]. The compressible fluid mechanics of the CFV are so well understood that analytical discharge coefficients agree with experimental values within 0.05% [99].

To use a nozzle as a primary standard (i.e., with low uncertainty without calibration versus another flow reference) requires good dimensional metrology of the inlet contour and especially the throat diameter (needed to calculate A). One pitfall is that the functional relationship between the discharge coefficient and Reynolds number depends upon whether the boundary layer is laminar or turbulent [99]. The transition to turbulence occurs at a Reynolds number (based on the throat diameter) on the order of 10^6. (See figure 34.) Near $\mathrm{Re} \approx 10^6$, the transition can introduce an uncertainty of 0.2% or more into critical-nozzle-based flow measurements.

The physical model for critical nozzles is well validated, but users must beware of species effects [100] especially vibrational relaxation effects for certain gases (e.g., SF_6 and CO_2) [101]. First-order effects of gas temperature are well accounted for in the baseline model (equation (19)) but thermal boundary layers are significant for nozzles at small Reynolds number [102]. For example, at Reynolds numbers $\mathrm{Re} < 2.5 \times 10^5$ (e.g., a 2 mm throat diameter flowing air at $P_0 = 1$ MPa), nozzles exhibit sensitivity to the environmental temperature of approximately 0.02%/K, primarily due to the difficulty of measuring the temperature (temperature 'sampling' errors) and the finite conductance of the thermal boundary layer. CFVs are best suited to flows $>2.2 \times 10^{-2}$ g s^{-1} (1 L min^{-1}) and throat diameters >0.4 mm for at least 3 reasons: (1) boundary layer effects increase as the nozzle's size decreases, (2) difficulties in machining small nozzles lead to comparatively larger uncertainties of their shapes and surface finishes, and (3) vibrational relaxation effects grow as the size of a nozzle decreases.

Figure 34 exemplifies the use of CFVs as rugged, precise transfer standards for large flows such as the flows that occur when NG is transported through pipelines at high pressures [103]. In this instance, four CFVs, each with an ASME/ISO standard shape and with a throat diameter $d = 25.4$ mm, were transported among flow calibration laboratories located in four different countries. The CFVs were calibrated in air and NG. A disadvantage of a nozzle-based comparisons of large flows is that each laboratory must have the very large pumping capacity needed to maintain critical conditions.

3.2. Laser Doppler anemometer

A one-dimensional (1D) LDA [104] splits a laser beam into two beams that intersect to produce a *sensing volume* with the shape of prolate ellipsoid of revolution. (Typical dimensions: long axis = 1 mm; other axes = 0.1 mm.) In the sensing volume, constructive and destructive interference produces light and dark bands that are parallel with the long axis and have an accurately known separation that is determined by the angle of intersection and wavelength of the laser beams. When particles entrained in the flow pass through the bands of light in the sensing volume, they scatter light (flicker) at a frequency that is proportional to the component of their velocity that is perpendicular to the bands. Optics collect the scattered light, and a burst spectrum analyzer calculates the flicker frequency. Usually the flow is *seeded* (via a Laskin nozzle upstream from the LDA) with oil droplets that are approximately 1 μm

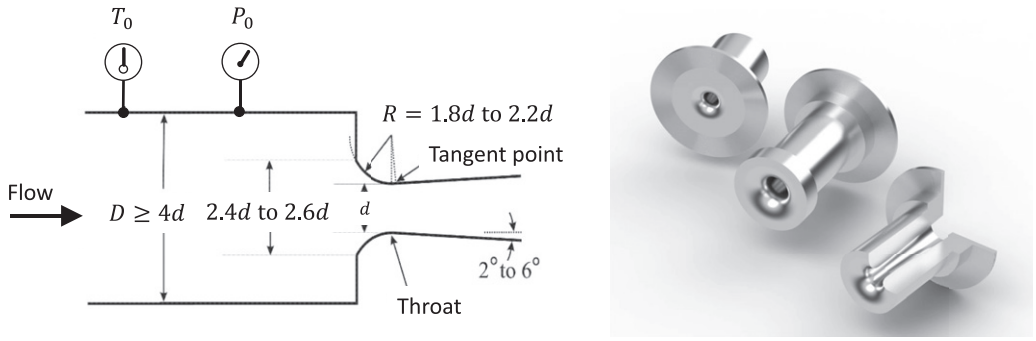

Figure 33. Left: geometry of a toroidal throat critical flow venturi as specified in the ASME/ISO standards and right: three CFVs, one with a cutaway view.

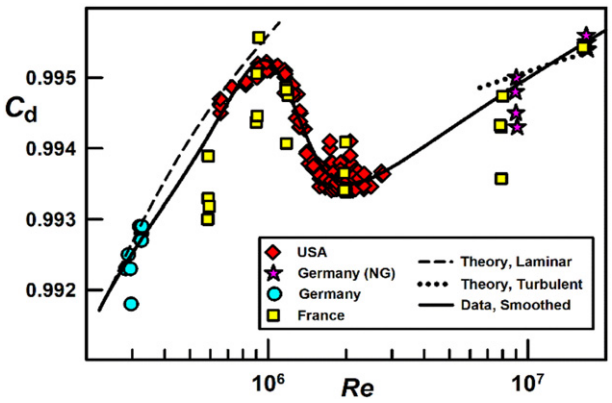

Figure 34. International comparison using four similar CFVs as transfer standards. The flows range from 0.11 kg s^{-1} to 4 kg s^{-1}. The discharge coefficient C_d = (actual flow)/(theoretical flow) is plotted as a function of Reynolds number (Re). Most of the data fall within ±0.05% of a smooth curve indicating that the laboratories are mutually consistent. The jog in the smooth curve near $Re = 1.5 \times 10^6$ occurs because the boundary layer flow near the nozzle walls transitions from laminar to turbulent.

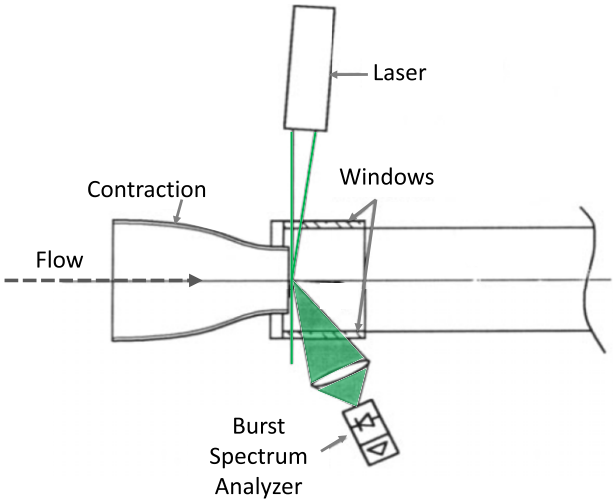

Figure 35. Dopheide *et al* [106] calculated flow by using a laser Doppler anemometer to measure the velocity profile of a free jet. The contraction flattens the velocity profile. The green lines represent the intersecting laser beams. The shaded cones represent the scattered light collected by the optical system leading to the burst spectrum analyzer. Reproduced from [106]. 1994 BIPM & IOP Publishing Ltd. All rights reserved.

in diameter. Such small droplets move at the same speed as the flowing gas. An LDA can be calibrated by replacing the scattering from entrained droplets with scattering from the edge of a spinning disk that has a known diameter and rotation frequency [105]. The speed of the disk's edge is easily made traceable to length and time standards.

Dopheide *et al* [106] designed a nozzle to produce a jet with a nearly symmetric 'top-hat shaped' (uniform) velocity profile (figure 35). They used a LDA to profile the jet and integrated the profile to determine the mean gas velocity in the cross section immediately downstream from the nozzle outlet. The nozzle diameter was 12 cm and the flow was up to 2 kg s^{-1} (93 m^3 min^{-1}). The expanded uncertainty was 0.1%. The challenges of this approach include: (1) accounting for large velocity gradients and von Karman vortices near the boundaries of the jet, (2) accurately defining the cross-sectional area of a free jet, and (3) knowing the pressure and temperature in the jet (to calculate the gas density).

Müller *et al* [107] used nozzles to produce a uniform velocity profile in a NG pipeline flowing in a 20 cm diameter pipe at flows up to 17.5 kg s^{-1} (1350 m^3 min^{-1}) and at pressure of 5 MPa (figure 36). Windows on opposite sides of the test section allowed the LDA transmitting and receiving optics to sense the velocity of seed droplets in the NG. The nozzles were designed to produce a uniform velocity at the outlet, but a boundary layer and a strong velocity gradient was unavoidable at the circumference of the jet, leading to an estimated volume flow uncertainty of 0.5%.

3.3. Ultrasonic time-of-flight flow meters

We consider three types of flow meter that use ultrasound to measure gas flow [2, 108, 109]: (1) Doppler flow meters that infer fluid velocity from the change in frequency of sound reflected by particles entrained in the flow, (2) cross-correlation meters that measure the time it takes particles or eddies (detected acoustically) to convect a known distance, (3) a time-of-flight (ToF) or transit-time meters that deduce an average fluid velocity from the difference in the time it takes sound to travel on a fixed path, in the upstream and downstream directions. Of these, the ToF meter has characteristics and performance suitable for use as a primary standard.

As shown in figure 37, a ToF meter uses two ultrasonic transducers mounted on opposite sides of a flow conduit that

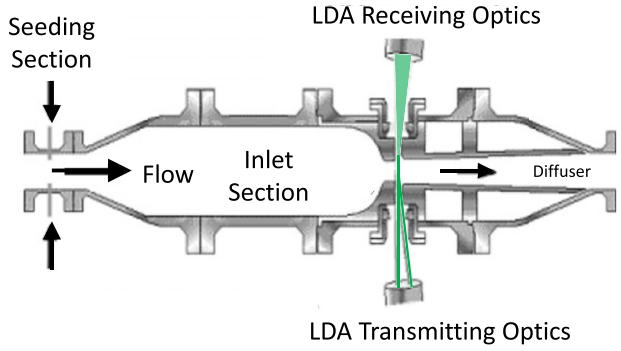

Figure 36. High pressure natural gas flow measured using a laser Doppler anemometer. Reproduced with permission from [107].

are offset in the stream-wise direction. Usually, the transducers are piezo-electric crystals that generate acoustic pulses (usually between 40 kHz and 250 kHz) into the flowing gas. The transducers are used alternately as receivers and transmitters. When the sound is transmitted in the downstream direction, the time required for the sound to travel between the two transducers (t_{down}) is shorter than when the roles of the transducers are reversed (t_{up}). Assuming: (1) that the flow field does not change during the sound propagation time, and (2) the gas's velocity is well below the speed of sound (Mach number < 0.1), the transit times are:

$$t_{\text{down}} = \frac{\ell}{a + V_\ell}, \tag{20}$$

$$t_{\text{up}} = \frac{\ell}{a - V_\ell}, \tag{21}$$

where ℓ is the distance between the transducers, a is the speed of sound, and V_ℓ is the component of average velocity of the flow along the sound path connecting the two transducers. If one makes the further assumption that there is only an axial velocity component to the gas flow V_{A} (no off-axis components or swirl), then

$$V_{\text{A}} = \frac{V_\ell}{\cos(\phi)}, \tag{22}$$

where ϕ is the angle between the ultrasonic path and the pipe axis.

The mass flow can be calculated by multiplying the average axial velocity by the cross-sectional area and the gas density. The gas density is calculated from pressure, temperature, gas composition and an equation of state.

Because the average axial velocity along the sound path is not equal to the velocity averaged over the cross-sectional area of the pipe, it is essential to apply a 'velocity profile correction factor' based on an assumed velocity profile. For a long, straight run of pipe, the velocity profile (and hence the correction) is a function of the Reynolds number and the pipe wall roughness [110]. It is impractical to predict the necessary corrections when the velocity profile is disrupted by valves, manifolds, pipe size changes, or elbows in the pipe upstream from the flow meter. Multipath ToF flow meters (such as those shown in figure 38) obtain line-average velocities over several strategically placed acoustic paths to reduce flow errors in distorted profiles [111]. The acoustic pulses can be reflected off the pipe walls one or several times so the paths sample more regions of the cross-sectional area. The cross-sectional average velocity (and flow measurement) can be improved if each path is weighted according to Gaussian quadrature based on the path locations and the anticipated velocity profile [112].

A ToF flow meter is also subject to errors due to off-axis fluid velocity components or swirl. Swirl errors can also be mitigated by multi-path ToF meters: the errors caused by non-axial velocity components largely cancel when the velocities measured by crossed acoustic paths are averaged [113].

Advances in multi-path ToF flow meters have been driven by the need for low-uncertainty flow measurements of feed water in nuclear power plants and of NG for in-pipeline custody transfer [114]. Multi-path ToF meters also measure flue gas flows in smokestacks for pollution control.

Uncertainty can be reduced by installing flow conditioners upstream from ToF meters to produce low swirl, predictable velocity profiles.

Manufacturers of ToF meters with diameter >20 cm often perform 'dry calibrations', i.e., flow calibrations that are based on the well-validated physical model for the flow meter and are directly traceable to length and time. Dry calibrations are practical for calibrating ToF meters for flows that exceed the capacity of other primary flow standards. Early ultrasonic meters were applied to measure liquid flows. In that context, 'dry calibration' indicated calibration done without a flow facility and 'wetted transducer' indicated that the acoustic transducers were in direct contact with the fluid instead of transmitting sound through pipe walls.

The acoustic path length ℓ can be determined *in situ* via equations (20) and (21). To do so, the flow is stopped and the meter is filled with a gas that has an accurately known speed of sound as a function of temperature and pressure $a(T, P)$. Then, measurements of the transit times, temperature, and pressure are combined with values of $a(T, P)$ from the literature to determine ℓ. Note that it is usually easier to obtain low uncertainty length and angle measurements in a large flow meter than in a small meter.

By making accurate time, diameter, path length, and angle measurements, a multi-path time-of-flight flow meter can provide a flow measurement with <0.5% uncertainty, without calibration in a flow facility and can be considered a primary flow standard.

Uncertainty analyses for flow measurements based on dry calibration and comparisons between dry-calibrated ToF flow meters and another flow reference are available in the literature. Drenthen and de Boer [115] and de Boer and Lansing [116] estimate the uncertainty of the velocity profile correction factor to be 0.3% and the uncertainty of the meter body geometry measurements to be 0.2%. Taking the root-sum-of-squares of these components gives 0.36% as the uncertainty of a flow measurement based on a dry calibration. When 48 dry calibrated ToF flow meters with diameter ranging from 20 cm to 61 cm were compared to reference standards, they agreed within 0.3%. Yeh and Mattingly [117] found that an 8-path, dry calibrated ToF meter and a gravimetric water flow standard agreed within 0.2%. On a cautionary note, Johnson *et al* [118] found that an 8-path, dry calibrated ToF meter differed from

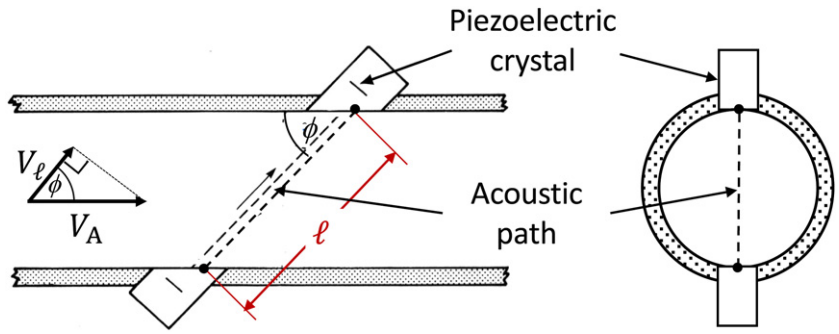

Figure 37. A single path ultrasonic time-of-flight flow meter measuring the axial velocity V_A of the flowing fluid along a path ℓ.

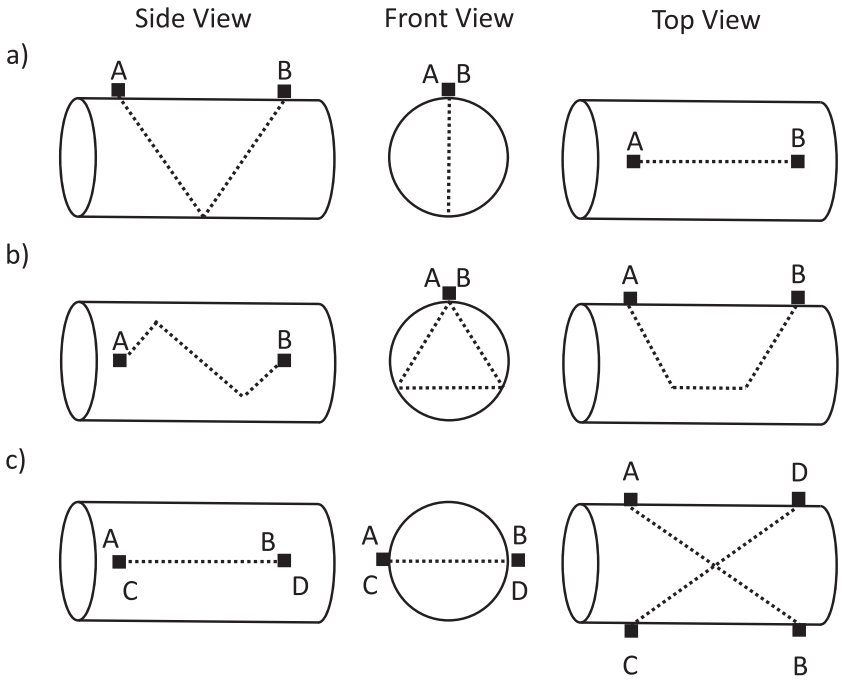

Figure 38. Multipath ToF flow meters are less prone to errors due to velocity profile effects and swirl than single path meters. A small sample of the many possible multi-path ToF configurations: (a) 2 paths with 2 transducers utilizing a reflection from the pipe wall, (b) 3 paths, 2 transducers, 2 reflections, (c) 2 paths, 4 transducers in a crossed pattern to counteract errors from swirl in the flow.

a gas flow working standard by −1.9%. The difference was attributed to a contracting upstream pipe configuration that produced a flatter velocity profile than the one used by the manufacturer to produce the Gaussian weights. Processing the line average velocities from multi-path ToF meters with computational fluid dynamics is fertile territory for machine learning and neural networks [112, 119].

4. Working standard flow meters and meters used in parallel

A calibrated flow meter can be subsequently used as a working standard, i.e. a reference for calibrating other flow meters. If the working standard and its associated instrumentation have good long term calibration stability, there is little increase in uncertainty compared to that of the flow reference used to calibrate it. Compared with primary standards, many working standards have advantages in operating simplicity, smaller size, easier maintenance, lower cost, and faster turnaround. Any stable flow meter (preferably with a well-developed physical model) is a candidate working standard. Examples are laminar, Coriolis, positive displacement, ultrasonic time-of-flight, positive displacement, and critical flow venturis [6].

The uncertainty of a working standard flow meter depends on: (1) the uncertainty of its calibration, (2) the uncertainty of its associated instrumentation (e.g. pressure, temperature, frequency, and gas composition sensors), (3) its reproducibility or long term calibration stability, (4) its sensitivity to environmental conditions, and (5) differences in the metered fluid between calibration and application conditions. The last two components have many facets: a meter's output is usually sensitive to the environmental temperature, the metered gas's pressure, temperature, and composition, and the velocity profile entering the flow meter. The meter's output may be sensitive

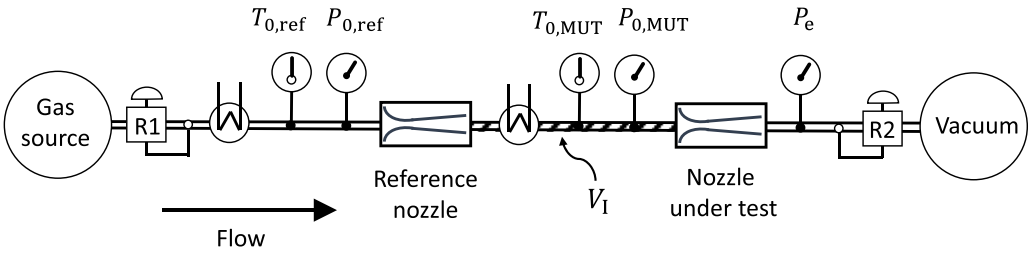

Figure 39. A schematic diagram of the nozzle-to-nozzle test system.

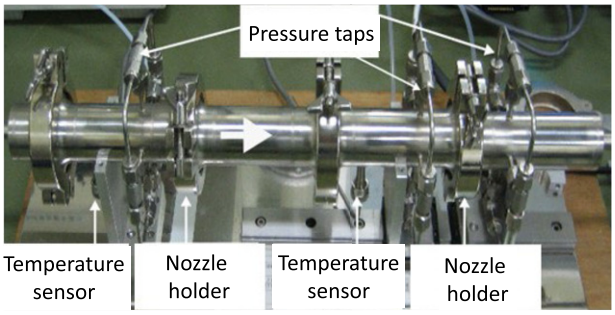

Figure 40. A picture of the nozzle-to-nozzle test system of NMIJ/AIST. Four pressure taps in the pipe wall are connected with a 3 mm tube and then connected to the pressure gauge.

to installation effects, including upstream pipe configuration, vibrations, and unsteady or pulsatile flow. Uncertainties from these sources are minimized by keeping the calibration and application conditions as similar as practical and by developing a physical model for how these quantities affect the meter output so that corrections can be made. Example uncertainty analyses are available in references [6, 94] and in the references related to each meter type given below.

Meters can be calibrated individually and then used in parallel in a manifold to measure larger flows, often with little increase in the measurement uncertainty. This approach is widely used and documented for turbine and ultrasonic meters for large, high-pressure NG flows and for critical flow venturis. The range of flows (turndown ratio) is limited by storage effects (line pack) in the connecting volume between the reference meters and the MUT. The size of the connecting volume should be optimized to achieve tolerable pressure losses with the largest flows while avoiding excessive storage effects that increase the uncertainty of the smallest flows.

Laminar flow meters: for a pipe Reynolds number of 2300 or less, flow is laminar and, to a good approximation, the volumetric flow is proportional to the pressure drop in the streamwise direction and inversely proportional to the dynamic viscosity of the gas (the Hagen–Poiseuille equation) [2, 92, 109]. Multiplying by the gas density gives the mass flow. Berg [120] published a physical model of the laminar meter that included five corrections to the Hagen–Poiseuille equation: (1) entrance and exit effects, (2) slip at the gas-wall boundary, (3) non-ideal gas effects, (4) gas expansion, and (5) transverse temperature distribution. Wright *et al* [121] applied the improved model to calibration data for three commercial laminar flow meters using five gases and found residuals <0.5% for Reynolds numbers <500. Hence it can be used to make corrections for differences between the calibration and application conditions. Laminar flow meters are particularly well suited to flows $<2.2 \times 10^{-2}$ g s^{-1} (1 L min^{-1}) but are commercially available for flows of 0.77 kg s^{-1} (60 m^3 min^{-1}) or more.

Laminar meters have no moving parts that might generate calibration instability; however, their calibration can change due to changes in the dimensions of the laminar flow path (corrosion or deposits of oil or dirt) and by calibration instability of the instruments (absolute and differential pressure sensors, thermometers, etc) needed to calculate mass flow. When a laminar meter is used in the same, filtered gas species, the main source of calibration changes is often the differential pressure sensor. There are several publications that quantify the calibration stability of laminar meters. Wright [122] examined 16 laminar meters that had been sent for periodic calibration versus the NIST piston and bell provers, some as many as seven times during a period of 22 years. For each laminar flow meter, the calibration drift was calculated by dividing the change in the meter factor by the time between calibrations. The standard deviation of the drift for the population of 16 laminar meters was 0.19% /year. Another study of four laminar meters calibrated seven times during a six-month period showed calibration changes of <0.05% [100].

Gas flow comparisons are a valuable source of calibration stability data because drift of the transfer standard is an important component of the comparison's uncertainty. The transfer standard's stability is evaluated by repeated calibrations in the pilot lab at the beginning and end of the inter-laboratory comparison. Rombouts *et al* [123] found uncertainty due to calibration stability of 0.04% ($k = 2$) for three laminar meters used over nearly three years at flows between 2.2×10^{-4} g s^{-1} (10 cm^3 min^{-1}) and 0.22 g s^{-1} (10 L min^{-1}). Chiang *et al* [14] used four laminar meters in a comparison with flows between 4.3×10^{-5} g s^{-1} (2 cm^3 min^{-1}) to 0.22 g s^{-1} (10 L min^{-1}) and found calibration stability uncertainty of 0.06% to 0.03% over a period of two years.

Critical flow venturis (nozzles): it is practical to measure CFV stagnation pressure and temperature with uncertainties of 0.02% or better in both the calibration and application laboratories. Therefore, a CFV with a low-uncertainty calibration can be used to calibrate other flow meters with little increase in uncertainty relative to the primary standard. In fact, a well calibrated nozzle can provide reference flows as good, or better than some versions of the primary standards we have described above. This makes the critical nozzle an accurate,

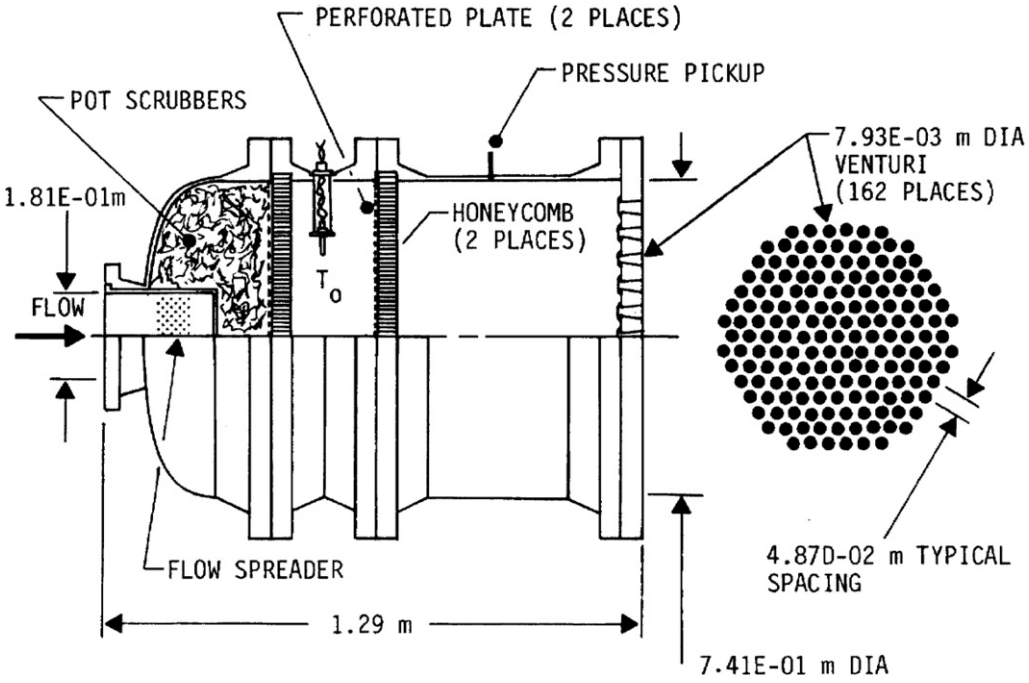

Figure 41. The multi-nozzle flow standard built by Stevens [125] is a manifold of 162 nozzles, each with a 7.9 mm throat diameter, that achieved air flows up to 18 kg s^{-1} (836 m^3 min^{-1}). Reproduced with permission from [125].

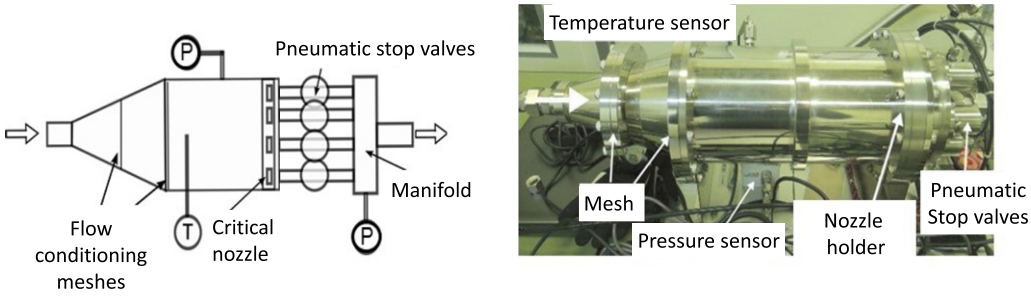

Figure 42. A schematic diagram and photograph of a multi-nozzle test system at NMIJ/AIST.

easily automated, low maintenance, robust, and economical way to calibrate other flow meters, including other critical nozzles.

The critical flow phenomenon makes CFVs largely immune to downstream pressure changes as long as the downstream-to-upstream pressure ratio is <0.5. This characteristic is useful when nozzles are calibrated by discharging their flow into a primary *PVTt* or RoR standard and when they are used as flow references.

Figure 39 is a schematic diagram of a reference CFV being used to calibrate another critical nozzle and figure 40 is a photograph of the nozzle-to-nozzle test system used at NMIJ/AIST. In figures 39 and 40, the reference nozzle is in the upstream position. The reference nozzle can also be in the downstream position but it is necessary to choose a reference nozzle and operating pressure such that both nozzles are in the critical flow condition.

Note the heat exchangers upstream from both nozzles shown in figure 39. Expansion through the pressure regulator cools the gas and it is easier to measure accurate gas temperatures if the gas is returned to room temperature before its temperature is measured. Also, the gas exiting the upstream nozzle produces a cold jet in the center of the exit pipe and temperature sampling errors are a concern if the gas is not returned to room temperature before reaching the downstream nozzle temperature sensor $T_{0,\mathrm{MUT}}$. These heat exchangers can be as simple as a long pipe with good heat transfer to the surroundings; however, such a pipe is a large contribution to the inventory volume. A large inventory volume requires a long wait for steady flow conditions to avoid errors due to storage effects. Time-stamped records of the pressure and temperature ($P_{0,\mathrm{MUT}}$ and $T_{0,\mathrm{MUT}}$) for the downstream nozzle can be monitored to assess whether steady conditions prevail.

Nozzles have no moving parts, so the long-term reproducibility of their discharge coefficients (calibration stability) depends on: (1) keeping the surfaces approaching the throat clean, undamaged by scratches, impact, and abrasive flows, and (2) the stability of the instruments that measure

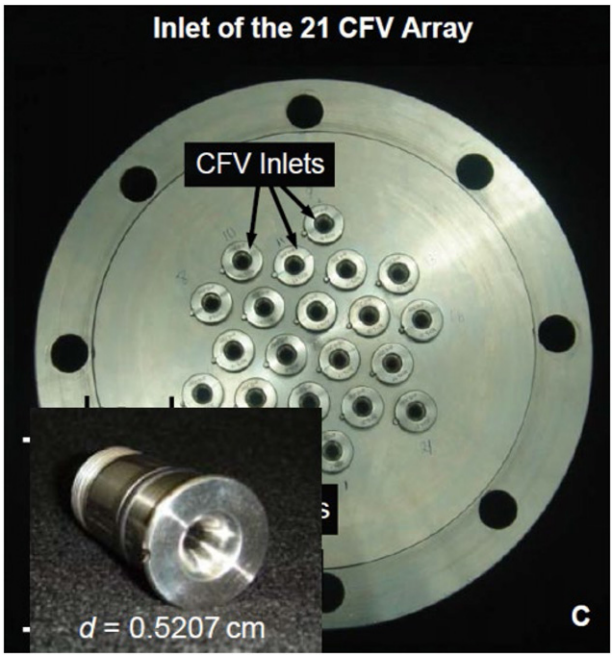

Figure 43. A nozzle plate used at NIST as a working gas flow standard. Eighteen nozzles have throat diameters of 5.2 mm, but three have diameters of 4.8 mm, 4.5 mm, and 3.2 mm to achieve smaller flow increments. Adapted with permission from [126].

$P_{0,\mathrm{MUT}}$ and $T_{0,\mathrm{MUT}}$. NIST calibrated 23 nozzles with diameters between 0.23 mm and 9 mm that were used by customers between calibrations. Some nozzles were calibrated five times over 26 years. The drift in the discharge coefficient C_d between the Nth and the $(N+1)$th calibrations was calculated via $\left(C_{\mathrm{d},N+1} - C_{\mathrm{d},N}\right)/\left(t_{N+1} - t_N\right)$. The standard deviation of the drift was 0.07%/year [122]. The uncertainty analysis for the NIST Working Gas Flow Standard uses a calibration stability uncertainty of 0.06% ($k = 2$) for the CFV discharge coefficient [6]: some of the NIST working standard nozzles show changes $<0.03\%$ over a period of 4 years [124]. The first low-pressure gas flow key comparison used critical nozzles and determined the uncertainty due to calibration instability to be $<0.05\%$ over a period of 14 months [12].

Multiple nozzles can be calibrated individually and then used in parallel to produce larger reference flows. In this way, a low-uncertainty primary standard with limited maximum flow can be applied to measure much larger flows economically and with a minor uncertainty increase. It is necessary to design the plenum for accurate pressure and temperature measurements and to separate the nozzles far enough from each other to avoid interference effects. Then, temperature and pressure measurements made in the plenum can be applied for all N nozzles.

In a properly designed multi-nozzle system, the nozzles have negligible interference effects, i.e., the discharge coefficient determined for each nozzle individually is unaffected by any combination of nearby nozzles that are used in parallel with it. The plenum should be large enough that that the gas in it is nearly at zero velocity (stagnant) and so that temperature measurements made in the plenum are accurate for each nozzle. This is achieved by (1) having a plenum with large cross-sectional area relative to the sum of the nozzle throat areas and (2) by separating the nozzles from the plenum walls and each other.

The upper limit of the flow for a multi-nozzle system is the capacity of the flow source. For the largest gas flows, it is economical to use a compressor for many hours to fill a blow-down tank to a high initial pressure. The tank is then discharged through a pressure regulator and a calibrated nozzle bank for as long as stable pressure conditions can be maintained at the test section. It is difficult to maintain steady-state gas and nozzle conditions in a blow-down system: the temperature of the gas exiting the blow-down tank falls as the pressure and mass of gas remaining in the blow-down tank decline. Furthermore, the approach pipe and nozzle body are cooling because of the cold, expanding gas flowing through them. Hence, uncertainty due to unsteady conditions in the plenum is important in blow-down systems and temperature and pressure instrumentation must be designed to account for this [118].

Most multi-nozzle systems are designed with valves (or manually screwed on caps) so that each nozzle can be individually opened or closed. The throat areas A_i are often sized in a factor-of-two sequence: ($A_i = 2^i A_1$, where A_1 is the throat area of the smallest nozzle) to provide reference flows over a wide range with resolution determined by the size of the smallest nozzle and/or the pressure at the manifold's inlet.

Figure 42 shows a multi nozzle test system used at NMIJ/AIST. In this system, five critical nozzles are installed in one plenum. Each critical nozzle can be stopped with an actuated valve, and the total flow is collected in a downstream manifold with a single outlet. The inlet plenum has a conical shape and contains two flow-conditioning meshes that suppress turbulence and prevent jet flows from directly hitting the nozzle entrances. In large plenums, the pressure is often measured via a pressure ring, a network of tubes that connects a single pressure sensor to multiple taps around the nozzle chamber.

Figure 43 shows a nozzle manifold used at NIST that holds 21 nozzles in a plate that is 20.3 cm in diameter [126]. When installed between flanges of a pipe, the plate is the downstream end of a plenum. Each nozzle was calibrated individually using the NIST 677 L *PVTt* standard. The temperature in the plenum is measured with three temperature sensors installed 120° apart around the chamber's circumference. The plenum's pressure is measured with a 4-tap pressure ring. The NIST multi-nozzle system covers flows from 4.3 g s^{-1} (200 L min^{-1}) to 0.93 kg s^{-1} (43 m^3 min^{-1}) with expanded ($k = 2$) uncertainty $<0.1\%$. Each nozzle has O-rings that prevent leakage between the nozzle body and the plate. Individual nozzles have removable, screw-on caps on their downstream sides so that the flow through each nozzle can be turned off by manually installing the cap.

Calibration of the NIST multi-nozzle system by the NIST 677 L *PVTt* standard (expanded uncertainty = 0.025%) is the first step in a five-step process to build a NG flow reference that operates at pressures up to 7.5 MPa with flows up to 520 kg s^{-1} (4×10^4 m^3 min^{-1}) with an expanded uncertainty $<0.27\%$ [127]. In the second step, four 25.4 mm nozzles are calibrated, one at a time, by flowing filtered dry air through

Figure 44. Working standard turbine meters used in parallel for natural gas flow measurement at (left) CEESI in Iowa. Reproduced with permission from [128] and (right) Pigsar in Germany. Reproduced with permission from [131].

Figure 45. Multipath ultrasonic time-of-flight meters at Trans Canada Calibrations are used in parallel to perform natural gas flow calibrations up to 12 kg s^{-1} (917 m^3 min^{-1}). Photo courtesy of TransCanada Calibrations Ltd.

each nozzle and then through the 21-nozzle plate shown in figure 43. The next two scale-up steps calibrate the same nozzles at higher pressures (and correspondingly higher flows and Reynolds numbers). In these steps, dry air flows through a single 25.4 mm nozzle and then through the four parallel 25.4 mm nozzles that had been calibrated in the previous step. The 5th scale-up step uses turbine meters, as described below and in [128]. The resulting flow reference measures NG flows 20 000 times larger than NIST's primary *PVTt* standard with the expanded uncertainty 0.27%, which is only 11 times larger than the uncertainty of the primary standard.

An essential assumption of multi-nozzle systems is that the discharge coefficient measured for each individual nozzle applies when the nozzles are used in parallel, i.e., that interference effects are negligible. If placed too close together or near the plenum's walls, one nozzle 'starves' its neighbor of gas. In this circumstance, the application conditions do not match the calibration conditions. Here, we cite measurements of interference effects as a function of L the separation of nozzles' centers from each other and as a function of the distance from the plenum's walls. The NMIJ/AIST design shown in figure 42 uses $L/d = 10$, where d is the throat diameter and the separation from the plenum wall is $10d$. Stevens (figure 41) [125] used nozzle spacing $L/d = 6.14$ and measured interference effects <0.01%. Choi *et al* [129] showed that $L/d > 3.7$ and distance from the plenum wall $>2.3d$ gave interference effects <0.05%. A second study by Choi *et al* [130] used three toroidal nozzles of different diameters (d = 4.3, 8.1, and 13.4 mm) in three plates that varied the distance between the nozzles and the plenum walls. They concluded that $L/d > 2.1$ and separation $>1.5d$ from the plenum walls produces interference effects <0.1%. The plate shown in figure 43 designed by Johnson *et al* [126] used $L/d = 6.15$ and plenum-wall separation $>6.15d$ and measured interference effects <0.01%.

Turbine meters and positive displacement meters: both of these meter types are used as working standards, often in parallel, to perform large NG flow calibrations. NIST uses nine turbine meters at the Colorado Engineering Experiment Station Inc. (CEESI) for NG calibrations at 7.5 MPa and flows from 15 kg s^{-1} (1.1×10^3 m^3 min^{-1}) to 520 kg s^{-1} (4×10^4 m^3 min^{-1}) with uncertainty of 0.27% or less (figure 44). Two calibrations of the nine turbines versus critical nozzle reference standards were performed 13 months apart and the standard deviation of the fits to the calibrations was <0.067% for all of the meters [128].

The national standard for NG flow measurement in Germany at Pigsar uses nine turbine meters at pressures from 1.4 MPa to 5 MPa and flows from 1.7 g s^{-1} (0.13 m^3 min^{-1}) to 1.4 kg s^{-1} (110 m^3 min^{-1}) [131, 132] (figure 44). Three calibrations performed over five years versus a piston prover showed changes of <0.2%. Calibrations of two turbines with diameter of 40 cm showed short term changes with standard deviation of <0.016% [132]. Shaw *et al* [133] used positive displacement and turbine meters with nominal diameters between 10 cm and 20 cm calibrated versus a gravimetric flow standard and estimated the reproducibility of the working standards to be <0.1% at the 95% confidence level. Benkova *et al* [13] used a positive displacement flow meter as the transfer standard in a key comparison for low pressure gas flow. The meter was calibrated versus a bell prover on seven occasions over 32 months and the uncertainty due to calibration stability was <0.06% at the 95% confidence level. Two 15 cm turbine meters used for an international comparison of high-pressure gas flow showed reproducibility during 22 months of <0.06% at the 95% confidence level [134].

The performance of turbine flow meters in gas flow depends on the meter design, bearing friction, the locations of pressure and temperature taps, gas composition, pressure, and temperature. An accurate physical model is not yet available; therefore, the performance of each working standard must be evaluated

Table 8. Calibration stability for six of ultrasonic ToF meters tested at CEESI Iowa.

Meter	Diameter/cm	Number of paths	Number of years	Number of calibrations	Calibration stability/%, $k = 2$
A	27	4	6.5	18	0.20
B	30.3	8	1.5	10	0.11
C	30.3	4	2.3	10	0.12
D	30.3	4	2.3	9	0.16
E	46.7	4	8.5	22	0.16
F	54.6	4	6.4	10	0.10

over the full range of conditions that it is applied. Normally, a polynomial fit of meter calibration factor versus Reynolds number works well for a range of gases and pressures [131]. Turbine meters are also susceptible to installation effects, especially swirl, so it is highly desirable to use the same piping and flow conditioners during calibration and application.

Ultrasonic time-of-flight meters: ultrasonic ToF meters have good long-term calibration stability that makes them well suited to serve as working standards. Figure 45 shows an example at TransCanada Calibrations Ltd. (TCC) where pairs of turbine and multipath ToF meters are used in series in eight parallel pipes ranging in diameter from 20 cm to 40 cm. The TCC facility calibrates meters in NG at flows between 2.2 g s^{-1} (0.17 m^3 min^{-1}) and 12 kg s^{-1} (917 m^3 min^{-1}) with uncertainty <0.25% and at pressures between 6 MPa and 7 MPa [135]. The turbine meters have repeatability of 0.2% or better (95% confidence level) and the ultrasonic meters have repeatability of 0.25% or better (95% confidence level). Calibrations of the turbine and ultrasonic meters conducted five years apart showed reproducibility of 0.1%.

Table 8 summarizes the calibration stability history for six multi-path ultrasonic ToF meters, each calibrated more than 9 times at CEESI in Iowa, over periods ranging from 1.5 years to 8.5 years. The calibration stability was quantified by fitting the error curves from the calibration with a second-order polynomial and calculating twice the standard deviation of the fit residuals (to obtain a 95% confidence level value). These meters were calibrated versus subsets of the nine parallel turbine meters described above, used in different combinations on different occasions, so the variance of the calibration results is dependent on both the reference turbine meters and on the ultrasonic meters.

Coriolis meters: when flow passes through a U-bend in a pipe, a Coriolis force proportional to the mass flow twists the U-bend (figure 46). Coriolis meters measure the twist imposed on the pipe by forcing a U-bend to oscillate and by accurately measuring the phase difference between two corners of the U-bend [2, 109]. The phase difference depends on the flow and on the elastic properties of the oscillating metal pipe. The temperature dependencies of the elastic properties of the metal flow tube must be known to accurately model Coriolis meters, particularly for cryogenic applications [136]. Coriolis meters can be subject to calibration changes caused by vibrations from external sources and details of their installation that influence the U-bend resonance.

Information about the calibration stability of Coriolis meters applied to gas flows is limited. Pope *et al* [137] found a calibration change of 0.14% in a Coriolis meter applied to hydrogen gas flow.

Figure 46. Twenty-seven Coriolis meters used in parallel at a natural gas storage facility in Hungary. Reproduced with permission from [138]. Photo courtesy of Emerson Automation Solutions.

Uncertainty of reference flow meters used in parallel: it is essential to take correlated uncertainties into account when estimating the uncertainty of meters used in parallel. Usually, the N flow meters are calibrated using the same primary standard, meaning their calibration uncertainties are highly correlated. Therefore, their calibration uncertainties are not combined by root-sum-of-squares. A more complex uncertainty formula such as that found in references [8, 10] is necessary. Combining uncertainties of meters used in parallel by RSS would lead to the incorrect conclusion that the uncertainty of the multi-meter system is smaller than the uncertainty of the flow reference used to calibrate each meter. It is challenging to assess the degree of correlation [8]; therefore, most analysts conservatively assume full correlation. References [128, 132] give example uncertainty analyses for nozzles and turbines used in parallel, respectively.

The uncertainty components of a multi-meter system include four components: (1) the uncertainty of a single meter used as a working standard (2) interference effects between the individual flow meters, (3) spatial non-uniformity of pressure and temperature in a plenum unless each of the parallel meters has its own sensors, and (4) extra storage effects resulting from larger pipe diameters needed to handle the combined flow.

5. Summary

This review article assembles the collective contributions of hundreds of flow metrologists who have worked to improve

gas flow measurements for a century. In sections 1 and 2, we described the volumetric and gravimetric primary standards used by national metrology institutes to provide traceability and proficiency testing to the flow meter manufacturing industry.

In sections 3 and 4, we described velocity × area methods, working standards, and calibrated meters used in parallel that are the most practical approaches for flows larger than about 0.3 kg s^{-1} (14 m^3 min^{-1}).

Acknowledgments

We thank Bobby Berg, Bill Johansen, and Wes Tew for reviewing and suggesting improvements to this manuscript before publication.

References

[1] 2008 International vocabulary of metrology—basic and general concepts and associated terms (JCGM 200: 2008) (https://bipm.org/utils/common/documents/jcgm/JCGM_200_2008.pdf)
[2] Baker R C 2016 *Flow Measurement Handbook* 2nd edn (Cambridge: Cambridge University Press)
[3] American Society of mechanical Engineers Measurement of gas flow by means of critical flow venturis and critical flow nozzles ASME MFC-7-2016
[4] ISO 9300 1990–2005 *Measurement of Gas Flow by Means of Critical Flow Venturi Nozzles, 1st edn, 1990, 2nd edn 2005* (International Organisation for Standardization)
[5] Wright J D, Kang W, Johnson A N, Khromchenko V B, Moldover M R, Zhang L and Mickan B 2021 Thermal boundary layers in critical flow venturis *Flow Meas. Instrum.* **81** 102025
[6] Wright J D, Kayl J-P, Johnson A N and Kline G M 2008 *Gas Flowmeter Calibrations with the Working Gas Flow Standard* (*NIST Special Publication 250-80*) (Gaithersburg, MD: National Institute of Standards and Technology)
[7] American Society of Mechanical Engineers 2021 *Boiler and Pressure Vessel Code*
[8] Coleman H W and Steele W G 1999 *Experimentation and Uncertainty Analysis for Engineers* 2nd edn (New York: Wiley)
[9] 2009 Evaluation of measurement data—an introduction to the guide to the expression of uncertainty in measurement and related documents (Joint Committee for guides in metrology, (JCGM) 104: 2009) (https://bipm.org/utils/common/documents/jcgm/JCGM_104_2009_E.pdf)
[10] 2008 Guide to the expression of uncertainty in measurement (JCGM 100) (https://bipm.org/utils/common/documents/jcgm/JCGM_100_2008_E.pdf)
[11] 2008 Evaluation of measurement data—supplement 1 to the guide to the expression of uncertainty in measurement-propagation of distributions using a Monte Carlo method (JCGM 101) (https://bipm.org/utils/common/documents/jcgm/JCGM_101_2008_E.pdf)
[12] Wright J D, Mikan B, Paton R, Park K-A, Nakao S-I, Chahine K and Arias R 2007 CIPM key comparison for low-pressure gas flow: CCM.FF-K6 *Metrologia* **44** 07008
[13] Benkova M *et al* 2014 Comparison of the primary (National) standards of low-pressure gas flow (CCM.FF-K6.2011) *BIPM Key Comparison Database*
[14] Chiang C-L *et al* 2021 CIPM low-pressure gas flow key comparison, (CCM.FF-K6.2017): comparison of primary gas flow standards spanning the range from 2 mL min^{-1} to 10 L min^{-1} *BIPM Key Comparison Database*
[15] Jousten K *et al* 2013 Final report of key comparison CCM.P-K12 for very low helium flow rates (leak rates) *Metrologia* **50** 07001
[16] Mickan B, Dopheide D, Kramer R, Vieth D, McLaren J, Haner W and Grudueski G 2007 *Final Report on the Bilateral CIPM Key Comparison for Natural Gas at High Pressure Conducted in October 2006, CCM.FF-K5.a.1, BIPM Key Comparison Database*
[17] Mickan B, Toebben H, Johnson A and Kegel T 2013 Final results of bilateral comparison between NIST and PTB for flows of high pressure natural gas *Metrologia* **50** 07004
[18] Lemmon E W, Bell I H, Huber M L and McLinden M O 2018 *NIST Standard Reference Database: Reference Fluid Thermodynamic and Transport Properties-REFPROP, Version 10.0* (Gaithersburg: National Institute of Standards and Technology, Standard Reference Data Program)
[19] Wright J D and Mattingly G E 1998 *NIST Calibration Services for Gas Flow Meters: Piston Prover and Bell Prover Gas Flow Facilities* (*NIST Special Publication 250-49*)
[20] Jousten K, Menzer H and Niepraschk R 2002 A new fully automated gas flowmeter at the PTB for flow rates between 10^{-13} mol s^{-1} and 10^{-6} mol s^{-1} *Metrologia* **39** 519–29
[21] Bellinga H and Delhez F J 1993 Experience with a high-capacity piston prover as a primary standard for high-pressure gas flow measurement *Flow Meas. Instrum.* **4** 85–9
[22] Kutin J, Bobovnik G and Bajsić I 2011 Dynamic effects in a clearance-sealed piston prover for gas flow measurements *Metrologia* **48** 123–32
[23] Barr G 1934 Two designs of flow-meter, and a method of calibration *J. Sci. Instrum.* **11** 321–4
[24] Harrison P and Darroch I F 1967 Air flow measurement by the soap film method *Report No. 302* National Engineering Laboratory, East Kilbride, Glasgow
[25] Kramer R, Mickan B and Kiesewetter P 2004 Traceability in gas flow measurements *55th Pittsburgh Conf. Analytical Chemistry & Applied Spectroscopy (PITTCON)* (Chicago IL, USA)
[26] Choi H M, Park K-A, Oh Y K and Choi Y M 2009 Improvement and uncertainty evaluation of mercury sealed piston prover using laser interferometer *Flow Meas. Instrum.* **20** 200–5
[27] Padden H 2002 Uncertainty analysis of a high-speed dry piston flow prover *Int. Symp. Fluid Flow Measurement* (Arlington, Virginia, USA)
[28] Padden H 2003 Development of a 0.2% high-speed dry piston prover *Measurement Science Conf.* (Anaheim, CA)
[29] Padden H 2009 Extending the range of gas piston provers *Int. Symp. Fluid Flow Measurement* (Anchorage, Alaska, USA)
[30] Bobovnik G, Kutin J and Bajsić I 2016 Uncertainty analysis of gas flow measurements using clearance-sealed piston provers in the range from 0.0012 g min^{-1} to 60 g min^{-1} *Metrologia* **53** 1061–8
[31] Bobovnik G and Kutin J 2019 Experimental identification and correction of the leakage flow effects in a clearance-sealed piston prover *Metrologia* **56** 015013
[32] Alasia F and Cignolo G 1985 Design criteria for a 1200 liter capacity piston prover for primary gas volume and flowrate measurements *FLOMEKO* (Melbourne, Australia) pp 123–8
[33] Cignolo G, Rivetti A, Martini G, Alasia F, Birello G and La Piana G 2000 The national standard gas provers of the IMGC-CNR *FLOMEKO* (Salvador, Brazil)

[34] Cignolo G, Alasia F, Capelli A, Goria R and La Piana G 2005 A primary standard piston prover for measurement of very small gas flows: an update *Sensor Rev.* **25** 40–5

[35] Park J T, Behring K A and Krueger P J 1995 *Metering Research Facility Program: Review of Field Meter Provers* (Gas Research Institute)

[36] van der Beek M P and van den Brink R 2015 Gas oil piston prover, primary reference values for gas-volume *Flow Meas. Instrum.* **44** 27–33

[37] Berg R F and Fedchak J A 2015 *NIST Calibration Services for Spinning Rotor Gauge Calibrations* (*NIST Special Publication*) pp 250–93

[38] McCulloh K E, Tilford C R, Ehrlich C D and Long F G 1987 Low range flowmeters for use with vacuum and leak standards *J. Vac. Sci. Technol.* A **5** 375–81

[39] Eckel S, Barker D S, Fedchak J, Newsome E, Scherschligt J and Vest R 2022 A constant pressure flowmeter for extreme-high vacuum *Metrologia* **59** 045014

[40] Berg R F, Gooding T and Vest R E 2014 Constant pressure primary flow standard for gas flows from 0.01 cm^3 min^{-1} to 100 cm^3 min^{-1} (0.007–74 μmol s^{-1}) *Flow Meas. Instrum.* **35** 84–91

[41] 2010 Calibration and measurement capabilities in the context of the CIPM MRA *CIPM MRA-D-04, Version 2*

[42] 2010 *ILAC Policy for Uncertainty in Calibration, ILAC-P14:12/2010*

[43] 2013 *Working Group for Fluid Flow Guidelines for CMC Uncertainty and Calibration Report Uncertainty* (https://bipm.org/documents/20126/44756349/ccm-wgff-guidelines.pdf/eda74c50-1192-a20e-fc16-a3760e11329e)

[44] Wright J D 2003 What is the best transfer standard for gas flow? *FLOMEKO* (Groningen, Netherlands)

[45] Kutin J, Bobovnik G and Bajsić I 2015 Heat exchange effects on the performance of a clearance-sealed piston prover for gas flow measurements *Metrologia* **52** 857–63

[46] Burick T E 1965 Automatic prover controls *Proc. 22nd Annual Appalachian Gas Measurement Short Course* vol 65 (West Virginia University Bulletin) pp 95–9

[47] Collett C T 1964 Calibration of bell-type provers by bottling and strapping *Proc. 24th Appalachian Gas Measurement Short Course* (Morgantown, WV) (West Virginia University) pp 59–66

[48] Smith A J W 1976 The effect of oil films on the performance of bell provers *Int. J. Mech. Sci.* **18** 135–43

[49] Wright J D, Sheckels S D, Lachance C, Sharifi F, Falicki A and Ondoro D 2015 The effect of liquid kinematic viscosity and drain time on the volume delivered from a test measure *Int. Symp. Fluid Flow Measurement* (Arlington, VA, USA)

[50] Ruegg F W and Johnson D P 1971 Dynamics of the bell prover *Flow: Its Measurement and Control in Science and Industry* (Pittsburg, PA: Instrument Society of America) pp 1297–307

[51] Ruegg F W and Ruegg F C 1990 Dynamics of the bell prover: II *J. Res. Natl Inst. Stand. Technol.* **95** 15–31

[52] Maginnis T O 2002 Dynamical effects in expanding volume flow calibrators *Int. Symp. Fluid Flow Measurement* (Arlington, VA, USA)

[53] Aschenbrenner A 1983 The main features of the new bell type prover of the Physikalisch-Technische Bundesanstaldt *FLOMEKO* (Budapest, Hungary)

[54] Bignell N and Choi Y M 2001 Volumetric positive-displacement gas flow standard *Flow Meas. Instrum.* **12** 245–51

[55] Wright J D, Moldover M R, Johnson A N and Mizuno A 2003 Volumetric gas flow standard with uncertainty of 0.02% to 0.05% *ASME J. Fluids Eng.* **125** 1058–66

[56] Ishibashi M, Takamoto M and Watanabe N 1990 New system for the pressurized gas flow standard in Japan *Proc. Int. Symp. Fluid Flow Measurement*

[57] Ishibashi M and Takamoto M 2000 Calibration of super-accurate critical nozzles at pressurized condition *Trans. Soc. Instrum. Control Eng.* **36** 1–9 (in Japanese)

[58] Li C, Cui L and Wang C 2013 The new PVTt facility in NIM *FLOMEKO* (Paris, France)

[59] Li C, Cui L and Wang C 2016 The uncertainty analysis and capability verification for the high pressure PVTt gas flow facility of NIM *FLOMEKO* (Sydney, Australia)

[60] Chahine K and Wang Z 2019 Establishment of an ultra-high accuracy 670 L PVTt gas flow primary standard at NMIA *FLOMEKO* (Lisbon, Portugal)

[61] Kuo C Y, Ho Y L, Lin W T and Su C M 2015 A new PVTt primary gas flow standard at CMS *9th Int. Symp. Fluid Flow Measurement* (Arlington, Virginia, USA)

[62] Olsen L and Baumgarten G 1971 Gas flow measurement by collection time and density in a constant volume *Flow: Its Measurement and Control in Science and Industry* (Pittsburg, PA: Instrument Society of America) pp 1287–95

[63] Wright J D and Johnson A N 2010 NIST lowers gas flow uncertainties to 0.025% or less *NCSL Int. Measure* **5** 30–9

[64] Wright J D and Johnson A N 2000 Uncertainty in primary gas flow standards due to flow work phenomena *FLOMEKO* (Salvador, Brazil)

[65] Johnson A N, Wright J D, Moldover M R and Espina P I 2003 Temperature characterization in the collection tank of the NIST 26 m^3 PVTt gas flow standard *Metrologia* **40** 211–6

[66] Nakao S-I 2006 Development of the system for very low gas flow rates *Flow Meas. Instrum.* **17** 193–200

[67] Pope J G, Gillis K A, Moldover M R, Mehl J B and Harman E 2019 Progress towards a gas-flow standard using microwave and acoustic resonances p 69

[68] Ishibashi M, Kato N and Harada H 2016 Dead-volume correction (DVC) for the calibration of CFVNs-differential calibration and optimum estimation *FLOMEKO* (Sydney, Australia)

[69] Žibret P, Bobovnik G and Kutin J 2022 Time-correction model based on diverter speed for a pVTt gas flow primary standard *Sensors* **22** 4001

[70] Wright J D, Johnson A N and Moldover M R 2003 Design and uncertainty analysis for a PVTt gas flow standard *J. Res. Natl Inst. Stand. Technol.* **108** 21–47

[71] American Vacuum Society 1968 Method for vacuum leak calibration, AVS standard 2.2-1968 *Vac. Sci. Technol.* **5** 219–22

[72] Wright J D, Johnson A N, Moldover M R and Kline G M 2018 Errors in rate of rise gas flow measurement from flow work *Proc. 10th Int. Symp. Fluid Flow Measurement* (Querétaro, Mexico)

[73] Brain T J S and Reid J 1978 Primary calibration of critical flow venturi nozzles in high pressure gas *FLOMEKO* (Groningen, Netherlands) pp 55–64

[74] Park J T, Behring K A and Grimley T A 1995 Uncertainty estimates for the gravimetric primary flow standards of the MRF *Int. Symp. Fluid Flow Measurement* (San Antonio, USA)

[75] Shaw J-H, Yang F-R and Chen Y-F 1995 A primary high-pressure air flow measurement standard in Taiwan *Int. Symp. Fluid Flow Measurement* (San Antonio, USA)

[76] Ren J, Duan J and Dong Y 2021 Application and uncertainty analysis of a balance weighing system used in natural gas primary standard up to 60 bar *Flow Meas. Instrum.* **77** 101836

[77] Nakao S-I and Takamoto M 1999 Development of the calibration facility for small mass flow rates of gases and the sonic venturi nozzle transfer standard *JSME Int. J.* B **42** 667–73

[78] Hayakawa M 2011 Development of high speed diverter using pneumatic valves *Hydrometrics and Pneumatics* pp 40–5 (in Japanese)

[79] Harris R E and Johnson J E 1990 Primary calibration of gas flows with a weight/time method *Int. Symp. Fluid Flow Measurement* (Calgary, Canada) pp 347–58

[80] Jaeger K B and Davis R S 1984 *A Primer for Mass Metrology* (*NBS Special Publication*) (National Bureau of Standards (US)) pp 700–1

[81] Picard A, Davis R S, Gläser M and Fujii K 2008 Revised formula for the density of moist air (CIPM-2007) *Metrologia* **45** 149

[82] Wright J D, Johnson A N and Moldover M R 2003 Design and uncertainty analysis for a PVTt gas flow standard *J. Res. Natl Inst. Stand. Technol.* **108** 21–47

[83] Berg R F and Tison S A 2004 Two primary standards for low flows of gases *J. Res. Natl Inst. Stand. Technol.* **109** 435–50

[84] Barbe J, Couette J, Picault J and Marschal A Traceability of standard gas mixtures prepared by the dynamic gravimetric method *Bull. Bureau Nat. Metrologie* 2001–2 120

[85] Knopf D and Richter W 1998 Highly accurate calibration gas mixtures by dynamic-gravimetric preparation *PTB-Mitteilungen* **108** 201–5

[86] Imamura K, Horinouchi O, Okuyama T and Isobe Y 2020 The primary gravimetric system for gas flow measurement *Flow Meas. Instrum.* **76** 101752

[87] Bair M and Rombouts C 2006 Typical measurement uncertainty in gas flow measured by GFS2102 gravimetric flow standard *Technical Note 6050TN09, DH Instruments*

[88] Barbe J and Rombouts C 2016 Improvements of the dynamic gravimetric flow standard (dGFS) below 0.2 mg·s^{-1} N2 (10 sccm) *FLOMEKO* (Sydney, Australia)

[89] Vičar M, Krajiček Z, Pražák D, Sedlák V, Gronych T, Hajdul T and Tesař J 2018 Gravimetric flow standard in the vacuum and hermetic modes *Meas. Sci. Technol.* **29** 095011

[90] Sillanpää S and Heinonen M 2008 The contribution of varying shear stress to the uncertainty in gravimetric gas mass flow measurements *Metrologia* **45** 249–55

[91] Grinten V d and Jos G M 1993 The primary standard for gas flow measurement in The Netherlands *Int. Conf. Flow Measurement, FLOMEKO* (Seoul, Korea)

[92] White F M and Majdalani J 2022 *Viscous Fluid Flow* 4th edn (New York: McGraw-Hill)

[93] Johnson A N, Shinder I I, Filla B J, Boyd J T, Bryant R, Moldover M R, Martz T D and Gentry M R 2020 Faster, more accurate, stack-flow measurements *J. Air Waste Manage. Assoc.* **70** 283–91

[94] Carter M, Johansen W and Britton C 2010 Performance of a gas flow meter calibration system utilizing critical flow venturi standards *FLOMEKO* (Taipei, Taiwan)

[95] Hall I M 1962 Transonic flow in two-dimensional and axially-symmetric nozzles *Q. J. Mech. Appl. Math.* **15** 487–508

[96] Tang S P and Fenn J B 1978 Experimental determination of the discharge coefficients for critical flow through an axisymmetric nozzle *AIAA J.* **16** 41–6

[97] Geropp D 1971 Laminare grenzschichten in ebenen und rotationssymmetrischen lavaldusen *Deutsche Luft- und Raumfahrt Forschungsbericht* pp 71–90

[98] Ishibashi M and Takamoto M 2000 Theoretical discharge coefficient of a critical circular-arc nozzle with laminar boundary layer and its verification by measurements using super-accurate nozzles *Flow Meas. Instrum.* **11** 305–13

[99] Johnson A N and Wright J D 2008 Comparison between theoretical CFV models and NIST's primary flow data in the laminar, turbulent, and transition flow regimes *ASME J. Fluids Eng.* **130**

[100] Wright J D 2003 What is the best transfer standard for gas flow? *Proc. FLOMEKO* (Groningen, Netherlands)

[101] Johnson A N, Wright J D, Nakao S, Merkle C L and Moldover M R 2000 The effect of vibrational relaxation on the discharge coefficient of critical flow venturis *Flow Meas. Instrum.* **11** 315–27

[102] Wright J D, Kang W, Johnson A N, Khromchenko V B, Moldover M R, Zhang L and Mickan B 2021 Thermal boundary layers in critical flow venturis *Flow Meas. Instrum.* **81** 102025

[103] Mickan B, Kramer R, Dopheide , Hotze H-J, Johnson A, Wright J and Vallet J-P 2002 Comparisons by PTB, NIST, and LNE-LADG in air and natural gas with critical venturi nozzles agree within 0.05% *Int. Symp. Fluid Flow Measurement* (Arlington, VA, USA)

[104] Drain L E 1980 *The Laser Doppler Technique* (New York: Wiley)

[105] Shinder I I, Moldover M R, Hall J M, Duncan M and Keck J 2012 Airspeed calibration services: laser Doppler anemometer calibration and its uncertainty *8th Int. Symp. Fluid Flow Measurements*

[106] Dopheide D, Strunck V and Krey E-A 1994 Three-component laser Doppler anemometer for gas flowrate measurements up to 5 500 m^3 h^{-1} *Metrologia* **30** 453–69

[107] Müller H, Strunck V, Kramer R, Mickan B, Dopheide D and Hotze H-J 2004 Germany's new optical primary standard for natural gas OF high pressure at Pigsar *FLOMEKO* (Beijing, China)

[108] Lynnworth L C 1989 *Ultrasonic Measurements for Process Control: Theory, Technique, Applications* (New York: Academic)

[109] Spitzer D W (ed) 2001 *Flow Measurement: Practical Guides for Measurement and Control* 2nd edn (Instrument Society of America, Research Triangle Park, NC)

[110] Yeh T T and Mattingly G E 1997 Computer simulations of ultrasonic flowmeter performance in ideal and non-ideal pipeflows *1997 ASME Fluids Engineering Division Summer Meeting*

[111] Moore P I, Brown G J and Stimpson B P 2000 Ultrasonic transit-time flowmeters modelled with theoretical velocity profiles: methodology *Meas. Sci. Technol.* **11** 1802–11

[112] Zheng D, Zhao D and Mei J 2015 Improved numerical integration method for flowrate of ultrasonic flowmeter based on Gauss quadrature for non-ideal flow fields *Flow Meas. Instrum.* **41** 28–35

[113] Johnson A, Shinder I, Moldover M, Boyd J and Filla J 2018 Progress towards accurate monitoring of flue gas emissions *Int. Symp. Fluid Flow Measurement* (Querétaro, Mexico)

[114] American Gas Association (AGA) 2007 Measurement of gas by multipath ultrasonic meters *Transmission Measurement Committee Report No 9* 2nd edn ((AGA9), AGA)

[115] Drenthin J G and de Boer G 2001 The manufacturing of ultrasonic gas flow meters *Flow Meas. Instrum.* **12** 89–99

[116] de Boer G and Lansing J 1997 Dry calibration of ultrasonic gas flow meters *North Sea Flow Measurement Workshop, Paper 18* (Kristiansand, Norway)

[117] Yeh T T and Mattingly G E 2000 Ultrasonic technology: prospects for improving flow measurements and standards paper A2 *FLOMEKO* (Salvador, Brazil)

[118] Johnson A N, Harmon E and Boyd J T Blow-down calibration of a large ultrasonic *flow meter Flow Meas. Instrum.* **77** 101848

[119] Yeh T T, Espina P I and Osella S A 2001 An intelligent ultrasonic flow meter for improved flow measurement and flow calibration facility *IEEE Instrumentation and Measurement Technology Conf.* (Budapest, Hungary)

[120] Berg R F 2005 Simple flow meter and viscometer of high accuracy for gases *Metrologia* **42** 11–23
Berg R F 2006 *Metrologia* **43** 183 (erratum)

[121] Wright J D, Cobu T, Berg R F and Moldover M R 2012 Calibration of laminar flow meters for process gases *Flow Meas. Instrum.* **25** 8–14

[122] Wright J D 1998 The long term calibration stability of critical flow nozzles and laminar flow meters *National Conf. Standards Laboratories Conf. Proc.* (Albuquerque, New Mexico) pp 443–62

[123] Rombouts C, Bair M, Barbe J, Wright J D, Kramer R and Krajicek Z 2014 A comparison of primary gas flow standards spanning the range 10 sccm N2 to 10 slm N2 *NCSLI Conf. Proc.* (Orlando, Florida, USA)

[124] Wright J D, Kang W, Zhang L, Johnson A N and Moldover M R 2015 Thermal effects on critical flow venturis *Proc. 9th Int. Symp. Fluid Flow Measurement* (Arlington, Virginia, USA)

[125] Stevens R L 1986 Development and calibration of the Boeing 18 kg s^{-1} airflow calibration transfer standard *Int. Symp. Fluid Flow Measurement* (Arlington, Virginia, USA) pp 80–96

[126] Johnson A N, Li C H, Wright J D, Kline G M and Crowley C J 2012 Critical flow venturi manifold improves gas flow calibrations *Int. Symp. Fluid Flow Measurement* (Colorado Springs, Colorado, USA)

[127] Johnson A N and Johansen B 2008 US National standards for high pressure natural gas flow measurement *Proc. 2008 Measurement Science Conf.* (Anaheim, California, USA)

[128] Johnson A N 2008 NIST measurement services: natural gas flow calibration service *NIST Special Publication 250-1081* (Gaithersburg, MD: National Institute of Standards and Technology)

[129] Choi Y M, Park K A and Park S O 1997 Interference effect between sonic nozzles *Flow Meas. Instrum.* **8** 113–9

[130] Choi Y M, Park K A, Park J T, Choi H M and Park S O 1999 Interference effects of three sonic nozzles of different throat diameters in the same meter tube *Flow Meas. Instrum.* **10** 175–81

[131] Mickan B, Kramer R, Hotze H-J and Dopheide D 2002 Pigsar—the extended test facility and new German national primary standards for high pressure natural gas *Int. Symp. Fluid Flow Measurement* (Arlington, VA, USA)

[132] Bremser W, Hasselbarth W, Hirlehei U, Hotze H-J and Wendt G 2002 Traceability and uncertainty of the German national flow rate measurement standard Pigsar *Int. Symp. Fluid Flow Measurement* (Arlington, VA, USA)

[133] Shaw J-H, Yang F-R and Ho Y-L 2006 Construction of a recirculation type high pressure air flow measurement facility and uncertainty evaluation *Int. Symp. Fluid Flow Measurement* (Querétaro, Mexico)

[134] Dopheide D, Mickan B, Kramer R, Hotze H-J, Vallet J-P, Reader-Harris M, Shaw J-H and Park K-A 2006 *Final Report on the CIPM Key Comparisons for Compressed Air and Nitrogen Conducted in November 2004/June 2005 (CCM.FF-5.b)*

[135] Mantilla J and Haner W 2006 Process variable stability, data processing, and installation and environmental influences during ultrasonic meter calibration *Int. Symp. Fluid Flow Measurement* (Querétaro, Mexico)

[136] Costa F, Pope J and Gillis K 2020 Modeling temperature effects on a Coriolis mass flowmeter *Flow Meas. Instrum.* **79** 101811

[137] Pope J G and Wright J D 2015 Hydrogen field test standard: laboratory and field performance *Flow Meas. Instrum.* **46** 112–24

[138] Calame S 2013 *Fundamentals of Coriolis Meters AGA Report No. 11* (American School of Gas and Measurement Technology)